Aus der Klinik für Neurologie
(Prof. Dr. med. M. Bähr)
der Medizinischen Fakultät der Universität Göttingen

Regulation des Autophagieproteins ULK1 im MPTP-Mausmodell des Morbus Parkinson

INAUGURAL-DISSERTATION

zur Erlangung des Doktorgrades
der Medizinischen Fakultät der
Georg-August-Universität zu Göttingen

vorgelegt von

Dirk Balke

aus

Warburg

Göttingen 2021

Dekan:	Prof. Dr. med. W. Brück

Betreuungsausschuss

Betreuer/in	Prof. Dr. med. P. Lingor
Ko-Betreuer/in:	Prof. Dr. med. C. Stadelmann-Nessler

Prüfungskommission

Referent/in	Prof. Dr. med. P. Lingor
Ko-Referent/in:	Prof. Dr. med. C. Stadelmann-Nessler
Drittreferent/in:	……...

Datum der mündlichen Prüfung: 15.11.2022

Hiermit erkläre ich, die Dissertation mit dem Titel "Regulation des Autophagieproteins ULK1 im MPTP-Mausmodell des Morbus Parkinson" eigenständig angefertigt und keine anderen als die von mir angegebenen Quellen und Hilfsmittel verwendet zu haben.

Göttingen, den …… ……

(Unterschrift)

Die Daten, auf denen die vorliegende Arbeit basiert, wurden publiziert:

Balke D, Tatenhorst L, Dambeck V, Ribas VT, Vahsen BF, Michel U, Bähr M, Lingor P (2020): AAV-mediated expression of dominant-negative ULK1 increases neuronal survival and enhances motor performance in the MPTP mouse model of Parkinson's disease. Mol Neurobiol 57, 685–697

Table of contents

List of figures

List of tables

List of abbreviations

3-MA	3-Methyladenine
6-OHDA	6-Hydroxydopamine
AAD	Acute axonal degeneration
AADC	Aromatic L-amino acid decarboxylase
AAV	Adeno-associated virus
ALP	Autophagosme-lysosome pathway
AMP	Adenosinmonophosphate
AMPK	AMP activated protein kinase
ATG	Autophagy-related, refers to the protein, genes are printed in italics
Atg	Autophagy-related, refers exclusively to yeast proteins
ATP	Adenosine triphosphate
bw	Body weight
CMA	Chaperone-mediated autophagy
CNS	Central nervous system
COMT	Catechol-O-methyltransferase
CSF	Cerebrospinal fluid
CTRL	Control
DA	Dopamine
DAB	3,3′-Diaminobenzidine
DAT	Dopamine transporter
DLB	Dementia with Lewy bodies
DNA	Deoxyribonucleic acid
DOPAC	3,4-Dihydroxyphenylacetic acid
ER	Endoplasmic reticulum
ERK1/2	Extracellular signal-regulated kinase 1/2
FAK	Focal adhesion kinase
FIP200	FAK family kinase interacting protein of 200kDa
GABA	Gamma amino-butyric acid
GABARAP	Gamma amino-butyric acid receptor-associated protein
GATE-16	Golgi-associated ATPase enhancer of 16kDa
GDNF	Glial cell line-derived neurotrophic factor
GP	Globus pallidum
GPe	Globus pallidum externum
GPi	Globus pallidum internum
HPLC	High-performance liquid chromatography
HRP	Horseradish peroxidase
HSC70	Heat shock cognate 70
HVA	Homovanillic acid
IHC	Immunohistochemistry
ITR	Inverted terminal repeat
IVC	Individually ventilated cage

LC3	Microtubule-associated protein 1 light chain 3
L-DOPA	Levodopa
MAO-B	Monoamine oxidase B
MAPK	Mitogen-activated protein kinase
miRNA	Micro RNA
MPDP	1-Methyl-4-phenyl-2,3-dihydropyridium
MPPP	1-Methyl-4-phenyl-4-propionoxypiperidine
MPP+	1-Methyl-4-phenylpyridinium ion
MPTP	1-Methyl-4-phenyl-1,2,3,6-tetrahydropyridine
mRNA	Messenger RNA
mtDNA	Mitochondrial DNA
mTOR	Mammalian target of rapamycin
NGS	Normal goat serum
ORF	Open reading frame
PAS	Phagophore assembly side
PBS	Phosphate buffered saline
PD	Parkinson’s disease
PFA	Paraformaldehyde
PI3K	Phosphatidylinositol 3-kinase
PI3P	Phosphatidylinositol 3-phosphate
RBD	REM sleep behavior disorder
REM	Rapid eye movement
RNA	Ribonucleic acid
ROS	Reactive oxygen species
RT	Room temperature
S6	Ribosomal protein S6 kinase beta-1
SCI	Spinal cord injury
SEM	Standard error of the mean
siRNA	Small interfering RNA
SN	Substantia nigra
SNpc	Substantia nigra pars compacta
STN	Nucleus subthalamicus
TBS	Tris buffered saline
TBS-T	Tris buffered saline with Tween 20
TH	Tyrosine hydroxylase
TU	Transforming units
Tris	2-Amino-2-hydroxymethyl-propane-1,3-diol
ULK1	Unc-51 like autophagy activating kinase 1
ULK1.DN	Dominant negative ULK1
UPS	Ubiquitin-proteasome system
wt	Wild type

1 Introduction

1.1 Parkinson's disease

Parkinson's disease (PD) belongs to the big field of neurodegenerative diseases. Among those it is the second most common disease and the one that has been described first of all, already in 1817 by James Parkinson (Parkinson 2002), a British doctor and surgeon. A characteristic feature of PD is the loss of dopaminergic (DAergic) neurons in the Substantia nigra pars compacta (SNpc) and its striatal projections (Beck et al. 2018). After loss of an estimated amount of 30 % of this particular neuronal cell population, patients start to present motor symptoms like a resting tremor or gait disturbances (Tagliaferro and Burke 2016). The histopathologic hallmark of PD is the occurrence of intracellular, alpha-synuclein immune-positive Lewy bodies in surviving neurons (Bengoa-Vergniory et al. 2017). The precursors of these protein aggregates, the alpha-synuclein oligomers are considered to contribute to the neuronal cell death by hampering essential cell functions (Wilkaniec et al. 2019). Several years of intense research led to the development of a broad spectrum of pharmacological agents being used for symptomatic therapy and providing normal life expectancy for the patients but there still is no curative treatment available yet (Connolly and Lang 2014). Therefore, further studies are required to illuminate the pathophysiology and causes of the disease in order to identify new targets and develop a potential therapy, which can stop or at least decelerate the progression of the disease (Tagliaferro and Burke 2016).

1.1.1 Epidemiology

PD as a neurodegenerative disease predominately affects the older population aged 60 years and higher. Beyond the age of 60 the prevalence is about 1 % and it might rise up to 4 % in the group of people aged 80 years and older (de Lau and Breteler 2006). PD is 1.5 times more frequent in men than in women. Based on population-based health claims data, the number of PD patients in Germany alone lies around 275,000 (Nerius et al. 2017). Due to the demographic development and increasing life expectancy in the western world but also fueled by declining smoking rates and increasing emission of industrial

by-products in the developing countries, patient numbers are expected to continuously rise in the near future: They are expected to double until 2050 compared to 2010 considering only Europe, Canada and the US (Bach et al. 2011; Dorsey et al. 2018).

1.1.2 Symptomatology & diagnosis

It is assumed that PD usually develops slowly within several years or even decades. Different studies suggest that nigro-striatal pathologies, like changed dopamine turnover and synthesis in the caudate and putamen, occur at an average of 5 – 10 years before the appearance of first clinical symptoms (Salat et al. 2016). These studies are based on brain imaging of patients with early PD or subclinical genetic forms of PD, post-mortem neurochemical analysis and animal models (Schapira and Tolosa 2010). However, a safe diagnosis cannot be made until the typical clinical motor symptoms, which define parkinsonism are clearly visible: bradykinesia and at least a resting tremor or/and rigidity have to be present. Then the clinical diagnosis of PD is made in a second step according to the MDS diagnostic criteria (Postuma et al. 2015b): For diagnosis of clinically established PD absolute exclusion criteria and red flags must be absent, while at least two supportive criteria are present. For diagnosis of clinically probable PD up to two red flags may be present but each red flag has to be balanced by at least one supportive criterion. Supportive criteria are defined as good response to dopamine therapy, levodopa-induced dyskinesia, rest tremor of an extremity and MIBG (metaiodobenzylguanidine) scintigraphy showing either olfactory loss or sympathetic denervation of the heart (Postuma et al. 2015b). Non-motor symptoms like hyposmia and autonomic dysfunction often occur years ahead of the manifestation of motor disturbances and can be equally relevant to patients. Moreover, cognitive deficits/dementia represent an important non-motor symptom that usually appears in late disease stages (Salat et al. 2016). The most meaningful pre-motor symptoms to support a diagnosis of early PD are hyposmia, REM (rapid eye movement) sleep behavior disorder (RBD), depressive or anxious mood alterations and constipation. In contrast to healthy individuals RBD patients do not lose muscle tone during REM sleep. This can lead to a vivid and potential harmful enactment of their dreams (Tekriwal et al. 2016). RBD can be idiopathic but patients with RBD may also develop PD or atypical parkinsonian disorders like Dementia with Lewy Bodies (DLB) or multiple system atrophy (MSA). For example, over 40 % of the patients suffering from RBD develop PD within four years and over 60 % within 10 – 30 years

(Postuma et al. 2012; Postuma et al. 2015a). Nevertheless, the sequence of symptoms and the speed of development is highly variable among the PD patients. A reliable identification of threatened individuals is difficult because symptoms like impaired smelling or constipation are very common in the elderly population (Salat et al. 2016). Despite intense research, there is no single reliable PD marker, neither in imaging, nor in cerebrospinal fluid (CSF)/serum or tissue available yet (Cooper and Chahine 2016). However, when combining several markers, recent studies show quite promising results for the future (Postuma and Berg 2016). Most recently, with the help of machine learning algorithms a study identified a discriminating cluster of six elements (Se, Fe, As, Ni, Mg, Sr) in CSF that might be used to distinguish between PD and age matched controls (Maass et al. 2018). This cluster of six was successfully validated in a new cohort at the local study centre, but failed in new cohorts from external centres, most likely due to centre effects (Maass et al. 2020). Therefore, further refinement seems to be necessary. In another recent pilot study the very first proteomic analysis of tear fluid was conducted. It revealed disease specific protein patterns, thereby suggesting potential biomarker candidates, but also needs further investigation (Boerger et al. 2019).

1.1.3 (Patho)physiology & pathology

PD has been identified to be a systemic disorder, as it affects the central nervous system (CNS) as well as the peripheral nervous system (PNS). The underlying pathology of alpha-synuclein aggregation has been intensively analyzed by Braak and colleagues in brain sections from PD patients. The authors developed a six-stage scheme for its classification and concluded that the pathology begins in the dorsal motor nucleus of the IX/X nerve and the anterior olfactory nucleus. From this origin the pathology likely ascends through the brain stem, progressing to the basal ganglia and other midbrain nuclei, finally reaching the neocortex (Braak et al. 2003). However, this spreading theory has been intensively discussed and doubted due to some uncertainties and contradictions (Burke et al. 2008; Salat et al. 2016). In one explanation attempt Engelender and Isaacson propose a threshold theory in which they connect pathologic features time-wise with the appearance of clinical symptoms. Thereby concluding that there is parallel degeneration in the PNS and CNS but a greater functional dopamine reserve in the midbrain, which might explain the emergency of early non motor symptoms (Engelender and Isacson 2017).

When trying to understand the emergence of PD motor symptoms, one aspect of high interest is the loss of nigral DAergic neuronal cell bodies and their striatal projections (Obeso et al. 2008): The SN and its main projection target, the striatum (consisting of the putamen and the nucleus caudatus), are part of the basal ganglia which also include the globus pallidus (with its pars externus (GPe) and internus (GPi)), the nucleus subthalamicus (STN) and the nucleus accumbens. The basal ganglia form a circuitry, which is upstream of the motor cortex and essential for the initiation of voluntary movements (Obeso et al. 2008). Normally the nigral DAergic neurons affect the striatal, inhibitory, GABAergic neurons via the D1-dopamine receptor on the one and via the D2-dopamine receptor on the other hand. An activation of the first one leads to an inhibition of inhibitory, GABAergic neurons in the GPi, which regularly inhibit glutamatergic thalamic neurons (direct pathway) (Smith et al. 1998). The resulting disinhibition of this highly spontaneously active neuronal population leads to an excitatory input to the motor cortex and consecutive motor activity. The activation of the second receptor supports this effect of movement initiation by reduction of signaling via the alternative, indirect pathway (Smith et al. 1998). In this pathway, striatal neurons inhibit GABAergic neurons in the GPe, which regularly inhibit the GABAergic neurons in the GPi and the glutamatergic neurons in the STN (Smith et al. 1998). Thus, by activating this pathway the GPi neurons are disinhibited and consequently suppress the activity of thalamic neurons, causing impairment of movements (Smith et al. 1998). In PD patients, the huge compensation capability of remaining dopamine neurons and synapses might conceal neuronal degeneration for years (Cheng et al. 2010). At a certain point, though, the remaining synapses are not numerous enough anymore, and the decreasing dopamine levels result in a disparity between the two pathways of the basal ganglia. The reduced stimulation of the direct pathway in the process is believed to be responsible for akinesia, bradykinesia, freezing episodes and postural instability, while the disinhibition of the indirect pathway with its overactive STN accounts for increased muscle tone, rigor and tremor (Smith et al. 1998). However, this is a simplified approximation as more and more details about the way dopamine depletion alters cellular excitability and synaptic transmission in and outside of the striatum are unraveled (Mallet et al. 2019).

Post-mortem and imaging studies were able to show that patients at the point of clinical disease onset (when motor symptoms are visible for the first time) usually had already lost 2/3 of nigrostriatal projections, but only 1/3 of corresponding perikarya in the SNpc, indicating that PD's pathology starts in the axons and consecutively leads to cell death

(Cheng et al. 2010; Kurowska et al. 2016; Balke et al. 2020). Therefore, it is assumed that axonal degeneration is takes part in the early phase of PD's pathogenesis (Lingor et al. 2012; Tagliaferro and Burke 2016). However, we only obtained little knowledge about the underlying mechanisms by now. It has been shown that neurotoxin-induced neuropathies but also neurodegenerative disorders are characterized by retrograde axonal degeneration, which starts at the axon terminals. Contrary to this, distal axonal compartments after acute injury show Wallerian (anterograde) degeneration (Tagliaferro and Burke 2016). Studies of acute axonal degeneration (AAD) in a model of an optic nerve crush lesion in rats revealed a massive increase of intracellular Ca^{2+} levels shortly after the injury (Lingor et al. 2012). Ca^{2+} levels could be linked to increased numbers of LC3 (microtubule-associated protein 1 light chain 3) positive vesicles, indicating Ca^{2+} dependent upregulation of autophagy, promoting the axonal degeneration (Knöferle et al. 2010). Findings of studies with the autophagy inhibitor 3-methyladenine (3-MA) in the same model (Koch et al. 2010), but also in models of spinal cord injury (Kerschensteiner et al. 2005; Ribas et al. 2015) and toxin models of PD (Lingor et al. 2012; Burke and O'Malley 2013) underline the important function of (macro)autophagy in axonal degeneration.

1.1.4 Etiology

In terms of disease etiology, a distinction between familiar and sporadic/idiopathic cases of PD can be made. In total, inherited, monogenetic variants of the disease only account for 5 to 10 % of the patients. Here autosomal mutations in *LRRK2* (encoding the leucine-rich repeat kinase 2, most frequent), *SNCA* (encoding alpha-synuclein) or *VPS35* (encoding vacuolar protein sorting ortholog 35) or autosomal recessive mutations in *PINK-1* (encoding the serine/threonine protein kinase PINK1), *PARK7* (encoding the protein/nucleic acid deglycase DJ-1), *Parkin* (encoding the E3 ubiquitin ligase Parkin) and others are found (Pan and Yue 2014; Lill 2016; Rosenbusch and Kortholt 2016). To date, 90 gene loci linked with enhanced risk for PD development have been discovered (Bandres-Ciga et al. 2020) and consideration of these genes' functions has been very helpful in understanding the sporadic cases of PD and underlying mechanisms, because they are sufficiently overlapping with those in familiar forms of PD (Dauer and Przedborski 2003; Dexter and Jenner 2013). While the exact causes for the occurrence of sporadic PD are still vague, these idiopathic cases are assumed to be the result of a

complex interplay between multiple environmental factors, like e.g. intoxication, drugs, head trauma, and genetics (Dexter and Jenner 2013).The currently discussed mechanisms leading to neuronal cell death are reactive oxygen species (ROS), mitochondrial dysfunction, disrupted proteolysis, neuroinflammation and excitotoxicity (Salat et al. 2016). Recently, most attention has been paid to altered protein metabolism and mitochondrial impairment as these are probably major factors promoting neurodegeneration.

1.1.4.1 Disrupted proteolysis

Lewy bodies and neurites, discovered by Friedrich Lewy in 1912, represent the pathological hallmark of PD (Holdorff 2002). These intracytoplasmic, insoluble aggregates are composed of neurofilaments, ubiquitin and several proteins, among them the presynaptic protein alpha-synuclein as the major constituent (Spillantini et al. 1997; Goedert et al. 2013). While the discussion on whether Lewy bodies are harmful or protective (Beyer et al. 2009; Eisbach and Outeiro 2013) is still ongoing, the effects of alpha-synuclein aggregation on autophagy (in terms of upregulation or impairment) are also still under debate (Pan and Yue 2014). On the one hand Lewy bodies are found in most PD patients, the only exception being the ones becoming diseased by intoxication or the ones carrying a *Parkin* mutation (Branco et al. 2010). On the other hand only a small portion of Lewy positive patients carries mutations or multiplications of *SNCA* (Ibáñez et al. 2004), which encodes alpha-synuclein and thereby is able to enhance alpha-synuclein production and aggregation. Therefore, it is assumed that a disrupted proteolysis must lead to its accumulation and aggregation (Dexter and Jenner 2013). Generally, there are two major players in protein degradation: The ubiquitin-proteasome system (UPS), which mainly dismantles smaller and transitory proteins, and the autophagosome-lysosome pathway (ALP), which is possibly of even higher importance when it comes to degradation of aggregation-prone proteins and damaged organelles (Banerjee et al. 2010). Both systems take part in the clearance of alpha-synuclein and their impairment causes increased alpha-synuclein levels within the cells (Webb et al. 2003). It is assumed that under normal conditions the breakdown of alpha-synuclein is conducted by the UPS, while the ALP is only recruited when the alpha-synuclein burden is rising (Ebrahimi-Fakhari et al. 2011).

Rott and colleagues postulated that the ubiquitination status of the alpha-synuclein is crucial for the way of its degradation: The deubiquitinated protein is mostly broken down

by the ALP, while the monoubiquitinated protein is degraded by the UPS (Rott et al. 2011). There is also genetic evidence for the importance of these pathways: Mutations in *Parkin* and *ULCH1* lead to alterations in the function of the UPS and cause familiar forms of PD (Branco et al. 2010). *Parkin* is encoding the ubiquitin E3 ligase, which catalyzes the ubiquitin transfer to a recruited substrate, and *ULCH1*, encoding the ubiquitin C-terminal hydrolase L1, is an enzyme which is responsible for deubiquitination and thereby maintains a progressive proteolysis by mono-ubiquitin recycling (Branco et al. 2010). On top of this, Parkin and ULCH1 are frequently found as components of Lewy bodies (Lowe et al. 1990; Schlossmacher et al. 2002), and by that are autophagy-related proteins (Tanji et al. 2011). The D620N mutation in *VPS35*, encoding the vacuolar protein sorting ortholog 35 which participates in the formation of the so-called retromer complex, has also been disclosed as a rare reason for late-onset PD (Singleton 2011; Goedert et al. 2013). Normally, this retromer complex mediates endosome to trans-Golgi retrieval of membrane proteins but in cells which express PD-mutant VPS35 an impairment of the autophagic process has been described (Zavodszky et al. 2014). This might be due to an abnormal trafficking of ATG9A (autophagy-related protein 9A), but further investigations are necessary.

1.1.4.2 Mitochondrial dysfunction

Evidence for mitochondrial impairment in PD patients was first found by Schapira and colleagues (Schapira et al. 1989) in terms of reduced complex I activity in postmortem analysis of the SN of diseased patients' brains. The incentive to investigate this was coming from the observation of PD symptoms in drug abusers who injected themselves with a 1-methyl-4-phenyl-1,2,3,6-tetrahydropyridine (MPTP) contaminated batch of the analgesic opioid 1-methyl-4-phenyl-4-propionoxypiperidine (MPPP) (Langston et al. 1983). MPTP occurs as a byproduct of MPPP-synthesis if the reaction temperature rises above a certain threshold during the production process. After MPTP had been identified as the possible cause for the Parkinsonian syndrome, its mechanism was thoroughly investigated in several animal studies (Kolata 1983; Heikkila et al. 1984). The mechanism of the MPTP toxin is well-known (Schober 2004) (see Figure 1): As a highly lipophilic agent MPTP easily moves across the blood-brain barrier after intravenous or intraperitoneal administration. Then this protoxin is converted to the intermediate 1-methyl-4-phenyl-2,3-dihydropyridium (MPDP) via monamine oxidase B (MAO-B) in astrocytes and MPDP consequently spontaneously oxidizes to the toxic 1-methyl-4-

phenylpyridinium ion (MPP^+) (Nicklas et al. 1987). While the mechanism by which MPP^+ is unleashed from the astrocytes remains unknown, it is predominately incorporated by DAergic neurons due to its high specificity for the dopamine transporter (DAT) (Javitch et al. 1985). Additionally, MPP^+ can be taken up by cells carrying noradrenaline and serotonin transporters. Within the dopaminergic neurons MPP^+ can be sequestered in vesicles after binding to vesicular monoamine transporter (VMAT), remain in the cytosol or accumulate within the mitochondria (Del Zompo et al. 1993). Here it exerts its toxic effect via binding itself to and inhibition of complex I of the respiratory chain (Mizuno et al. 1987).

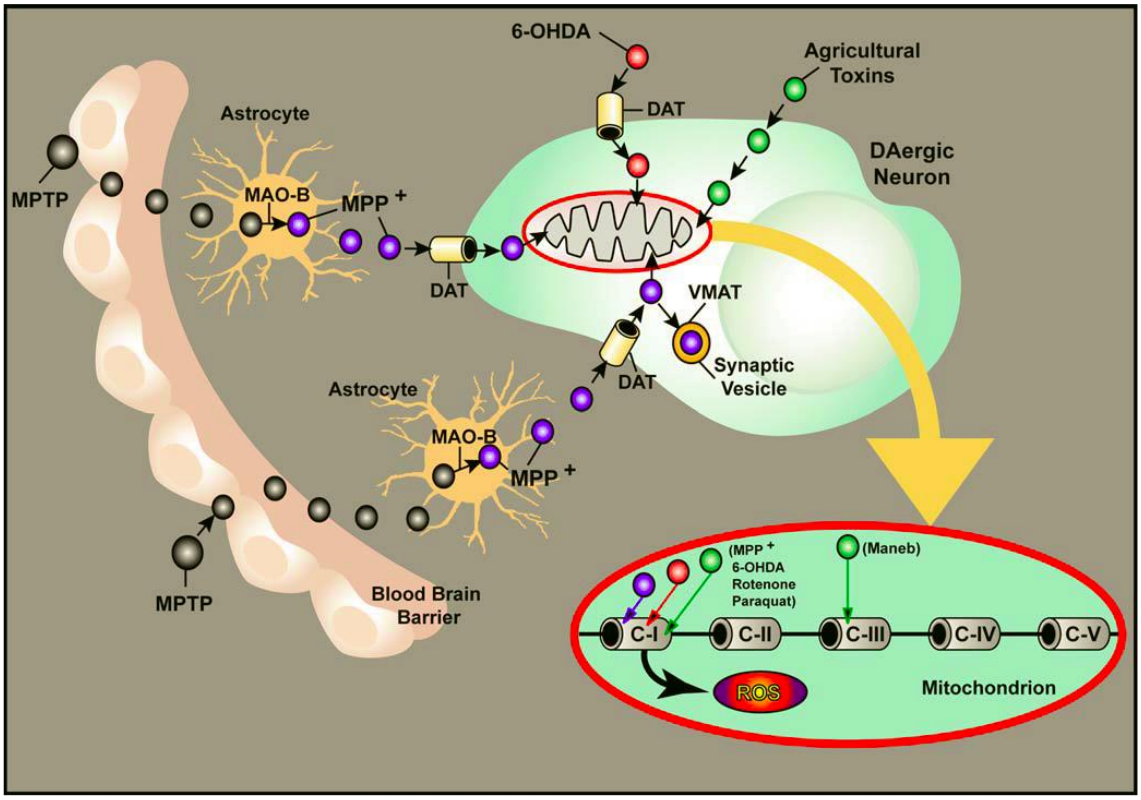

Figure 1 Metabolism of selected neurotoxins
After passage through the blood-brain barrier, the highly lipophilic MPTP is taken up by astrocytes. Resident Monoamine oxidase B leads to conversion of MPTP into the toxic metabolite MPP^+ with high affinity to the DAT, causing a predominant uptake in dopaminergic neurons. In the mitochondria of DAergic neurons MPP^+ binds itself to complex I, mediating oxidative stress and cellular toxicity. Modified from Schober (2004), reprinted by permission from Springer Nature. The figure is part of the licensed content title "Classic toxin-induced animal models of Parkinson's disease: 6-OHDA and MPTP", published by Andreas Schober in Cell and Tissue Research. https://link.springer.com/journal/441 © Springer Nature (2004)

Besides MPTP, there are other agents like paraquat, an herbicide with structural similarity to MPP^+, or rotenone, an insecticide, which are also used to model PD due to their effect

on mitochondrial respiratory function, and due to the hypothesis that they might contribute to the disease's development as environmental factors (Liou et al. 1997; Elbaz and Tranchant 2007). However, recent investigations were not able to reproduce a consistent relation in this context (Breckenridge et al. 2016). Therefore, until today, the MPTP model is the one which is most widely studied due to its clear link to human parkinsonism (Dauer and Przedborski 2003) and its specificity for dopaminergic structures (Schober 2004).

Generally, an impairment of complex I leads to a shortage of adenosine triphosphate (ATP) and increased oxidative stress (Andreyev et al. 2005). This subsequently favors damage of mitochondrial DNA (mtDNA) and enzymes and causes stronger malfunction and further ROS production (Lin and Beal 2006; Banerjee et al. 2009), enhancing a process that can finally lead to apoptosis and cell death.

Dopaminergic neurons are extraordinarily susceptible to this pathology due to their high energy demand due to strong axonal arborization and extraordinary long processes. Moreover, already the physiological dopamine metabolism leads to increased ROS production by autoxidation and H_2O_2 formation, which is scavenged also with the help of DJ-1, due to dopamine recycling (Sidhu et al. 2004).

Besides environmental agents, a complex I deficiency in PD patients' dopaminergic neurons might occur due to mutations in the mtDNA, which encodes at least 7 of the 45 subunits of complex I or mutations in the nuclear DNA as far as the affected gene is involved in mtDNA maintenance (Simon et al. 1999; Thyagarajan et al. 2000). Aging as the major risk factor for PD can also be linked to mitochondrial impairment: A continuously increasing burden of mtDNA errors, clonal expansion of mutant variants and depletion of functional mtDNA (Bender et al. 2006; Kraytsberg et al. 2006) are considered to drive single neurons to energetic failure and cell death. Even alpha-synuclein is proposed to impair mitochondrial function: It binds itself to the outer mitochondrial membrane, thereby impeding mitochondrial fusion and promoting excessive fission instead (Kamp et al. 2010; Nakamura et al. 2011).

1.1.5 Therapeutic strategies

1.1.5.1 Established therapies for PD

Despite intense research in the field of neurodegeneration and PD, there is no curative treatment available until now. Although it had entered the market almost 40 years ago, levodopa (L-DOPA) remains the most valuable therapeutic compound to correct falling dopamine levels and thereby diminish PD motor symptoms (Connolly and Lang 2014). Unfortunately, the effects of L-DOPA tend to decrease after a relatively stable period of some years, and the patients then have to deal with increasing motor fluctuations (Salat et al. 2016). Besides L-DOPA, a row of other pharmacological agents such as D2-receptor agonists, MAO-(B) inhibitors, COMT (Catechol-O-methyltransferase) inhibitors and anti-cholinergics have entered the market. These are either used in mild, early stages to preserve L-DOPA as a later measure, or they are used to complement the therapeutic regimen in advanced stages of the disease to reduce L-DOPA induced dyskinesia and tackle non-motor symptoms like dementia or depression (Huynh 2011). An additional measure in PD therapy is the surgical implantation of electrodes for deep brain stimulation into the STN or GPi in order to reduce dyskinesia, stiffness and tremor in patients that still show response to the pharmacological therapy but suffer from these side effects (Umemura et al. 2016).

1.1.5.2 Therapeutic perspectives

There are different requirements for possible therapeutic agents: Because about 2/3 of nigrostriatal projections are irretrievably lost when the clinical diagnosis of PD is made (Beach et al. 2008; Balke et al. 2020), it is necessary to prevent further neurodegeneration. A neuroprotective drug is also what would be needed if an early biomarker for PD came up, to prevent the disease's onset. It would be desirable to stimulate neuro-regeneration in order to reverse disease progression, but this might be even more difficult due to the limited regeneration capacities of adult neurons. They display only limited neurogenic potential, which is additionally impaired by inhibitory signaling of glial cells (Fitch and Silver 2008). There is even evidence that in animal PD models as well as in human PD, adult neurogenesis is impaired (Le Grand et al. 2015).

The development of a causal therapy for PD is inevitably linked to a better understanding of disease pathogenesis. Our knowledge about the underlying mechanisms has continuously increased according to the successive discovery of PD-linked mutations, as

described above. Various approaches are currently examined in preclinical and clinical studies:

Micro ribonucleic acids (miRNAs) are currently considered to have great therapeutic potential. They are possibly able to activate or inhibit a whole group of genes and thereby combine different pathways for disease modification. For example, it is reported that miR-7 provided protection to different MPP^+ treated cell lines via a downregulation of the NF-kB component RelA (Choi et al. 2014). Additionally, miR-7 was found to mediate anti-oxidative effects by augmentation of glutathione levels and decrease of hydroperoxide levels (Kabaria et al. 2015). A third effect of this miRNA is the reduction of alpha-synuclein toxicity by binding to its mRNA (Messenger RNA) and consecutive downregulation of protein levels (Junn et al. 2009; Doxakis 2010). Of course, potential therapeutic effects are not exclusive to this miRNA, as miRNAs can have several and also overlapping targets. For instance, our group could show protective effects of miR-182/miR-183 treatment in a cell culture as well as in a mouse model of MPP^+/MPTP treatment (Roser et al. 2018).

Another approach is the grafting of fetal neuronal cells, or embryonal or induced pluripotent stem cells, to PD patients. The transplantation of both mesencephalic implants in rhesus monkeys (Bankiewicz et al. 1990) and of neuronal stem cells into the SN of MPTP-treated mice have already been successfully performed (Li et al. 2003) decades ago, and there have been multiple further studies in animals and also some in humans (reviewed by Pardal and López-Barneo 2012). Nevertheless, treatment with induced pluripotent stem cells, as the latest and most promising therapeutic strategy due to the fact that they can be produced autologously and in sufficient quantities, has to be strongly improved in terms of reprogramming efficiency and safety of use before an application in human trials is imaginable (Pen and Jensen 2017).

The observation that the transplantation of neuronal tissue also enhanced an outgrowth of the remaining host dopaminergic neurons, shed a light on therapeutic potential of neurotrophic factors. Among them the glial cell line-derived neurotrophic factor (GDNF) had been identified to be the most powerful one in the context of PD (reviewed by Sullivan and Toulouse 2011). GDNF is strongly involved in the promotion of survival and differentiation of dopaminergic neurons (Lin et al. 1993), and both cell culture and animal studies were able to show significant protective effects by GDNF delivery to MPTP-intoxicated monkeys and mice (Kordower et al. 2000; Wu et al. 2002). However,

human trials with intrastriatal GDNF infusions led to contradictory results and were immediately stopped after antibody production in 1/10 patients (Tatarewicz et al. 2007) and unaccountable cerebellar pathology in a rhesus monkey trial occurred (Hovland et al. 2007). Application of GDNF still seems a promising approach, but due to the sustained safety concerns, current research focus has shifted to the pharmacological modulation of disease-relevant signaling pathways and the targets they offer such as enzymes, receptors, transport proteins, DNA/RNA (reviewed by Imming et al. 2006). One promising example is the inhibition of the Rho kinase pathway, which normally mediates the phosphorylation of myosin light chain kinase (Mills et al. 1998). In the CNS in particular, it diminishes axonal growth and inhibits axonal regeneration (Liu et al. 2015). Accordingly, Rho kinase inhibition in combination with ciliary neurotrophic factor treatment has been described to be an effective measure to improve the regeneration of retinal ganglion cells after an optic nerve crush via Mitogen-activated protein kinase (MAPK) and Akt (also known as protein kinase B) pathway activation (Lingor et al. 2007). Subsequent studies could show that the isoquinoline derivate fasudil as a Rho kinase inhibitor could exert neuroprotective effects in toxin-induced models of PD (Tönges et al. 2011; Tönges et. al. 2012; Tatenhorst et al. 2014), leading to significantly increased numbers of DAergic nigral neurons and enhanced motor behavior of treated animals in comparison to untreated ones.

Finally, the most recent approach of our group targets the important role of autophagy in axonal degeneration. The Adeno-associated virus (AAV)-mediated overexpression of the C-terminal ULK1 (Unc-51 like autophagy activating kinase 1) domain (acting as a dominant-negative ULK1) (Chan et al. 2009) was successfully employed in cortical neurons *in vitro*, leading to significantly reduced numbers of degeneration bulbs after axotomy. In subsequent *in vivo* studies, comprising spinal cord injury as well as optic nerve crush experiments, these findings were confirmed. The dominant-negative ULK1 expression led to a reduced number of LC3 puncta and significantly attenuated axonal degeneration (Vahsen et al. 2020). Furthermore, mitigation of AAD in the optic nerve could also be shown employing the small molecule inhibitor SBI-0206965 (Egan et al. 2015), by that emphasizing the translational potential of ULK1 inhibition for future studies and possible clinical utilization.

1.2 Autophagy

The name “Autophagy” was established by Christian de Duve in 1963 according to the greek term *autóphagos*, meaning self-devouring (de Duve 1963; Harnett et al. 2017). Autophagy is an indispensable, continuously proceeding homeostatic breakdown process within every cell. It is involved in various physiological processes, like e.g. protein turnover, cellular differentiation or cell death. Autophagy is especially crucial in situations of nutritional scarcity as it ensures lysosome-bound degradation of marred organelles, malfunctioning proteins and redundant cell ingredients in order to provide energy and substrate for new proteins (Banerjee et al. 2010). Therefore, those intracytoplasmic components are sequestered into autophagosomes. These autophagosomes merge with lysosomes to facilitate the breakdown of the engulfed material by lysosomal hydrolases (Klionsky 2008). However, a disturbance of the delicate, balanced autophagic degradation procedure can cause cellular malfunction and diseases (Nah et al. 2015). A resulting profuse aggregation of autophagosomes is considered as a possible trigger for cell death or as a last effort to ensure viability of the cell (Mizushima et al. 2008; Banerjee et al. 2010). Especially neurodegenerative disorders could be linked to autophagy impairment (Wong and Cuervo 2010). The discussion whether an increased autophagosome number reflects increased levels of autophagy or if autophagosomes accumulate in consequence of decreased autophagic degradation is still ongoing. It is also controversial if autophagy induction actively leads to cell death via activation of the known preserved pathways, or if it just occurs alongside the other processes (Banerjee et al. 2010).

1.2.1 Types of autophagy

Until today, over 30 autophagy-related genes (*ATG*) have been discovered (Bednarczyk et al. 2018). Moreover, different kinds of selective autophagy have been described, which are all participating in organelle and protein turnover (Komatsu and Ichimura 2010). The three distinguished types of autophagy are termed: (Macro)autophagy, microautophagy and chaperone-mediated autophagy (CMA) (Pasquier 2016).

CMA considerably differs from macro- and microautophagy because it only degrades soluble proteins (Banerjee et al. 2010). The heat shock cognate 70 (HSC70), a cytosolic chaperone, and its co-chaperones recognize their designated proteins due to a unique

pentapeptide sequence (KFERQ) (Banerjee et al. 2010). After attaching itself to the protein, the HSC70 targets the protein to the lysosome. The lysosome-associated membrane protein type 2A (LAMP 2A) functions as a CMA receptor, detects the protein and initiates its unfolding and translocation across the membrane of the lysosome (Banerjee et al. 2010; Kaushik and Cuervo 2012). In contrast to macro- and microautophgy, substrates are not engulfed but transferred to the lysosome individually. While induction of macroautophagy by nutrient deprivation is short dated, CMA occurs for prolonged periods (Pan et al. 2008).

Microautophagy is quite comparable to macroautophagy, which is described below. The difference is that in microautophagy, the lysosome approaches its target by pinocytosis. Thus, there is no need for autophagosome formation. Opposed to macroautophagy, microautophagic activity does not increase under conditions of nutrient deprivation or stress (Pan et al. 2008).

1.2.2 The course of (macro)autophagy

Macroautophagy is a multi-step process inevitable for all mammalian cells to maintain vitality and functionality. Macroautophagy occurs constitutively at a low level but is enhanced under stress conditions or nutrient deprivation (Yorimitsu and Klionsky 2005). Under these circumstances, intracellular material is degraded for energy production or new biosynthesis to ensure cellular survival. Under normal growing conditions, the main function of macroautophagy is the degradation of damaged and dispensable cytoplasmic organelles and compounds in order to maintain cellular homeostasis (Yang and Klionsky 2010a). Although autophagy has primarily cytoprotective properties, it can harm the cell and even cause cell death if it is exaggerated (Booth et al. 2014).

1.2.2.1 Sequence of the macroautophagic process

In yeast, the autophagic process starts with the initiation of phagophore formation at one place, the phagophore assembly side (PAS). In mammals there is not just one corresponding equivalent to the PAS (Chen and Klionsky 2011). Phagophore formation can be initiated at multiple locations throughout the cytoplasm. There is strong evidence that endoplasmic reticulum (ER) derived membranes which are referred to as omegasomes act as site for initiation of phagophore formation (Molino et al. 2017a; Zhang et al. 2018). However, it is assumed that also other organelles like mitochondria,

Golgi and endosomes contribute to the phagophore (Molino et al. 2017b). Finally, it is still unclear whether the phagophore develops in a "de novo" lipid transfer from the ER as a single donor or through fusion of multiple preexisting organelles (Molino et al. 2017b). As the membrane at the initiation site starts expanding, it is called phagophore. This double membrane is the primary sequestering compartment and expands further to finally generate a spherical autophagosome (see Figure 2). Depending on the specific cargo, the size of the autophagosome ranges from 0.5 to 1.5 µm in mammals (Mizushima 2007).

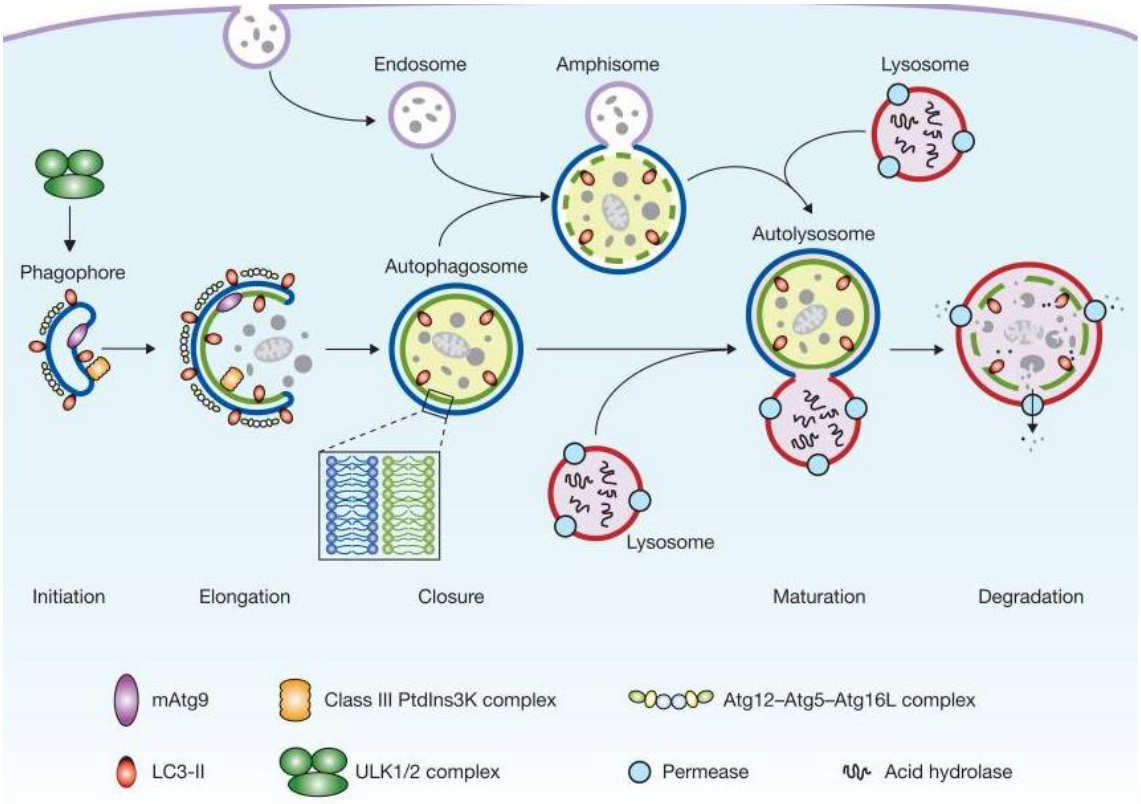

Figure 2 Sequence of the macroautophagic process
After induction through the ULK1/2 complex, the formation of the phagophore as initial sequestering vesicle takes place. Its elongation is aided by the class III PI3K (Phosphatidylinositol 3-kinase) complex, the ATG12-ATG5-ATG16L1 complex and ATG9. After maturation and closure of the autophagosome, LC3 is cleaved from the outer membrane, and the autophagosome undergoes fusion with the lysosome or with an endosome (forming an amphisome) before going into fusion with the lysosome, forming an autolysosome. Autoloysomal content is degraded by lysosomal enzymes and luminal acidity. Finally, break-down products are exported back into the cytoplasm. Modified from Yang and Klionsky (2010b), reprinted by permission from Springer Nature. The figure is part of the licensed content title "Eaten alive: a history of macroautophagy", published by Zhifen Yang et al. in Nature Cell Biology. https://www.nature.com/ncb/ © Springer Nature (2010)

To deliver its cargo, the autophagosome undergoes fusion with a lysosome, then being called an autolysosome. There is often a junction to the endocytic pathway, where the autophagosome merges with an endosome, forming a so called amphisome, which afterwards undergoes fusion with a lysosome to become an autolysosome (Parzych and Klionsky 2014). Resident hydrolases in the autolysosome and the acidic lumen lead to the decomposition of the former inner autophagosomal membrane and subsequently of its engulfed content. Afterwards, lysosomal permeases transfer the degradation products into the cytoplasm where they are used for biosynthesis or energy production (Yang and Klionsky 2010b).

1.2.2.2 The mammalian ULK1 complex

Unc-51 like autophagy activating kinase 1 (ULK1) is a serine/threonine protein kinase and it represents the mammalian orthologue of the Atg1 found in yeast (Zachari and Ganley 2017). Currently five ULK1 homologues are known the most important ones for autophagy initiation being ULK1 and ULK2 (Zachari and Ganley 2017). These two kinases share 52 % of their protein sequence and have a 78 % identical kinase domain which leads to similar interactions and causes a certain agonistic redundancy (Zachari and Ganley 2017). While just the loss of ULK1 reduces autophagic activity below a vital treshold in most cell lines (e.g. HEK293), in mice ULK1 and ULK2 need to be knocked out to reach a severe and deadly impairment of autophagy comparable to a knock-out of other core genes like *ATG5* (Chan et al. 2007; Lee and Tournier 2011). Yet no explanation for the ULK homologues and their redundancy exists (Zachari and Ganley 2017). However, the integrity and functionality of the kinase domain is crucial for successful initiation of the autophagic process. Kinase-inactivated ULK1 and also kinase inhibitors lead to a significant impairment of autophagy (Chan et al. 2009; Egan et al. 2015).

Autophagy induction is not signaled by ULK1 alone, but ULK1 acts as tetrameric initiation complex together with three other proteins: ATG13, FAK family kinase interacting protein of 200 kilodaltons (kDa) (FIP200) and ATG101 (Noda and Mizushima 2016). Under normal, homeostatic conditions, the exact location of ULK1 remains unclear by now. Upon amino acid starvation, which is the most precise characterized trigger for assembling of the ULK1 complex, ULK1 forms punctate structures close to the ER, where it colocalizes with omegasomes when Phosphatidylinositol 3-phosphate (PI3P) is present. Less frequently, ULK1 is found close to mitochondria (Karanasios et al. 2016).

1.2.2.3 Regulation of ULK1 activity

If amino acids are present, the serine/threonine kinase mammalian target of rapamycin (mTOR) usually associates with the ULK1 complex and inhibits autophagy by phosphorylation of ULK1 and ATG13 at multiple sites (Ganley et al. 2009). However, opposed to the modulation by mTOR activity, the ULK1 complex assembly itself is not nutrient dependent, ensuring an enduring, homeostatic autophagy process also under nutrient rich conditions. Under conditions of amino acid starvation, mTOR loses its inhibitory influence on the ULK1 complex, as its phosphorylation e.g. at Ser^{637} is no longer retained. So, ULK1 is activated and able to initiate autophagy (Rabanal-Ruiz et al. 2017). While mTOR negatively regulates ULK1 activity, AMP activated protein kinase (AMPK), another influential preceding regulator, induces ULK1 activity by phosphorylation at different sites (Lee et al. 2010). Furthermore, ULK1 activity is also increased by acetylation (Lin et al. 2012).

1.2.2.4 ULK1 inhibitors

Due to autophagy's involvement in various pathophysiological processes, modulation of autophagy is considered an attractive therapeutic and drug development target (Pasquier 2016). Thereby, inhibition of autophagy can take place at different levels: PI3K-inhibitors, like 3-MA, and ULK1 inhibitors block initial steps of the autophagy cascade, while lysosome inhibitors block the late stage (Pasquier 2016). Especially ULK1 represents an attractive drug target as it is the only serine/threonine kinase in the initial steps of the autophagy cascade (Egan et al. 2015; Ouyang et al. 2018). Therefore, its activity can be easily modulated by direct phosphorylation (Kim et al. 2011). Over the last years several ULK1 inhibitors like SBI-0206965, MRT67307 or ULK1-100 have been developed and successfully tested in the cell culture setup (Egan et al. 2015; Petherick et al. 2015; Martin et al. 2018). The SBI-0206965 for example is derived from a focal adhesion kinase (FAK), which showed great cross-reactivity towards ULK1/ ULK2. The inhibitor is highly selective for its kinase as it only inhibited 10 out of 456 tested kinases when applied in optimized dose. This selectivity is comparable to the one of kinase inhibitors like Imatinib, which is used for the treatment of chronic myeloid leukemia. (Egan et al. 2015). The more recently developed ULK1 inhibitors ULK-100/101 seem to be even more potent and selective (Martin et al. 2018). However, there are no *in vivo* studies utilizing these inhibitors published yet. The compound SBI-0206965 has already been used in an *in vivo* study (Vahsen et al. 2020): A rat optic nerve

crush experiment was performed to induce AAD and intravitreal SBI-0206965 injection attenuated the axonal damage (quantified as axon integritiy ratio)via autophagy inhibition, which was shown by an decreased number of LC3-positive punctae and increased p62-positive punctae distal to the lesion (Vahsen et al. 2020).

Besides the application of small molecule inhibitors, a dominant-negative variant of ULK1 (ULK1.DN) may be administered to suppress autophagic activity. ULK1.DN expresses only the C-terminal domain of ULK1 and therefore lacks the kinase domain and function as well as the most phosphorylation sites (see Figure 6) (Chan et al. 2009; Balke et al. 2020). The dominant-negative effect probably is the consequence of decreased kinase activity and a, due to the absence of large parts of the original molecule, exhibited C-terminal domain, which then engages in unconstrained interactions with other core components of the autophagic cascade, thereby hampering the autophagy flux (Chan et al. 2009). A possible way to implement ULK1.DN expression in target cells is the utilization of an AAV vector carrying DNA for ULK1.DN expression (see chapter 1.3 for more details). Another possibility of ULK1 inhibition is the use of small interfering RNAs (siRNAs) or short hairpin RNAs (shRNAs), which were successfully employed to knockout ULK1 by degradation of its mRNA (Corona Velazquez et al. 2018).

1.2.2.5 Autophagy induction

With regard to Kaur und Debnath (2015, Figure 3) the process of autophagosome formation comprises three stages: initiation, nucleation and expansion. As already mentioned, the process starts at the PAS with the assembly of the ULK1 complex consisting of ULK1, ATG13, FIP200 and ATG101, which directly binds to ATG13.

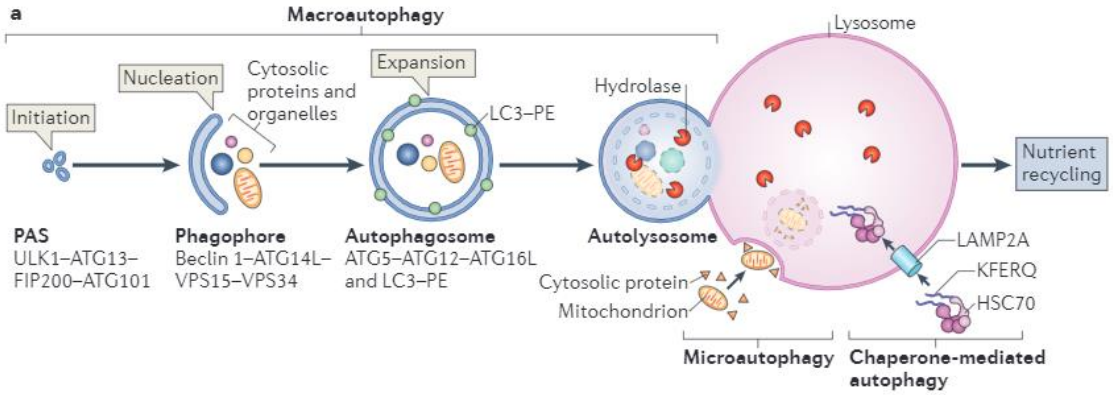

Figure 3 Overview of mammalian autophagy pathways and initial steps in macroautophagy

The initiation complex, which is necessary to recruit a membrane for phagophore formation, is formed of ULK1, ATG13, FIP200 and ATG101. The nucleation of the forming phagophore is promoted by the class III PI3K complex consisting of Beclin1, ATG14, VPS15 and VPS34. The ATG5-ATG12-ATG16L1 complex aids further expansion of the membrane as it binds itself to the growing phagophore membrane and mediates the covalent linking of LC3 with PE. See text below for more details. Modified from Kaur and Debnath (2015), reprinted by permission from Springer Nature. The figure is part of the licensed content title "Autophagy at the crossroads of catabolism and anabolism", published by Jasvinder Kaur and Jayanta Debnath in Nature Reviews Molecular Cell Biology. https://www.nature.com/nrm/ © Springer Nature (2015)

In the following nucleation stage, the recruited complex is the class III PI3K complex which is necessary to promote the production of PI3P that is specific to the autophagosomes (Nascimbeni et al. 2017). This complex comprises Beclin 1, vacuolar protein sorting 15 (VPS15), VPS 34 and ATG14. The regulation of this complex is mainly exerted by proteins which interact with Beclin 1. ULK1 induces autophagy by phosphorylation of Ser^{30} in association with ATG14 (Park et al. 2018). The antiapoptotic protein B cell-lyomphoma 2 (BCL2) exerts inhibitory influence on autophagy when it binds to Beclin 1, while Activating Molecule In Beclin-1-Regulated Autophagy (AMBRA1) and SH3 Domain Containing GRB2 Like, Endophilin B1 (SH3GLB1) are positive regulators of Beclin 1 (Pattingre et al. 2005; Fimia et al. 2007; Takahashi et al. 2007).

In the expansion stage, the ATG12-ATG5-ATG16 complex binds to the membrane of the growing autophagosome and promotes its elongation (Tanida 2011). Initially ATG12, a ubiquitin-like protein, is activated by ATG7 and ATG10 (ubiquitin-activating enzymes) before the covalent conjugate with ATG5 is finally formed (Kim et al. 1999). This last step differs from ubiquitination in so far as the binding is irreversible and no E3-ligase is required (Geng and Klionsky 2008). The mammalian orthologue of Atg16 in yeast, ATG16L1, then associates non-covalently to the ATG12-ATG5-conjugate in order to form a functional compound (Kuma et al. 2002). This functional ATG12-ATG5-ATG16 complex attaches to the membrane of the phagophore, probably acting as an E3-ligase which mediates the conjugation of Atg8 with phosphatidylethanolamine (PE) (Kirisako et al. 1999). To enable the lipidation, the protease ATG4 detaches designated arginine residues of ATG8. ATG7 activates the glycine residue, which is then exposed, and ATG3 acts as an E2-like enzyme before ATG12-5-16L1 mediates the covalent binding to PE (Ichimura et al. 2000). There are three subtypes of ATG8 in mammals: microtubule-associated protein 1 light chain 3 (LC3), Gamma amino-butyric acid receptor-associated protein (GABARAP) and Golgi-associated ATPase enhancer of 16 kDa (GATE-16), which may act on different steps of membrane expansion and final closure of the phagophore (Weidberg et al. 2011). While GABARAP and GATE-16 are crucial for late stage autophagosome maturation, LC3 is important for the elongation of the phagophore membrane (Weidberg et al. 2010). Usually, LC3-I describes the form of ATG8 after it has been processed by ATG4, while LC3-II defines the PE-conjugated form which is membrane-bound but can be released by a second ATG4 cleavage (Kirisako et al. 2000; Geng and Klionsky 2008). In a nutritious environment, LC3 is distributed in cytoplasm and nucleus in an acetylated form. If starvation is induced, a deacetylation leads to a redistribution of nuclear LC3 into the cytoplasm and it is able to interact with ATG7 (Huang and Liu 2015).

The process of autophagosome closure is still poorly understood. However, there is evidence for involvement of soluble N-ethylmaleimide-sensitive-factor attachment receptor (SNARE) proteins and a regulatory influence of ATG2A and ATG2B (Moreau et al. 2011). These proteins seem to have a crucial relevance for successful autophagosome fusion because a knock out leads to accumulation of unclosed autophagosomes (Velikkakath et al. 2012; Pfisterer et al. 2014).

1.3 Adeno-associated virus (AAV) and its role as gene delivery vector

1.3.1 Biology of AAV

AAVs belong to the family of parvoviruses and have a single stranded deoxyribonucleic acid (DNA) of roughly 4.7 kilobase pairs length. The genomic structure consists of two open reading frames (ORF) between two inverted terminal repeats (ITR) (Srivastava et al. 1983). The first ORF (*Rep*) is needed for viral replication and encrypts four proteins. The other ORF (*Cap*) encrypts the three viral capsid proteins (VP1-3) which originate from only one mRNA and are processed via alternative splicing (Berns and Linden 1995). To form the capsid, 60 of these structure proteins self-assemble. In the following, viral genome loads into it. Therefore, *Cap* plays a major role for virus transduction properties. When constructing an AAV transfer plasmid, these properties are exploited: *Rep* and *Cap* are cut out and the transgene is placed between the two ITRs there instead. *Rep* and *Cap* are supplied *in trans* to support the package of the transgene (Grieger et al. 2006; Kwon and Schaffer 2008). Twelve human serotypes of AAV have been identified by now, AAV2 being the one best characterized and most commonly used (Daya and Berns 2008). These serotypes differ in their tropism and preferentially infected cell types. For example, CNS is transduced optimally by AAV1,2,4,5,8 or 9. Tropism of the AAV can be refined further by pseudotyping which means the combination of the genome and capsid of different serotypes. AAV1/2 for example contains the genome of AAV1 packed with the capsid of AAV2 (Auricchio et al. 2001). Furthermore, it is possible to employ cell-specific promotors to increase the transduction efficiency of a certain cell population.

1.3.2 Viral integration and gene delivery

Initially in AAV infection a binding to the cellular membrane of the host is required. It is followed by uptake via endocytosis. This step is particularly important for virus tropism and transduction efficiency. AAV2 exploits superficial heparan sulfate proteoglycan as primary receptor to initiate the uptake into the host cell (Summerford and Samulski 1998). Intracellularly, one part of the viral vector remains in the cytoplasm, another part is translocated into the nucleus, where the uncoating of the virus takes place. Then the viral single-stranded DNA is converted into double-stranded DNA and integrated into the host cells genome. Eventually, it comes to the viral gene expression (Bartlett et al. 2000). Due to the fact that AAV is inherently a defective virus, it needs support of a helper virus to

successfully replicate after arriving at the nucleus (Weindler and Heilbronn 1991). In the absence of an adenovirus or herpes simplex virus, the AAV DNA can only integrate in the chromosomal genome of its target and cause a latent infection. Consequently, for AAV production, which is most commonly conducted in HEK cells, a helper virus or its protein is required. However, for research/therapeutic approaches *Rep/Cap* and the helper virus proteins may be combined into a single plasmid to facilitate the process (Kotin et al. 1990).

1.3.3 Clinical implications

AAV is a well characterized and very promising medium for gene therapy (Choi et al. 2006). Thus, it is not the wild-type but a recombinant variant (rAAV) that is utilized for gene therapy (Naso et al. 2017). The rAAV is free of viral DNA. The therapeutic transgenes incorporated within the rAAV are able to generate circular DNA strands that persist as so-called episomes in the nucleus of transduced cells but are not incorporated into the chromosomal genome (Choi et al. 2006). Because of its early discovery and well-known properties, AAV2 was the model for most of rAAV vectors used nowadays. The rAAV vectors employ the AAV2 ITRs and in between they likely carry a target compatible promoter, the gene/s of choice and a termination signal (Naso et al. 2017). A difficulty in utilization of AAVs is the pre-existing immunity. In various studies animals that have been pre-exposed to AAV were significantly less susceptible for AAV-mediated gene therapy because of production of neutralizing antibodies. Investigation in human collectives also revealed the presence of these AAV neutralizing antibodies in 20-60 % of the cases (Kwon and Schaffer 2008). Furthermore, capsid-specific T-cells targeting AAV-expressing cells can limit the duration of gene expression (Masat et al. 2013). Currently patients with detectable AAV neutralizing antibodies are excluded from clinical trials and there is a strong need to make gene therapy available for these seropositive patients. In the past plasmapheresis and transient immunosuppression with rituximab have been tested to reduce antibody levels. However, their effect was only modest in patients with high titer levels (Masat et al. 2013). A more promising alternative may be the use of AAV capsids isolated from other vertebetrates, as they have a lower likelyhood of pre-excisting immunity (Wang et al. 2019). Especially, some porcine AAVs showed promising results: In mice they easily crossed the blood-brain barrier and were not neutralized by human immunoglobulin G (Wang et al. 2019).

Depending on which pathology or organ one wants to address, there are different possible ways of AAV administration. Even considering only CNS diseases, a variety of delivery strategies has been developed. Initially, the gene delivery relied on intraparenchymal injections directly into the disease-affected area(s) of the brain, which is an approved and straightforward concept e.g. for PD. But even for disorders affecting larger areas of the brain like lysosomal storage disease (LSD), several animal studies and also clinical trials provided proof of efficiency and excellent safety of the method (Hocquemiller et al. 2016). Another way to address the CNS are lumbar/cisternal intrathecal or intracerebroventricular injections. Possible disadvantages are a requirement of higher quantities of the vector as well as leakage into the vascular system with off-target tissue expression, particularly in the liver (Gray et al. 2013; Meyer et al. 2015). The latest approach is the intravenous administration of AAV9 and AAVrh.10 which cross the blood-brain barrier in an unimpeded manner but do not reach the same transduction rate as the previously described methods (Zhang et al. 2011). Moreover, while AAV9 provides a suitable neuronal transduction efficacy in neonatal mice, it shifts to transduction of glial cells when administered to primates (Gray et al. 2011).

The current AAV-based treatment approaches in PD can be divided into two strategies (Choudhury et al. 2017): 1) the overexpression of enzymes involved in neurotransmitter synthesis in order to decelerate transmitter loss, and 2) the overexpression of neurotrophic factors in order to promote neuronal survival. There was a trial with injections of glutamic acid decarboxylase (GAD) encoding AAV2 into the STN to restore levels of the inhibitory transmitter gamma amino-butyric acid (GABA), or another trial focusing on infusion of aromatic L-amino acid decarboxylase (AADC) encoding AAV into the putamen, as well as a third trial using a lentiviral vector encoding TH, AADC and GTP cyclohydrolase 1 (GCH1) (Kaplitt et al. 2007; Christine et al. 2009; Palfi et al. 2014). All these therapeutic regimes were well tolerated and considered safe in phase I clinical trials but had only modest effects which declined over time (Mittermeyer et al. 2012). They may be less effective due to their symptomatic approach and the continuing neuronal loss. However, they argue for AAV vectors as safe and effective tools to be used in patients.

1.4 Aims of this thesis

This thesis aims to examine the therapeutic effects of AAV-mediated gene transfer inhibiting the key autophagic protein ULK1 in an MPTP mouse model of PD.

The MPTP primate model is the gold standard in animal models of PD (Jenner 2003, Masilamoni and Smith 2018). Although mice do not develop real parkinsonism like primates, they are widely used to unravel the underlying mechanisms of neuronal dopaminergic demise (Zhang et al. 2017). ULK1 was chosen as a target for autophagy inhibition because it is a key kinase regulating initial steps of the autophagy cascade (Noda and Mizushima 2016). Furthermore, ULK1 knockdown via siRNA expression proved to improve axonal regeneration of DAergic neurons after scratch lesion (Loh et al. 2008). AAVs are a safe tool for gene transfer because the gene of interest remains episomal (Choi et al. 2006). Furthermore, AAV-mediated ULK1.DN expression already succeeded in previous cell culture experiments (Vahsen et al. 2020).

The following questions should be answered:

1) Does inhibition of autophagy by expression of ULK1.DN attenuate degeneration of dopaminergic neurons and their axons induced by MPTP application?

2) Is inhibition of autophagy by expression of ULK1.DN able to enhance neuronal and axonal regeneration after MPTP treatment?

3) Does ULK1.DN gene expression affect the animals' motor behavior?

4) Which molecular players are regulated by the expression of ULK1.DN gene product?

2 Material & methods

2.1 Material

2.1.1 Chemicals

Table 1 Chemicals

Chemical	**Supplier**
0.9 % Saline	Braun (Melsungen, Germany)
APS	Sigma Aldrich (Taufkirchen, Germany)
B27 supplement	Gibco (Karlsruhe, Germany)
Bepanthen eye ointment	Braun (Melsungen, Germany)
Bromphenol blue	Sigma Aldrich (Taufkirchen, Germany)
BSA	Applichem (Darmstadt, Germany)
Citric acid	Roth (Karlsruhe, Germany)
DAPI	Sigma Aldrich (Taufkirchen, Germany)
Dermabond Topical skin adhesive	Ethicon (Norderstedt, Germany)
EDTA	Applichem (Darmstadt, Germany)
Entellan	Merck Millipore (Darmstadt, Germany)
Ethanol	Applichem (Darmstadt, Germany)
Glycerol	Roth (Karlsruhe, Germany)
Glycine	Applichem (Darmstadt, Germany)
HEPES	Applichem (Darmstadt, Germany)
HPLC water	Merck (Darmstadt, Germany)
Ketamine	Medistar (Ascheberg, Germany)
Laminin	Sigma Aldrich (Taufkirchen, Germany)
Methanol	Applichem (Darmstadt, Germany)
Mineral oil	Sigma Aldrich (Taufkirchen, Germany)
Mowiol	Sigma Aldrich (Taufkirchen, Germany)
MPTP (1-Methyl-4-phenyl-1,2,3,6-tetrahydropyridin)	Sigma Aldrich (Taufkirchen, Germany)
NaN_3 (sodium acid)	Sigma Aldrich (Taufkirchen, Germany)
NGS	Biochrom; PAA (Berlin; Pasching, Germany)

Chemical	Supplier
NHS	Biochrom; PAA (Berlin; Pasching, Germany)
Non-fat dried milk	Applichem (Darmstadt, Germany)
Octane sulphonic acid solution	Fluka (Seelze, Germany)
p-cumaric acid	Applichem (Darmstadt, Germany)
PFA	Applichem (Darmstadt, Germany)
PBS	Applichem (Darmstadt, Germany)
Roti-Histol	Roth (Karlsruhe, Germany)
SDS	Applichem (Darmstadt, Germany)
Sodium acetate	Roth (Karlsruhe, Germany)
Sterofundin	Braun (Melsungen, Germany)
Sucrose	Applichem (Darmstadt, Germany)
Sudan black	Applichem (Darmstadt, Germany)
TEMED	Roth (Karlsruhe, Germany)
Thionine acetate	Sigma Aldrich (Taufkirchen, Germany)
Tris	Applichem (Darmstadt, Germany)
TritonX 100	Applichem (Darmstadt, Germany)
Xylazine	Ecuphar (Greifswald, Germany)
Xylene	Sigma Aldrich (Taufkirchen, Germany)

2.1.2 Buffers & solutions

Table 2 Composition of buffers and solutions

Buffer/Solution	Composition
Blocking solution for IHC	10 % NHS, 5 % BSA (IgG free), 0.3 % TritonX, 25 mM glycine in PBS
Citrate buffer (100 ml)	10 mM citric acid (monohydrate 0.21 g) in H_2O, pH-value of 6.0 adjusted with 1N NaOH, 0.05 % Tween 20
DAPI solution	1 µg/ml DAPI in PBS
ECL component 1	10 µl/ml 250 mM luminol, 4.4 µl/ml 90 mM p-cumaric acid, 100 µl/ml 1M Tris pH 8.5 in distilled H_2O

Buffer/Solution	**Composition**
ECL component 2	0.9 µl/ml 30 % H_2O_2, 100 µl 1M Tris pH 8.5 in distilled H_2O
Electrophoresis buffer	192 mM glycine, 0.1 % SDS, 25 mM Tris-HCl, pH 8.3
HPLC buffer	6.973 g/l $NaO_2C_2H_3$, 7.365 g/l $C_6H_8O_7$ * H_2O, 0.105 g/l sodium octosulfonic acid, 0.048 g EDTA. pH adjusted to 4.3 using 1 M $C_6H_8O_7$, 105 ml/l CH_4O in 800 ml HPLC
Laemmli buffer	312.5 mM Tris pH 6.8, 10 % SDS, 50 % Glycerin, 0.005 % Bromphenolblau, 100 µM DTT
Mowiol	6 g glycerol, 2.4 g Mowiol, 6 ml H_2O, 12 ml Tris pH 7.2
PBS	9.5 mg/ml PBS in distilled water
PBS-T	0.1 % TritonX 100 in PBS
PFA (4 %) solution	40 mg/ml PFA, 9.5 mg/ml PBS, 1-3 pellets NaOH in distilled water
RIPA buffer	10 mM Hepes, 142 mM KCl, 5 mM $MgCl_2$, 1 mM EGTA and 1 % IGEPAL including complete proteasome inhibitor and phosphatase inhibitor
Running phase gel (10 %)	2.83 ml 30 % acrylamide bisacryl, 2.125 ml 4 x Tris pH 8.8, 3.54 ml distilled water, 4.25 µl TEMED, 42.5 µl 10 % APS
Stacking phase gel	0.65 ml 30 % acrylamid bisacryl, 1.25 ml 4 x Tris pH 6.8, 3.05 ml distilled water, 5 µl TEMED, 25 µl 10 % APS
Sudan black	0.3 g per 100 ml 70 % EtOH
TBS	10 mM Tris HCl, 150 mM NaCl in distilled water

Buffer/Solution	Composition
TBS-T	0.1 % Tween20 in TBS, pH 7.6
Transfer buffer	192 mM glycine, 20 % methanol, 25 mM Tris HCl, pH 8.3
Tris	10 mM Tris-buffered saline pH 8.0

2.1.3 Antibodies

Table 3 Primary antibodies

Origin	Antibody	Clonality	Supplier
Rabbit	Anti-AMPK	monoclonal	Cell Signaling Technology (Danvers, USA)
Rabbit	Anti-phosphorylated-AMPK	monoclonal	Cell Signaling Technology (Danvers, USA)
Rabbit	Anti-Atg1/ULK1	polyclonal	Sigma Aldrich (Taufkirchen, Germany)
Mouse	Anti-ß-Actin	monoclonal	Sigma Aldrich (Taufkirchen, Germany)
Rabbit	Anti-ERK1/2	polyclonal	Cell Signaling Technology (Danvers, USA)
Mouse	Anti-phosporylated-ERK1/2	monoclonal	Cell Signaling Technology (Danvers, USA)
Mouse	Anti-GAPDH	polyclonal	HyTest (Tuku, Finland)
Mouse	Anti-LC3-I/II	monoclonal	nanoTools (Teningen, Germany)
Rabbit	Anti-mTOR	polyclonal	Millipore (Burlington, USA)
Rabbit	Anti-phosphorylated-mTOR	polyclonal	Cell Signaling Technology (Danvers, USA)
Rabbit	Anti-p62	polyclonal	Sigma Aldrich (Taufkirchen, Germany)

Origin	Antibody	Clonality	Supplier
Rabbit	Anti-phosphorylated-S6	polyclonal	Cell Signaling Technology (Danvers, USA)
Mouse	Anti-ß-Tubulin	monoclonal	Millipore (Burlington, USA)
Rabbit	Anti-Tyrosin hydroxylase	polyclonal	Zytomed (Berlin, Germany)

Table 4 Secondary antibodies

Origin	Target	Labelling	Supplier
Donkey	Anti-mouse	Alexa Fluor 488	Dianova (Hamburg, Germany)
Goat	Anti-rabbit	Alexa Fluor 488	Dianova (Hamburg, Germany)
Goat	Anti-rabbit	biotinylated	Dianova (Hamburg, Germany)
Goat	Anti-mouse	Horseradish peroxidase	Cell Signaling Technology (Danvers, USA)
Goat	Anti-rabbit	Horseradish peroxidase	Cell Signaling Technology (Danvers, USA)

2.1.4 Kits

Table 5 Kits

Kit	Supplier
Peroxidase Substrate Kit DAB SK-4100	Vector Laboratories (Burlingame, USA)
Vectastain ABC Kit PK-6100	Vector Laboratories (Burlingame, USA)

2.1.5 Plasmids of AAV1/2 vector

The used AAVs both express mCherry under a Synapsin promoter for visual detection. The first AAV (AAV.ULK1.DN) additionally expresses the C-terminal domain of ULK1 (Chan et a. 2009; Balke et al. 2020). This domain is non-functional, by that being unable to induce autophagy. The overexpression of ULK1.DN therefore leads to competitive inhibition of the endogenous ULK1 (Chan et al. 2009). The second AAV is used as control (AAV.CTRL) and expresses a non-sense protein derived from pig.

Table 6 Plasmids

Plasmid	**Supplier**
p.AAV-hSyn-mCherry-hSyn-ULK1-CTD-WPRE	Kindly provided by Prof. Uwe Michel, University of Göttingen, Germany
p.AAV-hSyn-mCherry-hSyn-9(5)	Kindly provided by Prof. Uwe Michel, University of Göttingen, Germany

2.1.6 Equipment

Table 7 Equipment

Equipment	**Supplier**
Axioplan microscope	Carl Zeiss Microimaging (Oberkochen, Germany)
Bead mill homogenizer, Precellys 24	Peqlab (Erlangen, Germany)
Camera Legria HFM36	Canon (Krefeld, Germany)
Capillary puller	P-97, Sutter Instruments (Novato, CA, USA)
Catwalk XT gait analysis system	Noldus (Wageningen, the Netherlands)
Ceramin beads, 1.4 mm	Peqlab (Erlangen, Germany)
Coulochem II electrochemical detector	ESA (Bedfort, USA)
Cover slips 24 x 55 mm	Menzel (Braunschweig, Germany)
Cryomatrix (Shandon)	Thermo Scientific (Bremen, Germany)

Equipment	Supplier
Cryostat CM 3050S	Leica Microsystems (Mannheim, Germany)
Drying Oven	Thermo Scientific (Bremen, Germany)
Electrophoresis chamber	BioRad (München, Germany)
Electrophoresis power supply	BioRad (München, Germany)
Forceps	Fine Science Tools (Heidelberg, Germany)
Gilson pipettes	Gilson (Villiers de belle, France)
Glass capillaries	World Precision Instruments (Berlin, Germany)
Heracell 150i CO_2 incubator	Thermo Scientific (Bremen, Germany)
Ice machine	Scotman (Pogliano Milanese, Italy)
IVC animal cages	Tecniplast (Hohenpeißenberg, Germany)
Micro-centrifuge 5415R	Eppendorf (Hamburg, Germany)
Micro Injector Nanoliter 2000 Pump Head	World Precision Instruments (Berlin, Germany)
Microtome blades	Feather Safety Razor Co. (Seki, Japan)
Mini drill with 0.8 mm drill head	Proxxon NG2/S (Niersbach, Germany)
Mouse head holder	World Precision Instruments (Berlin, Germany)
MR 3000 Shaker	Heidolph (Schwabach, Germany)
Nitrocellulose transfer membrane	Applichem (Darmstadt, Germany)
Parafilm sealing film	Starlab International GmbH (Hamburg, Germany)
Peristaltic perfusion pump	Idex (Wertheim, Germany)
Petri dish	Sarstedt (Nümbrecht, Germany)

Equipment	Supplier
pH Meter	Sartorius (Göttingen, Germany)
Protein ladder	BioRad (München, Germany)
PVDF mebrane	Applichem (Darmstadt, Germany)
Rotarod for mice 47600	Ugo Basile (Comerio, Italy)
Scalpel, size 10	Bard-Parker (Singen, Germany)
Scissors	Fine Science Tools (Heidelberg, Germany)
Spacer plates/short plates	Biorad (München, Germany)
Stereotactic frame	David Kopf Instruments (Tujunga, CA, USA)
Super Frost Plus Microscope Slides	Menzel (Braunschweig, Germany)
SYS Micro4 controller	World Precision Instruments (Berlin, Germany)
Whatman gel blotting paper	GE Healthcare (Chalfont St. Gilles, UK)

2.1.7 Software

Table 8 Software

Software	Supplier
AxioVision 4.9	Carl Zeiss Microimaging (Oberkochen, Germany)
Catwalk XT 10.0 gait analysis software	Noldus (Wageningen, The Netherlands)
Chromeleon Chromatography Data System	Thermo Fisher Scientific (Waltham, USA)
CorelDRAWX3	Corel Corporation (Ottawa, Canada)
Fusion FX	Vilber (Collegien, France)
ImageJ 1.50b	National Institutes of Health (Rockville, USA)

Software	Supplier
KyPlot 5.0	KyensLab Incorporated (Tokyo, Japan)
Prism 4.0	GraphPad Software (La Jolla, USA)
SPSS Statistics 23.0	IMB (Armonk, USA)
Stereo Investigator 9.0	Micro Bright Field Inc. (Colchester, USA)

2.1.8 Animals

All animal experiments have been performed with C57BL\6 wt (wildtype) mice. These were purchased from Charles River Laboratories. The mice had an age of ten to twelve weeks and were group-housed with a maximum of four animals per cage in individually ventilated cages (IVCs) at the central animal facility of the University Medicine Göttingen. The mice were adapted to the new surrounding for one to two weeks before the experiments. Unlimited access to water and food was ensured and the mice were exposed to a standardized 12 h light/dark-cycle. All animal experiments were carried out in accordance with the national German animal protection laws and approved by the local authorities (LAVES Niedersachsen, approval number 33.9-42502-04-16/2239).

Mice were randomly allocated in the following treatment groups: CTRL PBS, ULK1.DN PBS, CTRL MPTP and ULK1.DN MPTP, see 2.3 for further details.

2.2 Methods

2.2.1 Stereotactic injections

2.2.1.1 Preparation and mice analgesia

Preoperative analgesic treatment was started three days before the operation by addition of Metamizole (1.5 mg/ml) to the animals' drinking water and continued for three more days after surgery to ensure effective reduction of postoperative wound pain.

Before surgery, the virus solutions or sterile PBS as vehicle control were prepared: Stored at -80°, the p.AAV-hSyn-mCherry-hSyn-ULK1-CTD-WPRE and p.AAV-hSyn-mCherry-hSyn-9(5) stocks were defrosted on ice, diluted with sterile PBS and centrifuged directly before the injection.

2.2.1.2 Surgical procedure

At first, mice were anaesthetized with a ketamine/xylazine injection. The mixture was dosed according to their actual body weight and delivered intraperitoneally: ketamine (150 mg/kg bw), xylazine (10 mg/kg bw) dissolved in Sterofundin infusion solution. Sufficient depth of anaesthesia was verified by checking the toe pinching and eye lid reflex. The eyes of the animals were covered with Bepanthene ointment to prevent them from desiccation. Next, the head of the mouse was fixed in a metal frame particularly designed for stereotactic surgery. Ear bars ensured the correct position of the skull in the sagittal plane and a jaw holder secured the horizontal alignment in the transversal plane. The skin on the skull was opened with a longitudinal incision of approximately one centimeter length. Then, the skin was moved aside with surgery hooks and the Bregma and Lambda points were determined. The coordinates of the dorso-ventral axis must not vary by more than 0.3 mm, otherwise Bregma had to be calibrated by careful adjustment of the jaw holder. The specific coordinates for the injection into the Substantia nigra of the right hemisphere were calculated separately for every mouse, based on its particular Bregma coordinates and the generally accepted adjustments for the SN – relative to Bregma – according to the Paxinos Mouse Brain Atlas (Paxinos and Franklin 2007):

Anteroposterior: -3.0 mm; Mediolateral: -1.2 mm; Dorsoventral: -4.5 mm

According to the target coordinates, the skull was opened using a mini-driller with a head size of 0.8 mm. Afterwards, the injector was introduced slowly into the brain parenchyma until it reached the correct depth. Then the injection of 1-5 x 10^8 TU of AAV.ULK1.DN

or AAV.CTRL in 2 µl total injection volume at an injection rate of 500 nl/min was performed via a delicate glass capillary (also see Figure 4 for illustration of stereotactic injection).

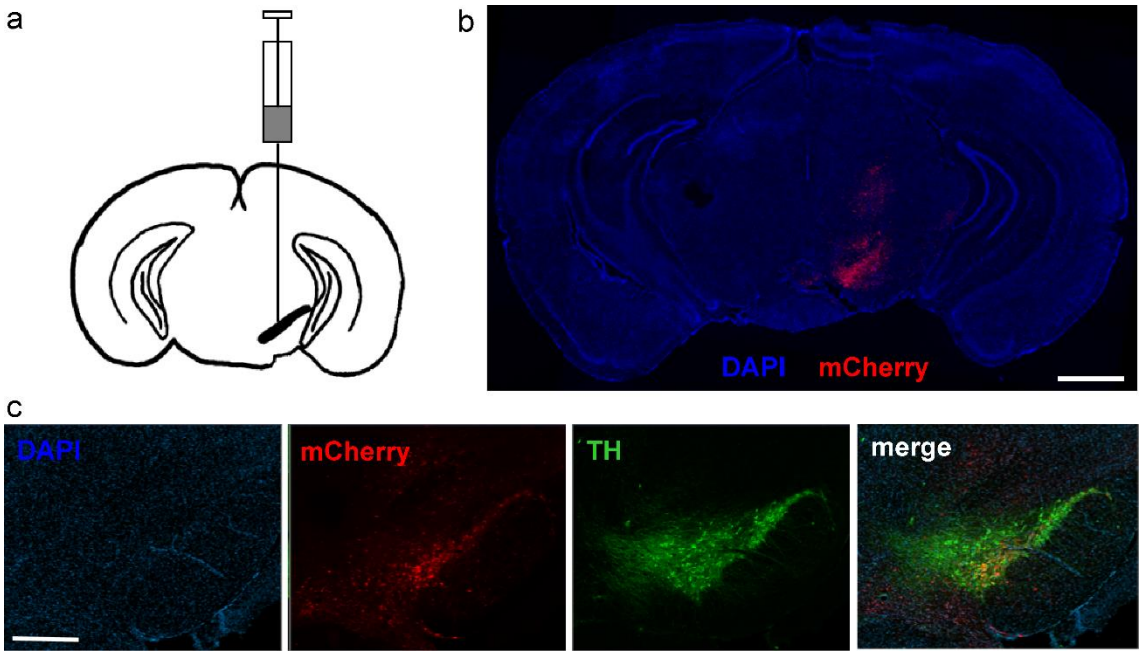

Figure 4 Illustration of AAV.ULK1.DN virus injection and cell transduction in the substantia nigra pars compacta (SNpc)

(A) Injection of the CTRL and ULK1.DN virus into the SNpc was performed during stereotactic surgery according to the coordinates relative to Bregma described in the Paxinos Mouse Brain Atlas (Paxinos and Franklin 2007): anterior posterior: -3.0 mm, mediolateral: -1.2 mm and dorsoventral: -4.5 mm. (B) Representative overview of mCherry expression after virus injection and DAPI staining to visualize cell nuclei and corresponding brain structures. Scale bar: 1 mm. (C) Representative micrograph of the mouse midbrain region visualizing the co-localization of mCherry expression and TH expression of dopaminergic neurons in the SNpc after AAV injections. Again cell nuclei were counterstained with DAPI. Scale bar: 500 µm. Modified from Balke et al. (2020), reprinted by permission from Springer Nature. The figure is part of the licensed content title "AAV-Mediated Expression of Dominant-Negative ULK1 Increases Neuronal Survival and Enhances Motor Performance in the MPTP Mouse Model of Parkinson's Disease", published by Dirk Balke, Lars Tatenhorst, Vivian Dambeck et al. in Molecular Neurobiology. https://link.springer.com/journal/12035 © Springer Nature (2020)

Afterwards, the capillary was left in its position for four minutes to prevent major reflux via the entry channel. Then the injection capillary was gradually removed and Dermabond tissue glue (15 µl) was applied to seal the skin incision. Finally, the mouse was unhitched from the stereotactic frame and received a subcutaneous injection of 1 ml pre-warmed (37°) Stereofundin, before it was put into a recovery cage on a warming pad under an infrared lamp.

2.2.2 Intraperitoneal injection of MPTP to create a subchronic PD model

We employed a subchronic MPTP mouse model to induce neuronal demise and analyze neuroprotective and neuro-restorative properties ofULK1-inhibition in this context (Vila et al. 2000; Tönges et al. 2012). The mice were intraperitoneally injected with 30 mg MPTP/kg bw per day for five days in succession, starting three weeks after the stereotactic surgery with injection of either AAV.ULK1.DN or AAV.CTRL. The MPTP was dissolved in 0.9 % saline for the injections and vehicle animals received injections of sterile PBS (200 µl/day). The injections and handling of the animals were performed with respect to current safety and utility guidelines for MPTP (Jackson-Lewis and Przedborski 2007).

2.2.3 Behavioral tests (Catwalk gait analysis, Rotarod, Cylinder rearing test)

At least once a week, and daily during the MPTP-treatment, the mices' weight was controlled. Besides, three behavioral tests were performed to investigate possible effects of the AAV and MPTP injection on the motor behavior of the animals. To get a baseline value, the mice were tested once before the MPTP or PBS injections took place. The further time points of behavioral testing were two, four and six weeks after the MPTP treatment for the animals in the "chronic cohort" and two weeks after the MPTP treatment for animals in the "acute cohort" (Balke et al. 2020). To grant the animals enough time to rest and sufficient stress relief, the tests were performed on separate days.

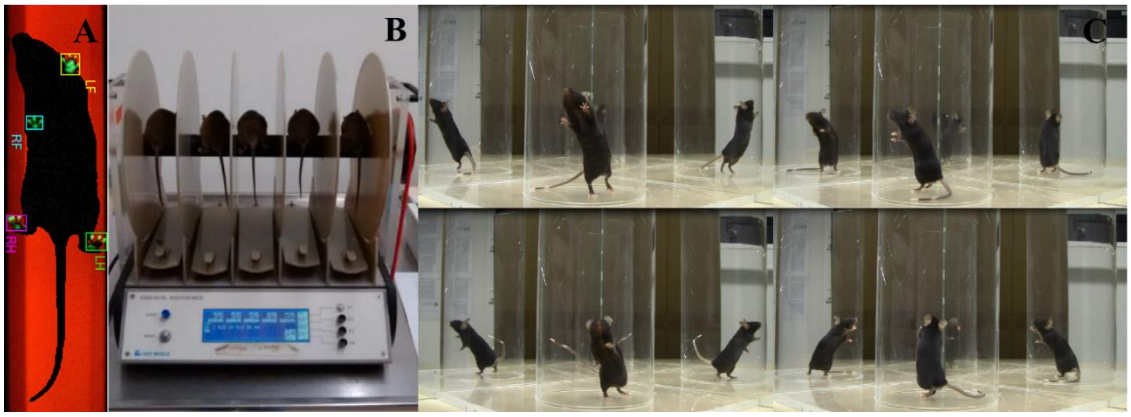

Figure 5 Summary of behavioral tests used in this thesis

(A) A still image from the Noldus catwalk gait analysis system, where the mouse is filmed from below while running on the walkway. The software automatically detects the paws for measurement of gait parameters. LF: left front; RF: right front; LH: left hind; RH: right hind; (B) Five mice on the rotarod during a test run. A downfall is registered by the rocker below each mouse and leads to an automatic indication of the endurance time on the screen. (C) Setup of the cylinder rearing test with two mirrors behind the plexiglass cylinder for better detection of paw usage during the rears. The mouse is videotaped for five minutes, and afterwards the number of freely conducted rears (top right), rears supported with both front paws (top left) or rears supported with one paw (left paw: bottom left; right paw: bottom right) is counted.

2.2.3.1 Catwalk gait analysis

The Noldus catwalk XT gait analysis system (see Figure 5 A) records and analyses more than 200 gait parameters of the tested animals (Tatenhorst et al. 2016): To acquire the necessary information to calculate these parameters, the mice run along a narrow walkway with a width of 4 cm on a glass floor, which allows to monitor the animals from below. The gait analysis software detects the paw prints and calculates stride length, toe spread, speed and several more parameters. In doing so, it provides detailed insights into motor behavior alterations of the animal, and after several tests it is also possible to evaluate the development of gait disorders in a very precise way. To form the mean values for the different treatment groups, each animal performed three runs on the catwalk and the average of these runs was calculated first. All runs were recorded with the very same detection settings: camera gain: 20; intensity threshold: 0.10; minimum run duration: 0.5 sec.; maximum run duration: 7 sec.; minimum number of compliant runs: 3; maximal allowed speed variation: 60 %.

2.2.3.2 Rotarod

The Ugo Basile Rotarod for mice 47600 (Tönges et al. 2012; Tatenhorst et al. 2016) is a device which has been developed for the purpose of analyzing mouse motor skills comprising running abilities, balance and stamina. The central element is a rotating rod with a diameter of three centimeters and space for five mice, separated by large plastic spacers, to be placed onto it simultaneously (see Figure 5 B). The initial speed of the rod was always adjusted to 5 revolutions per minute (rpm) and continuously and automatically accelerated to 40 rpm over a time period of five minutes. For statistical analysis the parameter "time on the rod" was noted for every animal. "Time on the rod" was defined as the timespan between start of the speed acceleration and the mouse's downfall or the end of the five minute period as the maximal value. On the day of data collection, every mouse was put onto the rotarod thrice with approximately 30 minutes intertrial interval to reduce stress and fatigue. For the evaluation of the data, again the average of the three iterations was determined for each animal, and based upon these values the average for every treatment group was determined. All mice were pretrained on three consecutive days two weeks before the first data collection to obtain reliable results. Furthermore, they were always put one the rotarod for one five minute-trial the day before each data collection to let them get used to the procedure again.

2.2.3.3 Cylinder rearing test

To analyze the mices' motor coordination in terms of forelimb usage, the well-established cylinder rearing test was utilized (Schallert et al. 2000; Tönges et al. 2012, Tatenhorst et al. 2014). For this purpose, the mice were put into an acrylic glass cylinder (height: 25 cm, diameter: 11.5 cm) and then videotaped for five minutes. In order to ensure reliable detection of forelimb usage in situations when a mouse did not face the camera, the glass cylinder was placed between the camera and a mirror (see Figure 5 C). The evaluation of the recorded behavior was performed manually by a blinded investigator: A "free rear" was noted if the mouse straightened itself without any assistance from the forelimbs. If the rear was supported with one forelimb, the rear was rated as either "right" or "left", depending on the forelimb that was used. If the mouse used both forelimbs to brace during the rear, this was rated as "both". The absolute numbers of different rears per animal were converted into relative numbers (%) to achieve a better comparability between very active and relatively calm animals. Afterwards, the means were compared between the different treatment groups and time points.

2.2.4 Euthanasia & perfusion

Depending on the cohort the mice belonged to, the scarification time point was two (acute model) or six weeks (chronic model) after the MPTP treatment (Balke et al. 2020). They were either perfused transcardially with PFA to preserve their brains for immunohistochemical stainings or the brains were taken out freshly after cervical dislocation for neurochemical analysis.

2.2.4.1 Transcardial perfusion

First the animals were sacrificed with CO_2, which was introduced to the IVC very slowly to assure that the animals fall asleep first and do not choke while being conscious. Then they were attached to a polystyrene sheet and their abdomen was opened with a longitudinal cut. The diaphragm was intersected and afterwards the thorax was opened by bilateral incisions. After removal of the pericardium, the heart was perforated with a cannula in the left ventricle. This allowed the entering PBS to rinse and clean the animal's vasculature. The right atrium was also incised to allow the PBS to leave the circulation again. When the animal's liver blanched and only clear fluid came out of the right atrium, indicating that the blood had been successfully removed out of the body, the perfusion liquid was changed from pure PBS to 4 % paraformaldehyde (PFA) in PBS to finally fix the tissue and preserve its structure and protein conformations. After 4 minutes of perfusion, the dead body was detached from the polystyrene sheet and decapitated. The skull was opened with a longitudinal cut and the brain was carefully retrieved and stored in a falcon tube filled with 4 % PFA over night at 4 °C. On the following day, dehydration of the brain tissue was conducted in 30 % sucrose in PBS. When the dehydrated brains were sunken down in the falcon tubes, then they were dried with a tissue, wrapped with aluminum foil and frozen at -80 °C until cryo-sectioning.

2.2.4.2 Preparation of specific brain regions for neurochemical analysis

For the neurochemical analysis of dopamine concentration and the corresponding levels of its metabolites in the substantia nigra and striatum as well as for the determination of autophagy protein concentrations in the SN, the tissue must not be fixed but native. Therefore, not transcardial perfusion but sacrification by cervical dislocation was employed. After decapitation of the animals, the brains were explanted and the regions of interest dissected on ice. The tissue was quick-frozen in liquid nitrogen and stored in the -80 °C freezer until further processing.

2.2.5 Immunohistochemistry

2.2.5.1 Cryo-sections

All stainings were performed with cryo-sectioned brain tissue. Therefore, the still frozen brains were embedded in cryo matrix and kept in the -22 °C cold Cryostat CM 3050S until they were processed. When the cryo matrix was cured, the brains were sectioned coronally and the 30 µm thick slices containing the area of the striatum (Bregma AP +1.18 to -0.70 mm) and SN (Bregma AP -2.18 to -4.04 mm) were collected in separate 24-well cell culture plates filled with PBS (for each animal). Afterwards, 0.1 % sodium azide was added to the PBS for a better conservation of the slices, the plates were wrapped in Parafilm and temporarily shelved at 4 °C.

2.2.5.2 DAB & Nissl staining protocol

For the purpose of a stereological quantification of dopaminergic cells in the SN, the corresponding cryo-sections were first stained free-floating for TH-positive neurons and then additionally for Nissl-positive neurons on slides, according to the following protocol: Every 4^{th} of the collected SN sections was transferred to net tubes and washed 3 x 5 min with Tris (2-Amino-2-hydroxymethyl-propane-1,3-diol) buffered saline (TBS). Then the endogenous peroxidases were quenched via incubation for 5 min in 10 % methanol and 3 % H_2O_2 dissolved in TBS. After washing again in TBS, the sections were incubated in TBS containing 10 % Normal goat serum (NGS) for 30 min at Room temperature (RT) to block out unspecific antibody binding. Then the sections were incubated with the primary rabbit anti-TH antibody for 48 h at 4 °C. The antibody was diluted 1:1000 in 2 % NGS in 0.1 M TBS. After removal of the first antibody and three washing steps in TBS (a 5 min), the secondary biotinylated anti-rabbit antibody diluted 1:200 in 2 % NGS in 0.1 M TBS was put onto the sections and incubated at RT for 1 h. Then again three washing steps in TBS were performed, followed by the incubation with the Vectastain ABC Kit PK-6100 for 1 h at RT, which was used to amplify signal power and detection. Eventually, sections were washed again in TBS (3 x 5 min) and the Peroxidase Substrate Kit DAB SK-4100 was used to accomplish the staining. The 3,3′-Diaminobenzidine (DAB) reaction was stopped after 4 min by addition of distilled H_2O, when a brownish glowing SN was clearly visible by eye. Subsequently, the sections were transferred to Super Frost Plus Microscope Slides and dried at RT in a light shielded surrounding for three days.

Afterwards, the Nissl-staining was conducted: For rehydration the slides were placed in a box with distilled H_2O for 5 min. Then they were incubated in 1 % thionine acetate solution for 7 min and subsequently washed in a box of distilled H_2O for 5 min. Next, alcoholic solutions of ascending concentrations were used to dehydrate the tissue: 70 % (2 min incubation), 90 % (2 min) and 96 % ethanol for 5 min; followed by 5 min in 100 % isopropanol and consecutive incubation in xylene (2 x 5min). At the end the xylene wet sections were immediately fixed with Roti-Histol and then left to dry at RT.

2.2.5.3 Stereological quantification of TH^+ neurons in the SNpc

The amount of TH^+ and $Nissl^+$ cells in the SNpc of the DAB-stained sections was determined by stereological counting. Therefore, a Zeiss microscope was utilized to image the slides and the linked Stereo Investigator 9.0 software was utilized to count the cells. The blinded investigator first manually outlined the SNpc at 2.5 x objective magnification and then counted the TH^+ and $Nissl^+$ cells on both hemispheres on every 4^{th} section through the SN at 40 x objective magnification according to the optical fractionator method (Tönges et al. 2012, Tatenhorst et al. 2014). The settings were adjusted as follows:

Counting frame size: 50 x 50 µm; grid size: 100 x 100 µm; interval: every 4^{th} section; focus: manually on top of the 30 µm thick section;

The calculation of the total amount of TH^+ as well as $Nissl^+$ cells for the right and left SN of each animal was done by the software, based on the number of manually counted and marked immunolabeled cells. The amount of $Nissl^+$ cells was determined to be able to rule out a sole reduction of TH-expression as an explanation for possibly decreasing numbers of TH^+ cells and instead to confirm a real cell loss.

2.2.5.4 Striatal density staining

For the staining of TH^+ striatal fibers, the cryo-sectioned slices between Bregma +0.62 mm and -0.10 mm were incubated in a chloroform-ethanol solution with subsequent dehydration and a TH/DAB staining according to the protocol above. For the striatal density staining, the nickel intensifier was used. Afterwards, the slices were formalin fixed, dehydrated and mounted with Roti-Histol.

2.2.5.5 Evaluation of striatal fiber density

To image the stained striatal cryo-sections an Axioplan microscope with an attached gray scale camera was employed. Surveys of the whole slices were taken through the 2.5-fold objective. Using the Image J software with the freehand selection tool, the cortex and striatum of both hemispheres were surrounded and the mean grey value was measured. Then the value was subtracted from 255 for the cortex and striatum and the difference of cortex – striatum was calculated to determine the final value for the section. For each of the eight to twelve animals per group, at least five sections were analyzed in order to get a reliable mean grey value per section. Subsequent calculations provided the mean grey value per treatment group. Finally, the signal was normalized to the CTRL PBS group.

2.2.5.6 Fluorescence staining of nigral p62 and mTOR

In order to investigate downstream autophagy regulation after expression of ULK1.DN, an immunostaining to visualize nigral p62 and mTOR expression was employed.

The staining was performed on every 8th section through the SN. First, the sections were rehydrated at 4 °C in PBS overnight. On the following day, the microscope slides were transferred into citrate buffer and then incubated at 80 °C in a hot water bath for 30 min. After cooling down to RT for ~ 60 min, they were washed two times in PBS for 10 min. Subsequently, they were incubated in 25 mM glycine in PBS for 20 min, followed by two washing steps in PBS. Afterwards, slides were incubated in 0.1 % Sudanblack solution for 15 min and then washed in PBS twice. Subsequently, the sections were outlined with lipid blocker. The slides were transferred into a dark box with damped air and they were incubated with the IHC blocking solution (150 µl per slide) for 1.5 h at RT to block unspecific antibody binding. Afterwards, the blocking solution was removed, and the sections were incubated with the primary rabbit anti-p62 or anti-mTOR antibody over night at 4 °C. The anti-p62 antibody was diluted 1:500, and anti-mTOR antibody was diluted 1:250 in the IHC blocking solution.

The next day, the slides were washed three times in PBS, before they were incubated with the secondary Alexa 488 goat anti-rabbit IgG F(ab)2 antibody, which was diluted 1:250 in the IHC blocking solution, at RT for 1.5 h. Subsequently, three washing steps in PBS were performed, followed by an incubation in DAPI solution for 2 min and another three times of washing in PBS. The sections were initially dehumidified at 60 °C, then mounted with Mowiol and finally dried at RT overnight.

2.2.6 Western blot

Six weeks post MPTP treatment, animals were sacrificed and SN lysates were produced for Western blot analysis. This was employed in order to evaluate the influence of ULK1.DN expression on downstream signaling of ULK1 and cell survival pathways (Balke et al. 2020).

2.2.6.1 Protein isolation from frozen tissue

Midbrain tissue was dissected on ice and snap-frozen as described above. In the following, according to the individual sample weight, cold Radioimmunoprecipitation assay (RIPA) buffer was appended to the samples. The frozen tissue was homogenized manually using plastic pistils, followed by sonication for 2 x 20 sec at 40 % intensity and centrifugation for 20 min at 4 °C and 14.000 rpm. Subsequently, the Pierce bicinchoninic acid (BCA) protein assay kit in combination with a Rainbow Spectra Tecan plate reader was employed to determine protein concentrations. In preparation of later electrophoresis, tissue samples were heated up to 95 °C for 7 min after addition of Laemmli buffer containing 10 % Dithiothreitol (DTT). Until electrophoresis samples were kept at -20 °C.

2.2.6.2 Sodium dodecyl sulfate-polyacrylamide gel electrophoresis (SDS-PAGE)

SDS-PAGE was employed to segregate the different proteins and allow a quantification. The denaturating detergent SDS has the advantage of a clear separation of proteins by size under exclusion of bias due to electric charge or conformation. For conduction of the SDS-PAGE always a stacking gel with 5 % polyacrylamide content and a pH of 6.8 was used. The resolving gels pH always was 8.8 and polyacrylamide content varied between 8 and 14 % according to the specific blotting targets. BioRad Mini-PROTEAN Tetran-Cell systems were used to conduct the electrophoresis. After placement of the gels, electrophoresis buffer consisting of 192 mM glycine, 0.1 % SDS and 25 mM Tris- HCl with pH adjusted to 8.3 was added into the system. The gel pockets were filled with a standard amounts of 25 µg protein. At the beginning of electrophoresis 50 V were applied for about 20 min to transfer the probes from the pockets into the stacking gel. Subsequently, voltage was increased to 100 V for optimal protein separation. When the small proteins approached the distal verge of the gel, the electrophoresis was terminated.

2.2.6.3 Immunoblotting

For a successful transfer of the separated proteins to a polyvinylidene fluoride (PVDF) membrane a blotting cassette was prepared as follows: After a short immersion in

methanol for half a minute to activate the membrane, it was placed in the middle of the cassette together with the gel. They were flanked by a piece of filter paper and a soaking wet sponge on each side. Then chilled transfer buffer and an additional ice pack were added to the cassette to complete the blotting system and to keep the temperature low. Protein transfer was performed overnight at steady voltage of 30 V and 4 °C, followed by another 45 min at 100 V. After successful transfer, the membrane was incubated in a blocking solution consisting of 5 % non-fat dry milk in Tris buffered saline with Tween 20 (TBS-T) for one hour at RT. Subsequently, three washing steps (each 10 min) in TBS-T were performed before the membranes were incubated with the respective primary antibody overnight at 4 °C. The primary antibodies were diluted as follows:

Table 9 Primary antibody solutions

Target	**Dilution ratio**	**Medium**
mTOR	1:1000	in 5 % BSA
p-mTOR	1:1000	in 5 % BSA
p62	1:500	in 5 % BSA
pS6	1:1000	in 5 % BSA
LC3	1:100	in 5 % milk
ERK1/2	1:2000	in 5 % BSA
pERK1/2	1:2000	in 5 % BSA
AMPK	1:1000	in TBS-T only
pAMPK	1:1000	in TBS-T only
GAPDH	1:1000	in 5 % milk
ß-Tubulin	1:5000	in 5 % milk
ß-Actin	1:2000	in TBS-T only

After incubation, the membranes were rinsed three times in TBS-T for 10 min each. Subsequently, the membranes were incubated with the horseradish peroxidase (HRP) coupled secondary antibody. The secondary antibodies were derived from goat, always diluted 1:1000 in 5 % non-fat dry milk in TBS-T and incubated for 1 hour. Afterwards, three washing steps in TBS-T were conducted. Finally, signal was detected using chemiluminescence: The ECL (Electrochemiluminescence) 1 and ECL2 component were

added to the rinsed membrane in equivalent amounts and left to incubate for about 90 seconds. Then the enhanced chemiluminescence signal was detected using the Vilber Fusion FX system.

2.2.7 HPLC

The high-performance liquid chromatography (HPLC) was employed to analyze the dopamine levels in striatal axonal terminals of mice two and six weeks post MPTP treatment. In order to do so, 50 µl 0.1 M perchloric acid ($HClO_4$) per mg striatal tissue were added to the previously snap frozen tissue. Using Precellys 1.4 mm ceramic beads, homogenization of the samples was conducted utilizing a bead mill. Following this, centrifugation of the specimens was performed at 13.4 g at 4 °C for 5 min. Afterwards, the supernatant was decanted and filled into fresh tubes, followed by another 10 min cycle of centrifugation. The subsequently obtained supernatant was used for HPLC analysis of dopamine (DA), 3,4-dihydroxyphenylacetic acid (DOPAC) and homovanillic acid (HVA) content of the samples. For this purpose, a volume of 50 µl supernatant was used per HPLC tube. This ensured a smooth uptake of the loading amount which was set to 20 µl per sample by the autosampler. The loading amount was automatically injected into the guard column with an applied voltage of 600 mV at 6 °C. The purpose of the guard column is protection of the analytical column from possible contaminants in the liquid solvent by oxidation. For analysis a C18 reverse-phase HR-80 catecholamine column was implemented and electrochemical detection was performed by an ESA Coulochem III with a 5010 analytic model detector (E1 = 50 mV, E2 = 400 mV). As mobile phase, a filtered and degassed HPLC buffer consisting of 6.9 g/l sodium acetate, 48 mg/l EDTA, 7.3 g/l citric acid, 105 mg/l octane sulphonic acid solution and 10 % methanol was used at a flow rate 0.4 ml/min and pH = 4.3. Samples of the different treatment groups were run alternately and DA, HVA and DOPAC standards (in concentrations of 0.15 µM, 0.3 µM and 1.5 µM) were run at regular intervals between the samples to ensure a precise and absolute measurement of the catecholamines. The Chromeleon Chromatography Data System was utilized to record and analyze data. Finally, the area under the specific peak was analyzed to determine the concentration of DA, DOPAC and HVA in ng per mg wet tissue.

2.2.8 Statistical analysis

Statistical analyses were performed employing Kyplot software (Version 5.0), Graphpad Prism software (Version 4.0) and IBM SPSS Statistics (Version 23.0). Parametrical statistics were utilized because they suit the majority of biological samples, e.g. animals behavior data or tissue. To compare values of two groups statistically, unpaired student's t-test was applied. For comparison of multiple groups always an one-way ANOVA with Tukey's posthoc test was performed . Striatal fiber density measurements, TH cell count evaluation and neurochemical metabolite analyses were conducted in a hierarchical design. The respective parameter was defined as the dependent variable, the treatment group (AAV.CTRL vs. AAV.ULK1.DN) as the independent variable. Generally, data are represented as mean ± SEM (standard error of the mean) and significances are defined with * $p < 0.05$, ** $p < 0.01$, *** $p < 0.001$.

2.3 Study design

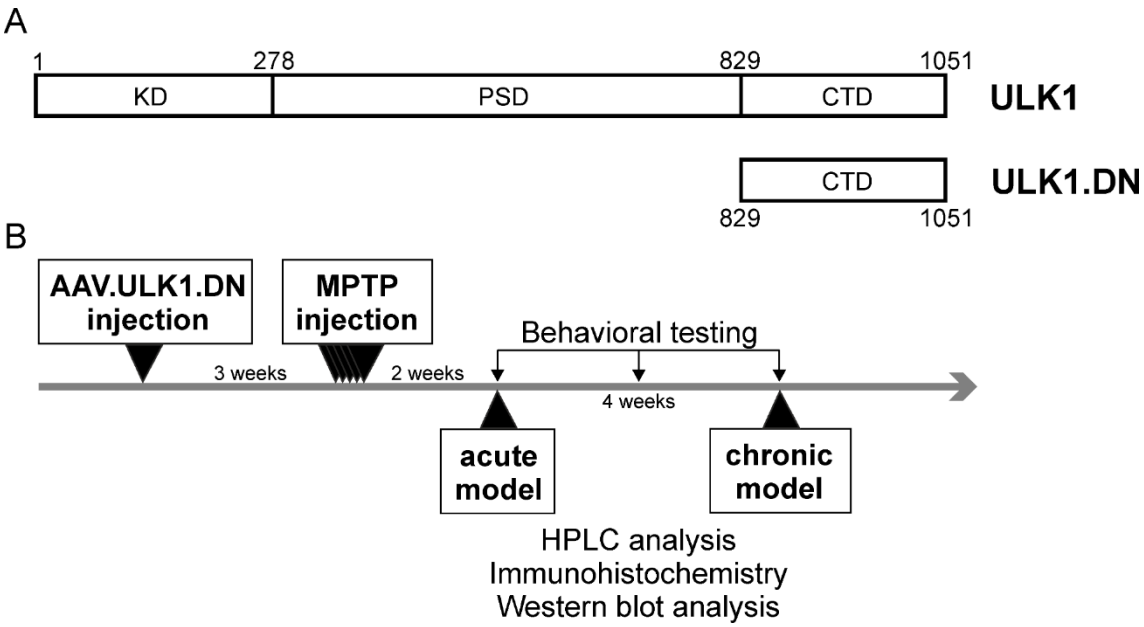

Figure 6 Structure of ULK1, its dominant negative variant ULK1.DN and treatment paradigm for animal experiments

(A) ULK1.DN represents only the C-terminal domain of physiological ULK1. KD: kinase domain; PSD: proline- and serine-rich domain; CTD: C-terminal domain. (B) All animals initially received stereotactic injection of either AAV.ULK1.DN or AAV.CTRL into the substantia nigra. Three weeks later, mice received intraperitoneal injections of MPTP or vehicle on five consecutive days. Animals were sacrificed either two (acute model) or six (chronic model) weeks after MPTP treatment and brain tissue was analyzed. Behavioral data was collected two, four and six weeks after MPTP treatment. Modified from Balke et al. (2020), reprinted by permission from Springer Nature. The figure is part of the licensed content title "AAV-Mediated Expression of Dominant-Negative ULK1 Increases Neuronal Survival and Enhances Motor Performance in the MPTP Mouse Model of Parkinson's Disease", published by Dirk Balke, Lars Tatenhorst, Vivian Dambeck et al. in Molecular Neurobiology. https://link.springer.com/journal/12035 © Springer Nature (2020)

In order to examine possible neuroprotective and neurorestorative properties of AAV-mediated ULK1 inhibition in the MPTP mouse model, a study design with two sacrifice time points was chosen (see Figure 6). For allocation and labelling of the treatment groups (see Table 10).

Table 10 Overview of the experimental groups

Treatment group	N	**Timepoint of sacrifice**	
		2 weeks post MPTP	6 weeks post MPTP
CTRL PBS	16	x	
CTRL PBS	24		x
ULK1.DN PBS	16	x	
ULK1.DN PBS	24		x
CTRL MPTP	16	x	
CTRL MPTP	24		x
ULK1.DN MPTP	16	x	
ULK1.DN MPTP	24		x

All experiments were conducted with C57BL\6 wt mice (as described above). At the corresponding timepoint (2 or 6 weeks), the whole treatment group (n = 16 or n = 24) was sacrificed. The brains of one half were fixed and sectioned for IHC analysis. The other half was used to prepare striata for HPLC analysis and SN for Western blotting. All animals underwent behavioral testing at two, respectively at two, four and six weeks post MPTP treatment.

3 Results

3.1 Neuronal cell survival and preservation after MPTP treatment

For the exploration of potential neuroprotective properties or possible supportive neuro-regenerative effects of ULK1.DN expression-mediated autophagy inhibition, the animals were sacrificed two weeks and six weeks post MPTP treatment for immunohistochemical analysis of TH and Nissl cell numbers in the SN as well as measurement of TH striatal density.

3.1.1 Quantification of DAergic neuronal cell survival in the SNpc two and six weeks post MPTP treatment

To evaluate possible neuroprotective properties of ULK1.DN expression, three weeks after stereotactic AAV.ULK1.DN injection the neurotoxin MPTP was administered in a subchronic regime. Then mouse brains were analyzed immunohistochemically two and six weeks after MPTP injections (Balke et al. 2020).

Two weeks after MPTP treatment, a loss of TH^+ DAergic neurons in the SNpc of the CTRL MPTP group was observed (see Figure 7 A). The stereological cell counting confirmed a significant decrease of > 50 % in TH^+ cell numbers in the CTRL MPTP group (5,095 ± 814 TH^+ neurons per SNpc) as compared to the CTRL PBS group (11,017 ± 511), as well as a decrease of > 40 % as compared to the ULK1.DN PBS group (9,033 ± 513). However, MPTP treatment did not significantly reduce the number of TH^+ cells in the ULK1.DN MPTP group (8,578 ± 254) as compared with ULK1.DN PBS. Yet after MPTP treatment, the TH^+ cell numbers in the ULK1.DN MPTP group were 40 % higher as compared with the CTRL MPTP group.

Similar ratios for the treatment groups were also obtained when the number of Nissl-stained nigral neurons was analyzed. A significant reduction in $Nissl^+$ cells in CTRL animals was seen when treated with MPTP (CTRL PBS: 13,081 ± 566, CTRL MPTP: 6,350 ± 936 $Nissl^+$ neurons per SN), while the number of $Nissl^+$ cells was not significantly lower in the ULK1.DN MPTP (10,114 ± 303) in comparison to the ULK1.DN PBS group (10,897 ± 635). Consequently, significantly more Nissl cells were preserved in the ULK1.DN animals after MPTP treatment compared to the CTRL MPTP animals.

The Nissl staining was conducted in addition to the TH staining to account for the total number of neuronal cells in the SNpc. It was thereby excluded that decreased TH^+ cell numbers occurred only due to TH downregulation because of MPTP administration, but it was rather due to real cell death.

Six weeks after MPTP treatment, still a clear and significant MPTP effect between the TH^+ cell numbers of the MPTP injected and the PBS injected groups was visible. However, in contrast to two weeks post MPTP treatment, no significant differences between CTRL MPTP and ULK1.DN MPTP groups were observable anymore (CTRL MPTP: 6,637 ± 428; ULK1.DN MPTP: 7,672 ± 325; CTRL PBS 10,728 ± 305; ULK1.DN PBS 11,892 ± 398, also see Figure 7 B) (Balke et al. 2020). Again, the results of the Nissl staining evaluation were perfectly in line with those of the TH staining: The number of $Nissl^+$ cells per SN was significantly higher in the PBS control groups than in the MPTP treated animals but no significant difference between CTRL MPTP and ULK1.DN MPTP could be detected anymore. (CTRL PBS: 12,989 ± 348; ULK1.DN PBS: 14,472 ± 464; CTRL MPTP: 8,291 ± 505; ULK1.DN MPTP: 9,640 ± 388; for all means± SEM, also see Table 11).

In summary, these results suggest that DAergic neurons in the SN are protected from acute MPTP-induced neurodegeneration by ULK1.DN expression-mediated inhibition of autophagy two weeks post MPTP. However, no statistically significant benefit in terms of enhanced neuro-regeneration or preservation of dopaminergic cell bodies could be detected six weeks post MPTP treatment.

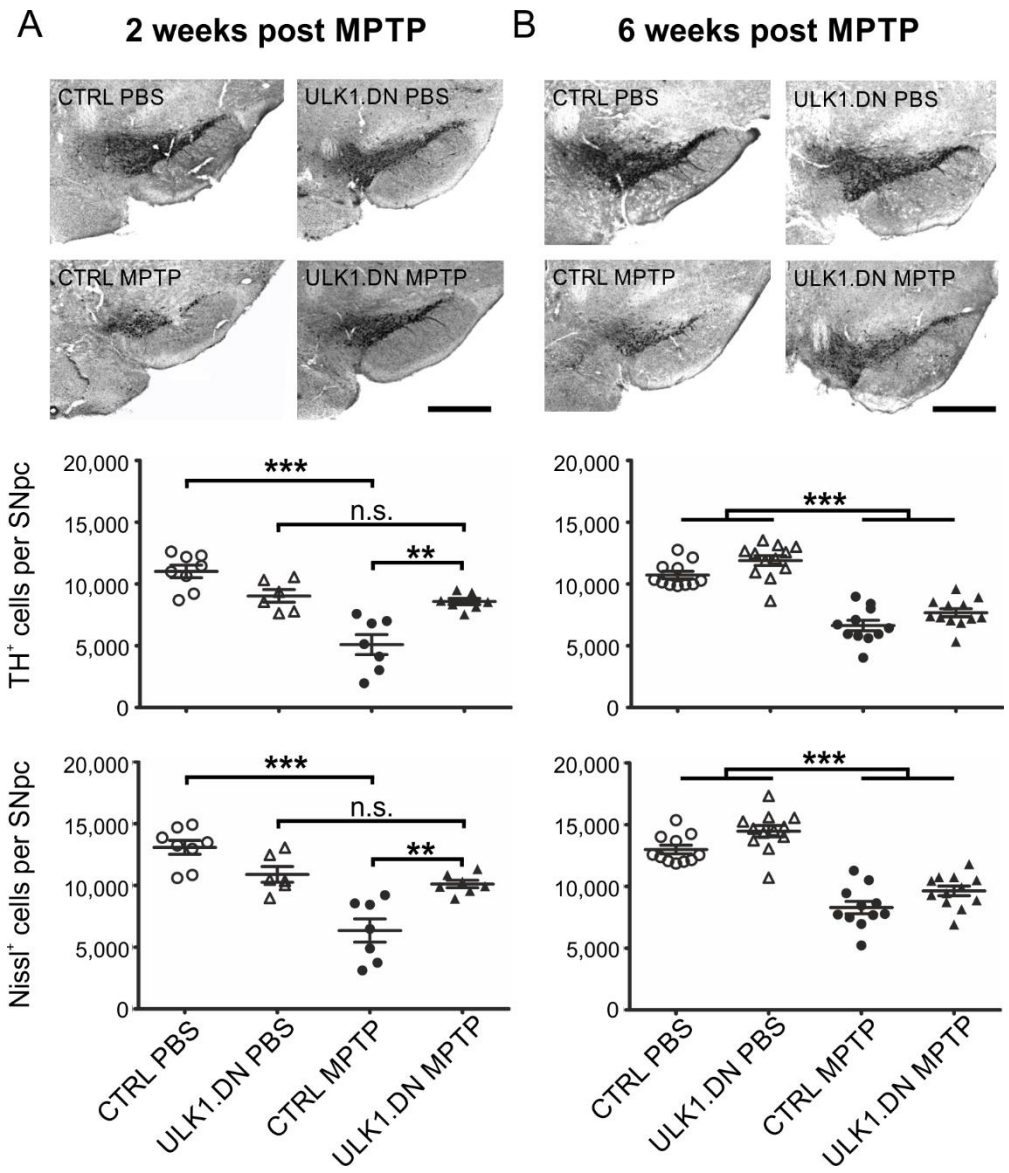

Figure 7 ULK1.DN prevents dopaminergic nigral neurons from MPTP-induced neurodegeneration

Immunohistological analysis of TH^+ and $Nissl^+$ cells in the substantia nigra pars compacta of MPTP treated mice expressing ULK1.DN and respective controls. (A) Analysis two weeks after MPTP treatment, data are presented including means ± SEM, n = 6-8, *** $p < 0.001$; ** $p < 0.01$; n.s. = not significant; ANOVA + Tukey posthoc test. Representative micrographs of substantia nigra are presented in the top panel, scale bar: 500 µm. (B) Analysis six weeks after MPTP treatment, data are presented including means ± SEM, n = 11-12, *** $p < 0.001$; ANOVA + Tukey posthoc test. Representative micrographs of substantia nigra are presented in the top panel, scale bar: 500 µm. Modified from Balke et al. (2020), reprinted by permission from Springer Nature. The figure is part of the licensed content title "AAV-Mediated Expression of Dominant-Negative ULK1 Increases Neuronal Survival and Enhances Motor Performance in the MPTP Mouse Model of Parkinson's Disease", published by Dirk Balke, Lars Tatenhorst, Vivian Dambeck et al. in Molecular Neurobiology. https://link.springer.com/journal/12035 © Springer Nature (2020)

Table 11 Nigral dopaminergic and total neuronal cell count in the SNpc

Experimental condition	TH^+ cells per SN	$Nissl^+$ cells per SN
2 weeks post MPTP		
CTRL PBS	11,017 ± 511	13,081 ± 566
ULK1.DN PBS	9,033 ± 513	10,897 ± 635
CTRL MPTP	5,095 ± 814	6,350 ± 936
ULK1.DN MPTP	8,578 ± 254	10,114 ± 303
6 weeks post MPTP		
CTRL PBS	10,728 ± 305	12,989 ± 348
ULK1.DN PBS	11,892 ± 398	14,472 ± 464
CTRL MPTP	6,637 ± 428	8,291 ± 505
ULK1.DN MPTP	7,672 ± 325	9,640 ± 388

Data given as mean ± SEM. Numbers given per complete SN, right hemisphere, injected side of the brain.

3.1.2 Quantification of striatal density two and six weeks post MPTP treatment

In order to investigate potential protective properties of ULK1.DN expression on nerve terminals of DAergic nigral neurons, striata were immunostained against TH 14 days after MPTP lesion (Figure 8 A). In addition, and with regard to feasible long-term or regeneration effects, the same staining was also performed six weeks after MPTP lesion (Figure 8 B) (Balke et al. 2020).

The representative micrographs in Figure 8 A show a similar signal of the TH staining for the PBS treated animals. Opposed to this, a significant reduction of TH^+ immune-reactive fibers in the CTRL MPTP treated animals is visible two weeks post treatment. The ULK1.DN MPTP animals also show reduced TH^+ signal compared to the PBS groups. However, the signal loss is less pronounced than in the CTRL MPTP group. This observation was consistent with the IHC analysis: Two weeks post MPTP treatment, the CTRL MPTP group showed a significantly diminished relative TH^+ fiber density in the striatum (44.9 ± 5.8 %) in comparison the CTRL PBS group (100 ± 9.8 %) as well as the

ULK1.DN PBS group (129 ± 14.0 %) (Balke et al. 2020). However, we observed a significantly, by > 45 % higher TH^+ fiber density in the striata of the ULK1.DN MPTP group (82.9 ± 7.1 %) in comparison to the CTRL MPTP group. Without the neurotoxin treatment, a higher striatal density in absolute numbers, but no statistically significant effect was observed for the ULK1.DN expressing experimental group.

Six weeks post MPTP treatment, the different micrographs of the experimental treatment groups look very much alike (Figure 8 B). IHC analysis showed similar levels of striatal density in all treatment groups (CTRL PBS: 100 ± 7.8 %; ULK1.DN PBS: 110 ± 11.3 %; CTRL MPTP: 104 ± 8.3 %; ULK1.DN MPTP: 125 ± 11.5 %).

In addition to neuroprotective effects of dominant negative ULK1 expression on the cell bodies two weeks post MPTP treatment revealed in the analysis of TH^+ and $Nissl^+$ cell counts, the results obtained from the striatal TH^+ fiber density staining point out an additive protection of DAergic terminals from acute MPTP-induced toxicity (Balke et al. 2020). Yet six weeks post MPTP treatment no significant beneficial effect of ULK1.DN was observed.

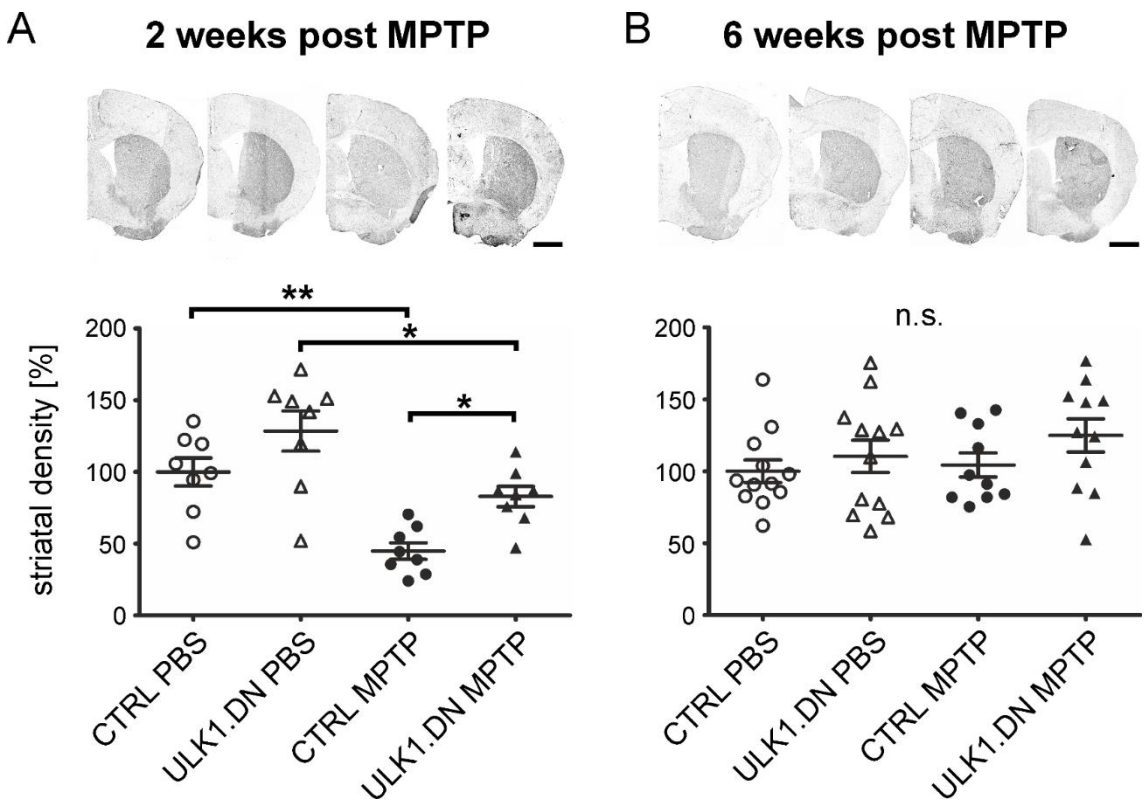

Figure 8 ULK1.DN protects dopaminergic nigrostriatal projections from MPTP-induced neurodegeneration

Immunohistological analysis of TH^+ striatal fiber density of MPTP treated mice expressing ULK1.DN and respective control. (A) Analysis two weeks after MPTP treatment, data are presented including means ± SEM, n = 8, ** $p < 0.01$; * $p < 0.05$; ANOVA + Tukey posthoc test. Representative micrographs of the striatum are shown in the top panel, scale bar: 1 mm. (B) Analysis six weeks after MPTP treatment, data are presented including means ± SEM; n = 10-12; n.s. = not significant; ANOVA. Representative micrographs of the striatum are presented in the top panel, scale bar: 1 mm. Modified from Balke et al. (2020), reprinted by permission from Springer Nature. The figure is part of the licensed content title "AAV-Mediated Expression of Dominant-Negative ULK1 Increases Neuronal Survival and Enhances Motor Performance in the MPTP Mouse Model of Parkinson's Disease", published by Dirk Balke, Lars Tatenhorst, Vivian Dambeck et al. in Molecular Neurobiology. https://link.springer.com/journal/12035 © Springer Nature (2020)

3.2 Analysis of dopamine and its metabolites in the murine striatum

For the evaluation of potential protective or restorative ULK1.DN expression-mediated effects on nigral DAergic nerve terminals in the striatum and their functional preservation, a HPLC analysis of DA and its metabolites DOPAC and HVA two and six weeks post MPTP treatment was performed (Balke et al. 2020).

3.2.1 Intrastriatal levels of DA, HVA and DOPAC two and six weeks post MPTP treatment

Two weeks after MPTP treatment, the neurochemical analysis showed a statistically very significant and with > 90 % nearly total depletion of DA in the animals striata (CTRL PBS: 9.35 ± 0.52; CTRL MPTP: 1.16 ± 0.09; ULK1.DN PBS: 8.90 ± 0.73; ULK1.DN MPTP: 1.12 ± 0.13 ng/mg wet tissue; Figure 9 A). The reduction of DOPAC (CTRL PBS: 3.56 ± 0.44; CTRL MPTP: 1.50 ± 0.16; ULK1.DN PBS: 2.95 ± 0.30; ULK1.DN MPTP: 1.42 ± 0.12 ng/mg wet tissue) and HVA (CTRL PBS: 1.81 ± 0.10; CTRL MPTP: 1.19 ± 0.08; ULK1.DN PBS: 1.72 ± 0.11; ULK1.DN MPTP: 1.20 ± 0.05 ng/mg wet tissue; also see Table 12 for all means ± SEM) levels upon MPTP treatment was also highly significant, although not as severe as the reduction of DA. These massive and nearly identical reductions in both ULK1.DN and CTRL treatment groups confirmed the functionality of the MPTP model but also revealed no DA preserving property of the ULK1.DN expressing construct.

Six weeks after MPTP treatment, still a significant MPTP effect on striatal DA levels of the animals could be detected (CTRL PBS: 9.83 ± 1.16; ULK1.DN PBS: 12.1 ± 1.19; CTRL MPTP: 2.65 ± 0.31; ULK1.DN MPTP: 2.93 ± 0.4 ng/mg wet tissue; Figure 9 B) (Balke et al. 2020). However, DA was partly restored compared to the lower absolute values two weeks post MPTP treatment. For DOPAC (CTRL PBS: 2.8 ± 0.43; ULK1.DN PBS: 3.41 ± 0.5; CTRL MPTP: 1.76 ± 0.17; ULK1.DN MPTP 1.41 ± 0.3 ng/mg wet tissue) and HVA (CTRL PBS: 1.75 ± 0.15; ULK1.DN PBS: 1.64 ± 0.12; CTRL MPTP: 0.99 ± 0.08; ULK1.DN MPTP: 0.91 ± 0.09 ng/mg wet tissue) also a prominent MPTP effect was still visible. In line with the measurements two weeks post MPTP treatment, levels of DA and its metabolites were not significantly altered by ULK1.DN expression could be shown (Balke et al. 2020).

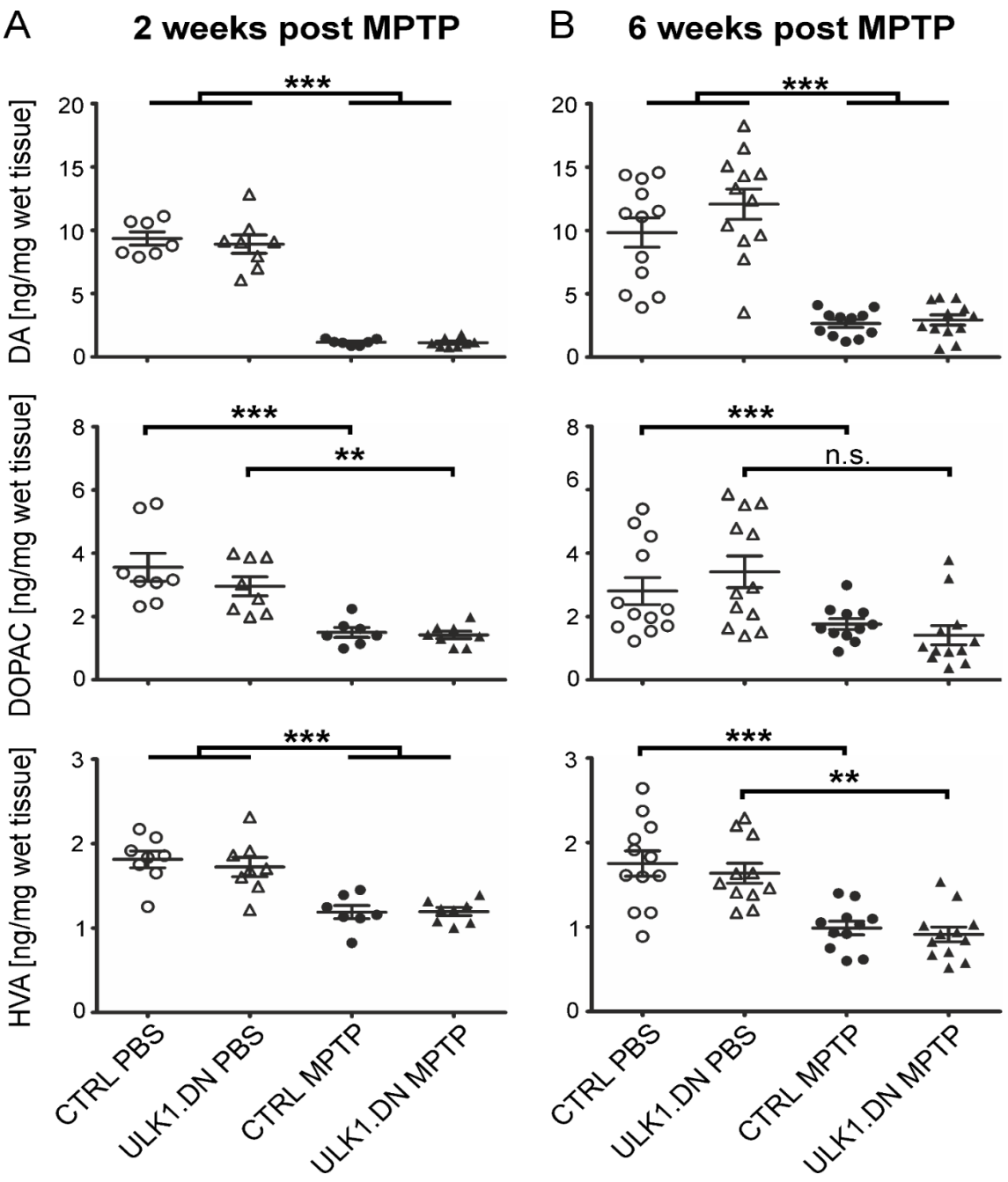

Figure 9 HPLC analysis of striatal dopamine and metabolites displays significant impairment of striatal dopaminergic terminals after MPTP treatment

Neurochemical detection of dopamine (DA) and its metabolites dihydroxyphenylacetic acid (DOPAC) and homovanillic acid (HVA) in the striatum of MPTP-treated mice expressing ULK1.DN and respective controls. (A) HPLC analysis two weeks after MPTP treatment, data are presented including means ± SEM; n = 7-8; *** $p < 0.001$; ** $p < 0.01$; ANOVA + Tukey posthoc test. (B) HPLC analysis six weeks after MPTP treatment, data are presented including means ± SEM; n = 11-12; *** $p < 0.001$; ** $p < 0.01$; n.s. = not significant; ANOVA + Tukey posthoc test. Modified from Balke et al. (2020), reprinted by permission from Springer Nature. The figure is part of the licensed content title "AAV-Mediated Expression of Dominant-Negative ULK1 Increases Neuronal Survival and Enhances Motor Performance in the MPTP Mouse Model of Parkinson's Disease", published by Dirk Balke, Lars Tatenhorst, Vivian Dambeck et al. in Molecular Neurobiology. https://link.springer.com/journal/12035 © Springer Nature (2020)

Table 12 Descriptive data of HPLC analysis

Experimental condition	**DA**	**DOPAC**	**HVA**
2 weeks post MPTP			
CTRL PBS	9.35 ± 0.52	3.56 ± 0.44	1.81 ± 0.10
ULK1.DN PBS	8.90 ± 0.73	2.95 ± 0.30	1.72 ± 0.11
CTRL MPTP	1.16 ± 0.09	1.50 ± 0.16	1.19 ± 0.08
ULK1.DN MPTP	1.12 ± 0.13	1.42 ± 0.12	1.20 ± 0.05
6 weeks post MPTP			
CTRL PBS	9.83 ± 1.16	2.80 ± 0.43	1.75 ± 0.15
ULK1.DN PBS	12.10 ± 1.19	3.41 ± 0.50	1.64 ± 0.12
CTRL MPTP	2.65 ± 0.31	1.76 ± 0.17	0.99 ± 0.08
ULK1.DN MPTP	2.93 ± 0.40	1.41 ± 0.30	0.91 ± 0.09

Levels of dopamine (DA), 3,4-dihydroxyphenylacetic acid (DOPAC) and homovanillic acid (HVA) in ng/mg wet tissue. Data given as mean ± SEM.

3.3 Behavioral tests

Due to the fact that MPTP has a systemic effect and causes DA degeneration in both hemispheres, its effects are not as easily detectable as in unilateral lesion models like the 6-hydroxydopamine model (Tatenhorst et al. 2014). However, I employed three different behavioral tests to detect potential alterations in animal motor behavior. The tests were conducted once before MPTP treatment started to get a baseline value, and then at two, four, and six weeks post MPTP treatment. If necessary, animals were pretrained before the first recorded testing.

3.3.1 Rotarod

Using the rotarod, mices' motor coordination, equilibrioception and endurance were tested. The test measured the time a mouse was running on the rotarod until it fell down. For statistical analysis, the mean of three runs was generated for each mouse.

After pretraining, but before MPTP treatment, all treatment groups showed a stable and comparable performance with no significant differences on the rotarod. Two weeks post MPTP treatment, surprisingly still no significant differences regarding the animals time on the rotarod were detectable (CTRL MPTP: 170 ± 11 s; ULK1.DN MPTP: 178 ± 25 s; CTRL PBS: 157 ± 17 s; ULK1.DN PBS: 159 ± 17 s; Figure 10 A) (Balke et al. 2020). Four weeks after MPTP treatment, also no significant difference was perceived when comparing the treatment groups (CTRL PBS: 183 ± 17 s; ULK1.DN PBS: 192 ± 15 s; CTRL MPTP: 172 ± 10 s; ULK1.DN MPTP 221 ± 21 s). Remarkably, at six weeks after MPTP treatment, a trend towards a longer timespan on the rotating rod in the ULK1.DN MPTP group ($p = 0.061$, ANOVA + Tukey posthoc test) compared to the CTRL MPTP group (CTRL PBS: 195 ± 16 s; ULK1.DN PBS: 215 ± 25 s; CTRL MPTP: 176 ± 19 s; ULK1.DN MPTP: 248 ± 16 s) was observed, thereby indicating a potential modulatory long-term effect of ULK1.DN expression on nervous connections involved in motor control after MPTP toxin exposure (Balke et al. 2020).

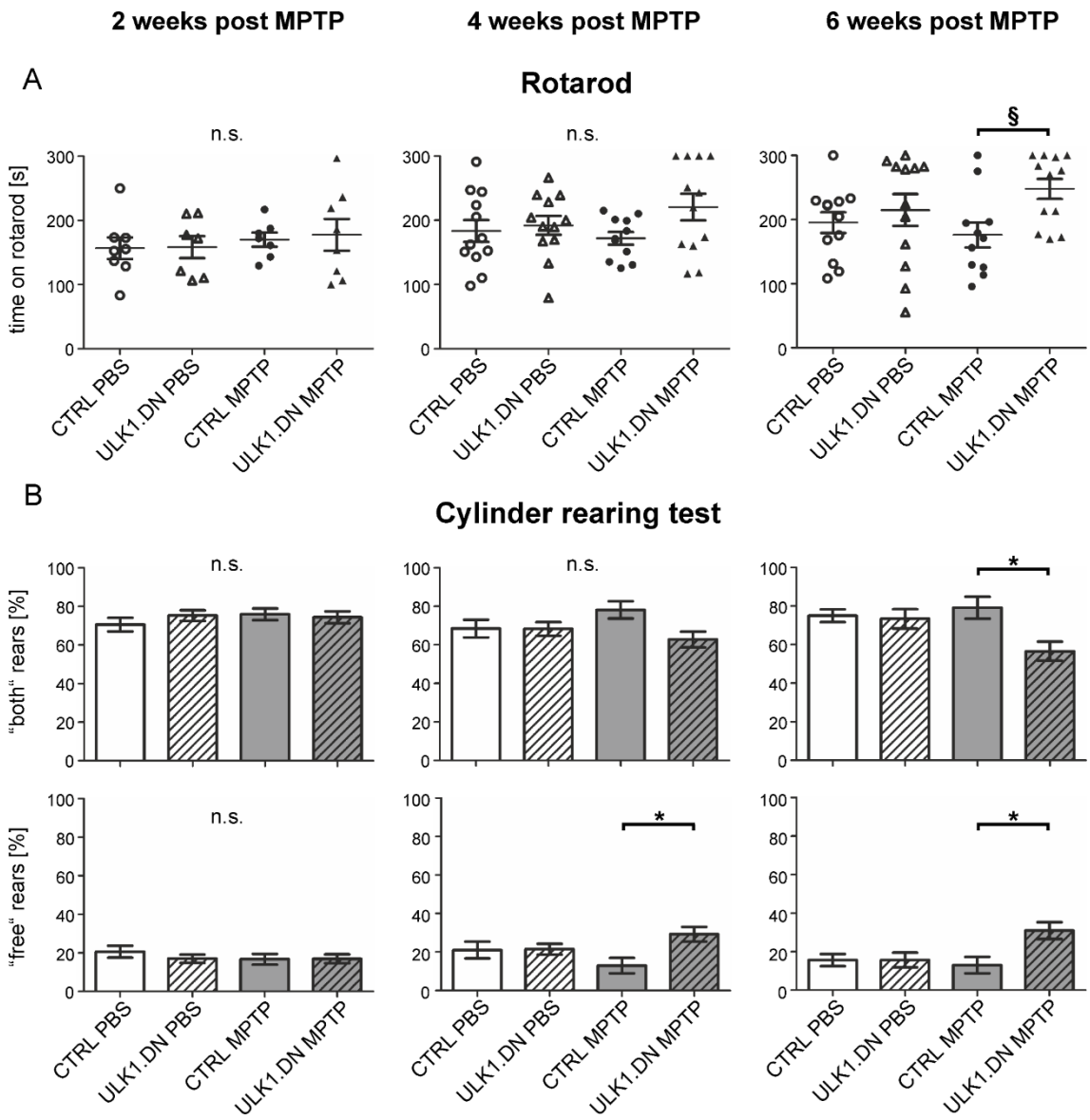

Figure 10 Behavioral analysis shows improved motor performance of mice expressing ULK1.DN after MPTP treatment

Analysis of motor behavior of MPTP-treated mice expressing ULK1.DN and respective controls was performed two, four and six weeks after MPTP intoxication. (A) Rotarod analysis showed a slightly improved motor performance after six weeks. Data are presented including means ± SEM; n = 7-8 (two weeks); n = 11-12 (four weeks); n = 11-12 (six weeks); § p = 0.061; n.s. = not significant; ANOVA + Tukey posthoc test. (B) Cylinder rearing test showed improved motor behavior at four and six weeks after MPTP treatment. Data are given as means ± SEM; n = 15-24 (two weeks); n = 15-24 (four weeks); n = 13-22 (six weeks); * $p < 0.05$; n.s. = not significant; ANOVA + Tukey posthoc test. Modified from Balke et al. (2020), reprinted by permission from Springer Nature. The figure is part of the licensed content title "AAV-Mediated Expression of Dominant-Negative ULK1 Increases Neuronal Survival and Enhances Motor Performance in the MPTP Mouse Model of Parkinson's Disease", published by Dirk Balke, Lars Tatenhorst, Vivian Dambeck et al. in Molecular Neurobiology. https://link.springer.com/journal/12035 © Springer Nature (2020)

3.3.2 Cylinder rearing test

Animals motor coordination and balance were also investigated with the help of the cylinder rearing. Since the stereotactic injections were only performed unilaterally into the right hemisphere, the test should also disclose possible side differences. For better comparison between relatively active and calm animals, the numbers of rears in the four categories (both, right, left or free) are given as relative numbers of the total rearing events (Balke et al. 2020).

Touches with only one paw against the cylinder wall were rare, each left and right accounting for about 5 % of all rears. Considering the proportion of right and left, a possible side effect due to the injection was successfully ruled out (see Figure 11; full data of means and respective SEM values are displayed in Table 13). There was no significant difference in right or left paw supported rears between the treatment groups, and also no preferability of one side in the total amount of one paw supported rears.

Two weeks post MPTP treatment, “both” assisted rears were most frequent (CTRL PBS: 70.6 ± 3.5; ULK1.DN PBS: 75.3 ± 2.8; CTRL MPTP: 75.9 ± 3.0; ULK1.DN MPTP: 74.4 ± 3.1; Figure 10 B), as has been described before (Tönges et al. 2012). However, no impaired sensorimotor coordination could be observed in the MPTP treated animals. The amount of “free” rears was smaller than the amount of “both” assisted rears (CTRL PBS: 20.6 ± 3.1; ULK1.DN PBS: 17.0 ± 2.2; CTRL MPTP: 16.7 ± 2.8; ULK1.DN MPTP: 16.9 ± 2.3), but also no significant differences in the amount of “free” rears between the treatment groups were found (Balke et al. 2020).

Four weeks after MPTP treatment, the number of “both” assisted rears was distinctly reduced in the ULK1.DN MPTP group, even though not yet statistically significant (CTRL PBS: 68.4 ± 4.5; ULK1.DN PBS: 68.3 ± 3.5; CTRL MPTP: 78.1 ± 4.4; ULK1.DN MPTP: 62.8 ± 4.0). However, the proportion of “free” rears was significantly elevated in ULK1.DN MPTP group after MPTP treatment in comparison to the CTRL MPTP group (CTRL PBS: 21.1 ± 4.3; ULK1.DN PBS: 21.5 ± 2.8; CTRL MPTP: 13.0 ± 4.0; ULK1.DN MPTP: 29.2 ± 3.8).

Six weeks after MPTP treatment, these differences were considerably larger, thereby a statistically significant effect was not only noted for “free” assisted rears (CTRL PBS: 15.7 ± 3.1; ULK1.DN PBS: 15.7 ± 3.8; CTRL MPTP: 13.1 ± 4.3; ULK1.DN MPTP: 31.0 ± 4.3), but also for “both” (CTRL PBS: 75.0 ± 3.3; ULK1.DN PBS: 73.3 ± 5.0; CTRL MPTP: 79.1 ± 5.6; ULK1.DN MPTP: 56.6 ± 5.0). These findings strongly suggest

genuine influence of ULK1.DN expression on animals motor performance in the MPTP mouse model (Balke et al. 2020). However, this significantly improved motor behavior of the ULK1.DN MPTP group six weeks post treatment is not reflected in higher striatal dopamine levels (Figure 8 B, Figure 9 B).

Table 13 Descriptive data of Cylinder rearing test analysis

Experimental condition	**Both [%]**	**Right [%]**	**Left [%]**	**Free [%]**
2 weeks post MPTP				
CTRL PBS	70.6 ± 3.5	5.5 ± 1.2	3.3 ± 1.0	20.6 ± 3.1
ULK1.DN PBS	75.3 ± 2.8	4.6 ± 1.1	3.2 ± 1.0	17.0 ± 2.2
CTRL MPTP	75.9 ± 3.0	2.4 ± 0.8	3.6 ± 1.4	16.7 ± 2.8
ULK1.DN MPTP	74.4 ± 3.1	3.0 ± 1.7	3.8 ± 1.0	16.9 ± 2.3
4 weeks post MPTP				
CTRL PBS	68.4 ± 4.6	6.3 ± 1.8	4.2 ± 1.3	21.1 ± 4.4
ULK1.DN PBS	68.3 ± 3.6	5.3 ± 1.8	3.5 ± 1.3	21.5 ± 2.8
CTRL MPTP	78.1 ± 4.5	2.7 ± 1.3	4.3 ± 1.4	13.0 ± 4.0
ULK1.DN MPTP	62.8 ± 4.1	5.1 ± 1.3	2.9 ± 1.0	29.2 ± 3.8
6 weeks post MPTP				
CTRL PBS	75.0 ± 3.4	4.4 ± 1.7	5.0 ± 1.6	15.7 ± 3.1
ULK1.DN PBS	73.3 ± 5.0	8.9 ± 2.6	2.1 ± 1.1	15.7 ± 3.8
CTRL MPTP	79.1 ± 5.6	3.8 ± 1.8	4.0 ± 1.6	13.1 ± 4.3
ULK1.DN MPTP	56.6 ± 5.0	3.2 ± 1.0	2.3 ± 0.9	31.0 ± 4.4

Number of rears supported by both paws, the left or the right paw as well as freely conducted rears in relation to the total number of rears [%]. Data given as mean ± SEM.

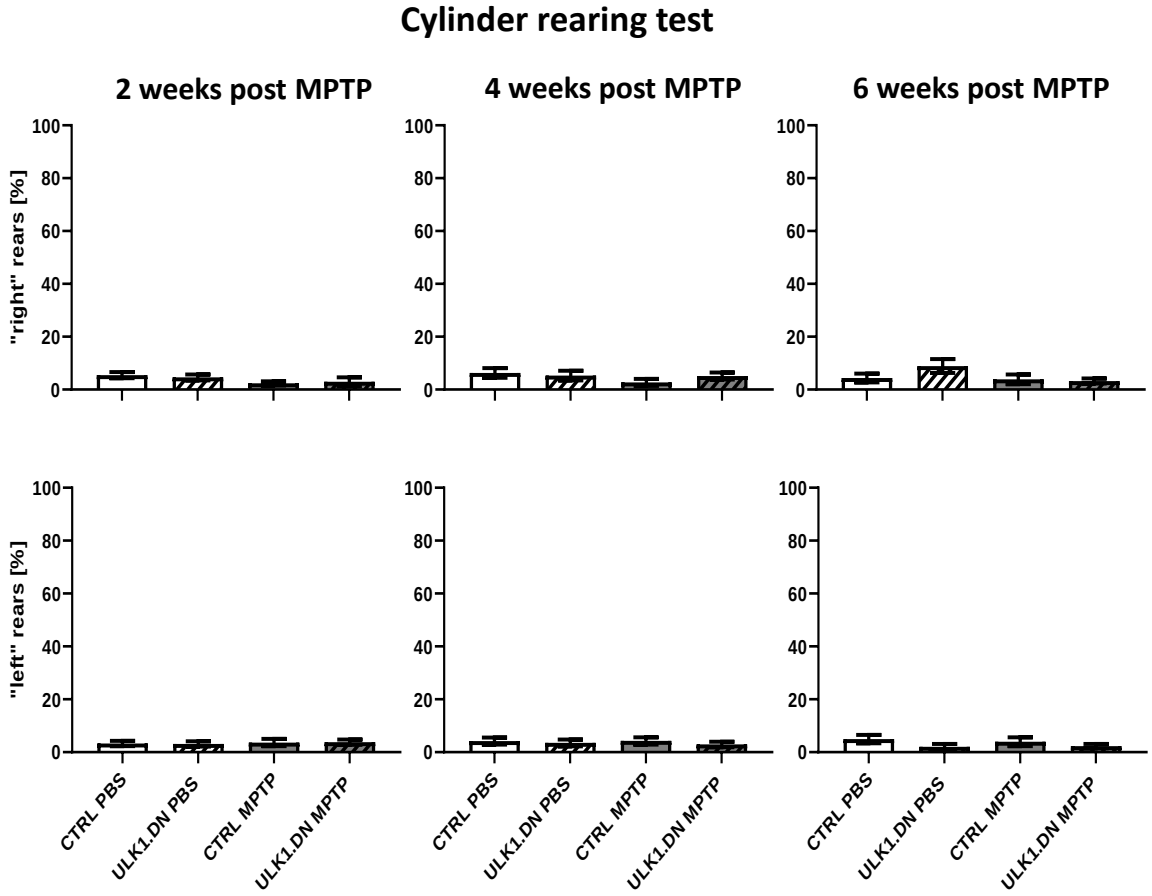

Figure 11 Cylinder rearing test revealed no unilateral preference in supportive paw use during rears

In addition to "both" and "free" rears also rears supported by either the right (A) or the left (B) paw were analyzed at the timepoints two, four and six weeks post MPTP treatment. Analysis of single paw-supported rears was conducted to reveal possible effects of the unilateral AAV injection. However, analysis did not disclose any side preferences as "left" and "right" rears were equally distributed. Data are given as means ± SEM; n = 15-24 (two weeks); n = 15-24 (four weeks); n = 13-22 (six weeks); n.s. = not significant; ANOVA + Tukey posthoc test.

3.3.3 Catwalk gait analysis

The Noldus catwalk XT is an automated system to gather 208 different variables in order to assess gait performance in rodents. It was employed to reveal possible motor deficits in the MPTP model as it has been useful in past studies of spinal cord injury (Bhimani et al. 2017) or synucleinopathy (Tatenhorst et al. 2016). For the analysis, special attention was paid to model-specific PD gait parameters like “run average speed”, “stride length” and “swing speed”. However, it turned out not to be sensitive enough as no significant changes could be detected between the different animal groups at all. A selection of exemplary gait parameters are depicted in Figure 12 with related means ± SEM in Table 14.

Table 14 Descriptive data of Catwalk gait analysis

Experimental condition	**Step sequence regularity index [%]**	**Run average speed [cm/s]**	**HP swing speed [cm/s]**	**HP stride length [cm]**
2 weeks post MPTP				
CTRL PBS	93.6 ± 1.5	16.1 ± 1.3	50.5 ± 3.3	5.9 ± 0.3
ULK1.DN PBS	95.6 ± 1.5	17.4 ± 1.6	50.8 ± 2.6	6.3 ± 0.3
CTRL MPTP	94.3 ± 1.5	13.7 ± 1.1	50.8 ± 4.0	5.7 ± 0.3
ULK1.DN MPTP	93.5 ± 2.3	13.2 ± 1.1	49.1 ± 2.2	5.3 ± 0.3
4 weeks post MPTP				
CTRL PBS	93.5 ± 1.5	16.5 ± 1.5	47.6 ± 2.9	6.0 ± 0.3
ULK1.DN PBS	95.7 ± 1.2	19.2 ± 1.1	53.1 ± 3.0	7.1 ± 0.4
CTRL MPTP	97.2 ± 0.7	17.7 ± 1.5	51.5 ± 3.5	7.3 ± 0.4
ULK1.DN MPTP	96.7 ± 1.1	20.2 ± 1.9	54.8 ± 1.8	6.8 ± 0.6
6 weeks post MPTP				
CTRL PBS	92.9 ± 1.1	21.1 ± 1.8	60.7 ± 2.6	6.2 ± 0.3
ULK1.DN PBS	96.9 ± 0.8	26.3 ± 3.2	60.2 ± 5.0	7.4 ± 0.5
CTRL MPTP	96.4 ± 1.7	20.1 ± 1.6	58.4 ± 3.2	6.5 ± 0.4
ULK1.DN MPTP	96.0 ± 0.6	22.9 ± 3.5	71.4 ± 8.0	6.8 ± 0.5

Data of four exemplary, potentially altered gait parameters given as mean ± SEM. HP: hind paw.

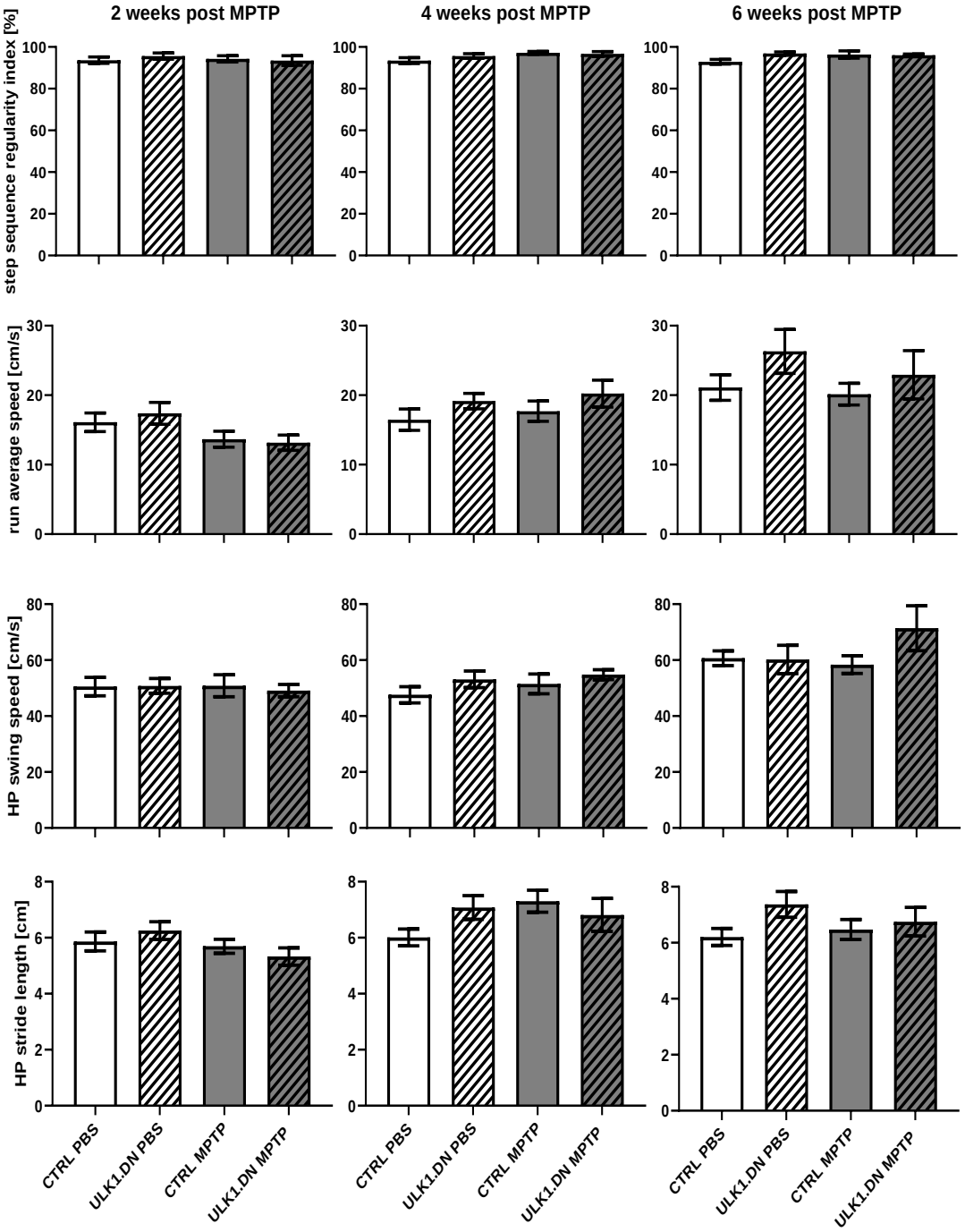

Figure 12 Catwalk gait analysis reveals no alteration in gait pattern post MPTP treatment

Gait analysis was conducted two, four and six weeks post MPTP treatment utilizing the Noldus software. Depicted parameters are exemplary for over 200 gait parameters analyzed and particularly prone to undergo changes in PD. However, no significant changes neither in the specific, displayed parameters step sequence regularity (A), run average speed (B), HP swing speed (C) and HP (hindpaw) stride length (D), nor in the other analyzed parameters (data not shown) were detected upon MPTP treatment. Data are given as means ± SEM; n = 7-8 (for all time points); ANOVA.

3.4 Western blot analysis

3.4.1 Quantification of autophagy and cell survival associated protein levels in mibrain tissue six weeks after MPTP treatment

Western blot analysis was conducted to investigate regulatory influences of ULK1.DN expression on autophagic and cell survival pathways six weeks post MPTP treatment. Due to methodical restrictions in preparation, tissue of the whole midbrain was used for the analysis. For a meaningful quantification of ULK1.DN expression-mediated effects on the downstream autophagy cascade, the LC3-II/-I ratio was determined (Balke et al. 2020). It is considered as a useful marker in monitoring of autophagy, as cytoplasmatic LC3-I hydrolyses a small polypeptide and turns into autophagosome membrane-associated LC3-II upon autophagy induction (Kang et al. 2019). The LC3-II/-I ratio was not found to be significantly altered in the ULK1.DN treatment group in comparison to controls (CTRL PBS: 1.0 ± 0.2; ULK1.DN PBS: 1.5 ± 0.2; CTRL MPTP: 1.2 ± 0.2; ULK1.DN MPTP: 1.8 ± 0.2; Figure 13 B) (Balke et al. 2020). Another well-established monitoring parameter for autophagy is p62. It delivers ubiquitinated proteins for autophagic degradation and accumulates if autophagic flux is impaired (Klionsky et al. 2016). Therefore, inhibitory properties of AAV-mediated ULK1.DN expression on autophagic activity were confirmed by significantly elevated p62 levels in the ULK1.DN MPTP group in relation to control (CTRL PBS: 1.0 ± 0.1; ULK1.DN PBS: 1.6 ± 0.2; CTRL MPTP: 0.9 ± 0.1; ULK1.DN MPTP: 2.0 ± 0.2; Figure 13 C) (Balke et al. 2020). A complementary immunohistochemical analysis confirmed the finding of increased p62 expression in the SNpc (see also Figure 14). Directly linked to ULK1 are its upstream regulators mTOR and AMPK (Kim et al. 2011), which were also analyzed. Apparently, ULK1.DN expression triggered activation of mTOR signaling, which was indicated by significantly increased levels of mTOR (CTRL PBS: 1.0 ± 0.08; ULK1.DN PBS: 1.5 ± 0.1; CTRL MPTP: 1.21 ± 0.1; ULK1.DN MPTP: 1.6 ± 0.1; Figure 13 D), as wells as p-mTOR (CTRL PBS: 1.0 ± 0.1; ULK1.DN PBS: 1.6 ± 0.2; CTRL MPTP: 1.2 ± 0.1; ULK1.DN MPTP: 1.8 ± 0.1; Figure 13 E) in ULK1.DN MPTP mice in comparison to controls (Balke et al. 2020). Again, a complementary immunohistochemical analysis confirmed the finding of increased mTOR expression in the SNpc (see Figure 15). However, no regulatory influence of ULK1.DN expression on AMPK and pAMPK levels was detected (Figure 13 F+G, for means ± SEMs see Table 15). Extracellular signal-regulated kinase (ERK) 1/2 are important components of the MAPK system, which

negatively regulate mTOR and thereby promote ULK1 protein expression (Xu et al. 2018). However, no significant regulation of ERK1/pERK1 (Figure 13 H+I), as well as ERK2/pERK2 (Figure 13 K+L) upon ULK1.DN expression could be observed. Finally, Ribosomal protein S6 kinase beta-1 (pS6), which also negatively regulates mTOR, was analyzed, but it was not found to be significantly regulated either (Figure 13 J, all corresponding means ± SEMs see Table 15).

Table 15 Descriptive data of Western blot analysis

	Experimental condition			
Analyzed protein	CTRL PBS	ULK1.DN PBS	CTRL MPTP	ULK1.DN MPTP
p62/GAPDH, normalized to CTRL PBS	1.0 ± 0.15	1.67 ± 0.21	0.97 ± 0.14	2.0 ± 0.25
AMPK/actin, normalized to CTRL PBS	1.0 ± 0.13	1.59 ± 0.31	1.11 ± 0.16	1.53 ± 0.30
pAMPK/actin, normalized to CTRL PBS	1.0 ± 0.14	1.29 ± 0.12	0.97 ± 0.13	1.31 ± 0.09
ERK1/tubulin, normalized to CTRL PBS	1.0 ± 0.24	1.08 ± 0.25	0.94 ± 0.40	1.25 ± 0.35
pERK1/GAPDH, normalized to CTRL PBS	1.0 ± 0.16	1.55 ± 0.29	1.06 ± 0.24	1.3 ± 0.31
ERK2/tubulin, normalized to CTRL PBS	1.0 ± 0.19	1.16 ± 0.26	1.41 ± 0.52	1.55 ± 0.40
pERK2/GAPDH, normalized to CTRL PBS	1.0 ± 0.33	0.82 ± 0.20	0.42 ± 0.13	0.74 ± 0.30
LC3ratio/tubulin, normalized to CTRL PBS	1.0 ± 0.29	1.53 ± 0.24	1.27 ± 0.26	1.8 ± 0.22
mTOR/actin, normalized to CTRL PBS	1.0 ± 0.08	1.49 ± 0.14	1.21 ± 0.13	1.6 ± 0.14
p-mTOR/actin, normalized to CTRL PBS	1.0 ± 0.13	1.65 ± 0.21	1.24 ± 0.15	1.85 ± 0.17
pS6/tubulin, normalized to CTRL PBS	1.0 ± 0.21	0.66 ± 0.12	0.79 ± 0.19	1.16 ± 0.18

Data given as mean ± SEM.

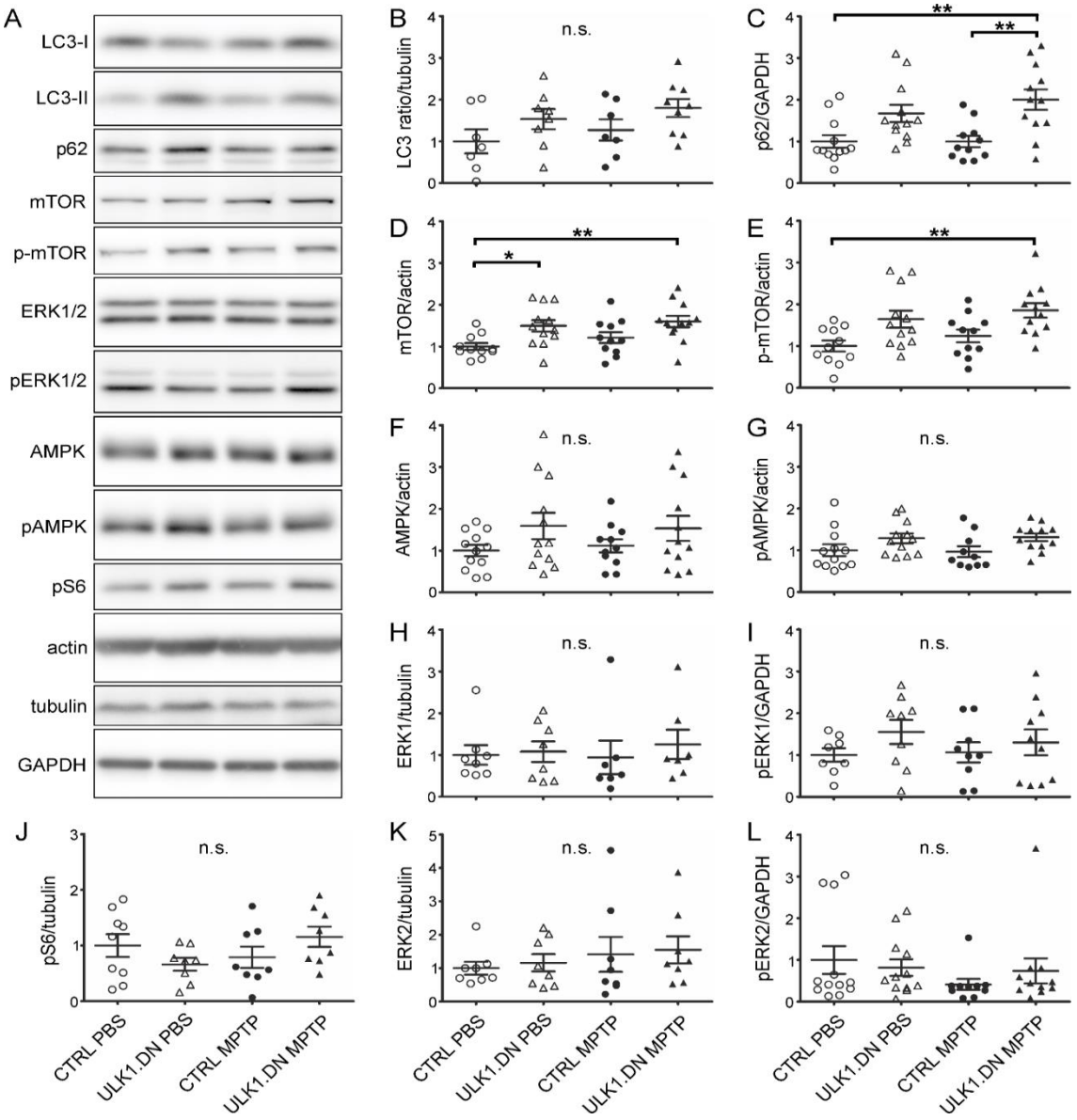

Figure 13 Western blot analysis reveals ULK1.DN-mediated down-regulation of autophagy and activation of mTOR signaling

Western Blot analysis was per formed from mouse midbrain tissue six weeks after MPTP treatment. (A) Representative Western blots of all analyzed proteins are displayed. The expression of each protein was adjusted to the respective housekeeping gene and normalized to sham control. (B) Analysis of LC3 ratio (n = 7-9) normalized to tubulin. (C) p62 levels (n = 11-12) normalized to GAPDH. (D, E) mTOR (n = 11-12) and p-mTOR (n = 11-12) levels normalized to actin. (F, G) AMPK (n = 11-12) and pAMPK (n = 10-12) normalized to actin. (H, I) ERK1 (n = 7-8) normalized to tubulin and pERK1 (n = 8-10) normalized to GAPDH. (J) pS6 (n = 8-9) normalized to tubulin. (K,L) ERK2 (n = 8) normalized to tubulin and pERK2 (n = 10-12) normalized to GAPDH. All data given including means and SEM; ** $p < 0.01$; * $p < 0.05$; n.s. = not significant; ANOVA + Tukey posthoc test. Modified from Balke et al. (2020), reprinted by permission from Springer Nature. The figure is part of the licensed content title "AAV-Mediated Expression of Dominant-Negative ULK1 Increases Neuronal Survival and Enhances Motor Performance in the MPTP Mouse Model of Parkinson's Disease", published by Dirk Balke, Lars Tatenhorst, Vivian Dambeck et al. in Molecular Neurobiology. https://link.springer.com/journal/12035 © Springer Nature (2020)

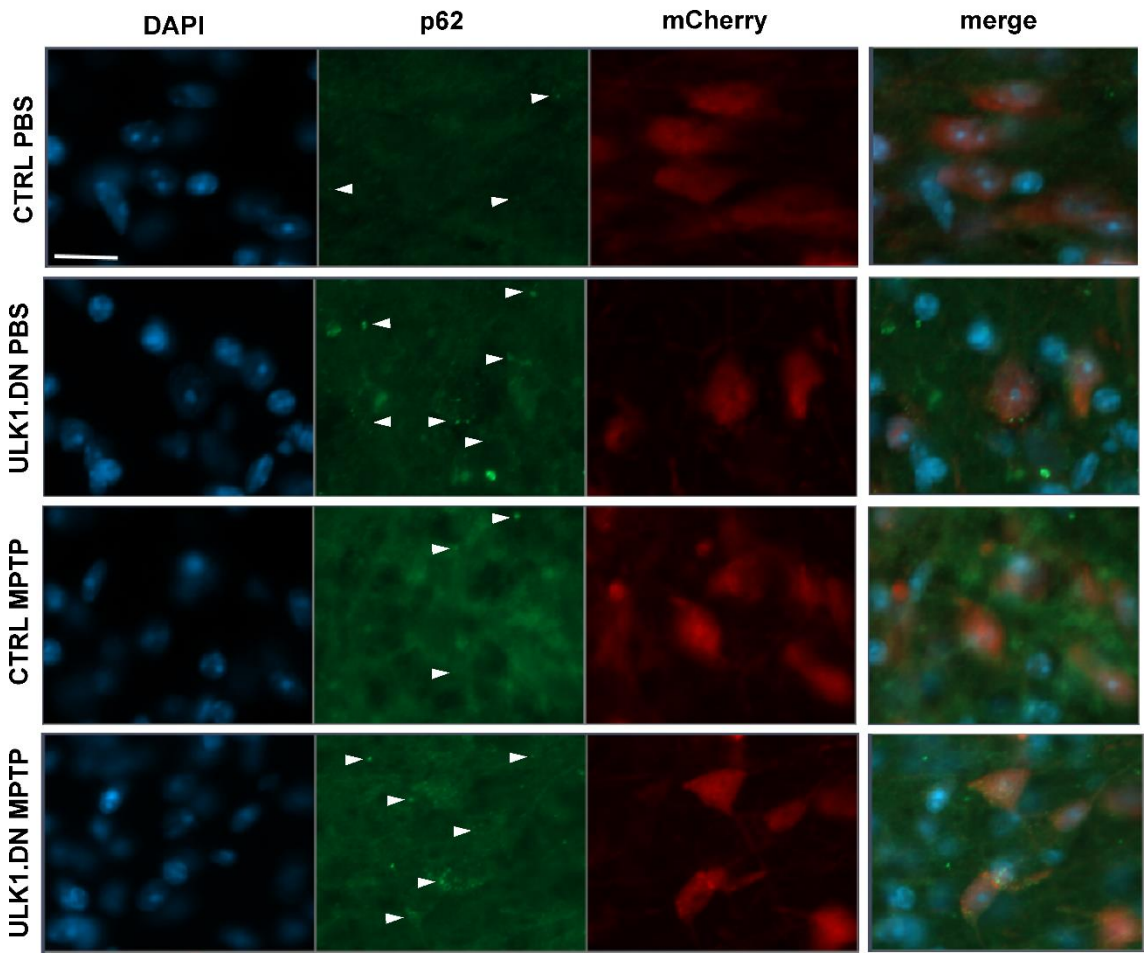

Figure 14 Immunohistochemical analysis of p62 in the substantia nigra pars compacta (SNpc)

Representative micrographs of the SNpc of each treatment group. All sections are stained for p62, cell nuclei are counterstained with DAPI and virus-transduced cells display the mCherry signal. There is a visible increase of p62 protein after ULK1.DN expression. White arrowheads indicate p62 signal. Scale bar: 50 µm. Modified from Balke et al. (2020), reprinted by permission from Springer Nature. The figure is part of the licensed content title "AAV-Mediated Expression of Dominant-Negative ULK1 Increases Neuronal Survival and Enhances Motor Performance in the MPTP Mouse Model of Parkinson's Disease", published by Dirk Balke, Lars Tatenhorst, Vivian Dambeck et al. in Molecular Neurobiology. https://link.springer.com/journal/12035 © Springer Nature (2020)

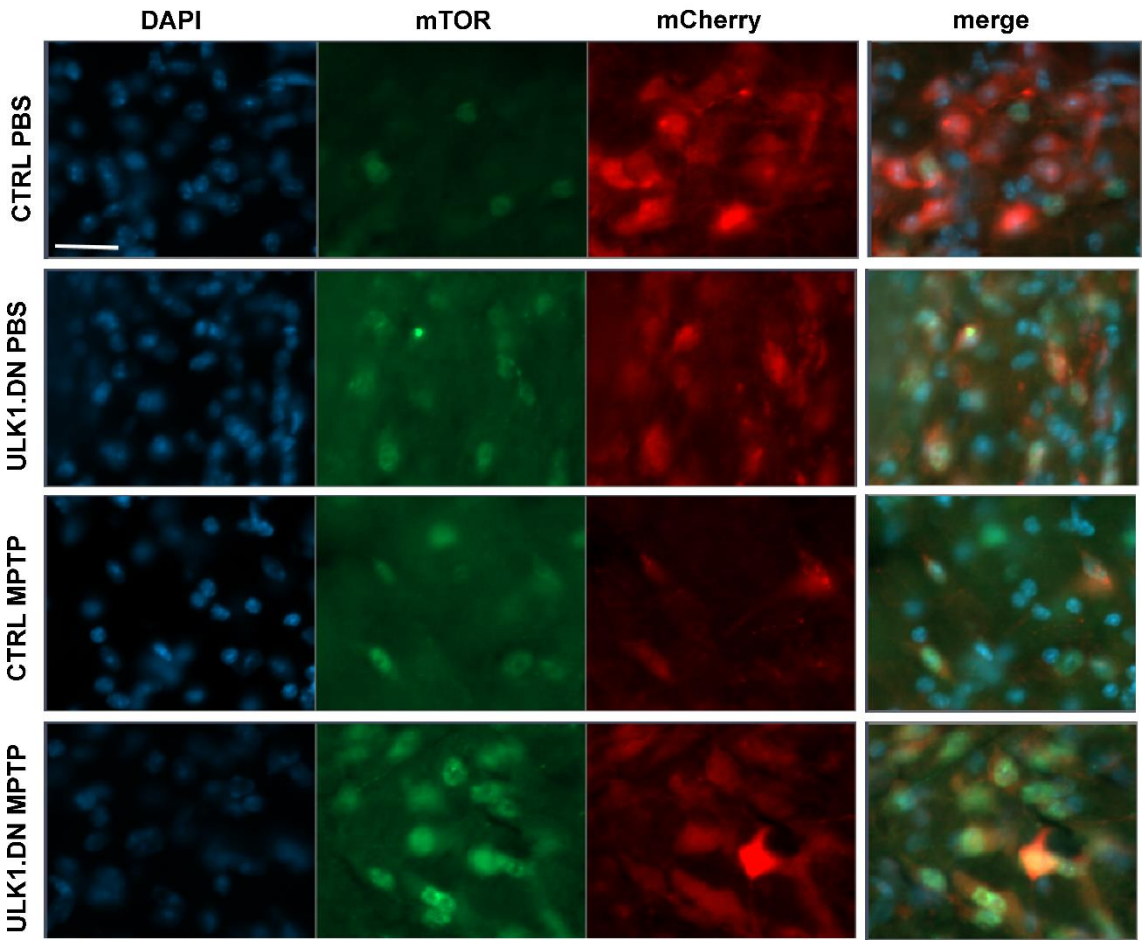

Figure 15 Immunohistochemical analysis of mTOR in the substantia nigra pars compacta (SNpc)

Representative micrographs of the SNpc of each treatment group. All sections are stained for mTOR, cell nuclei are counterstained with DAPI and virus-transduced cells display the mCherry signal. There is a visible increase of mTOR protein after ULK1.DN expression. Scale bar: 50 µm. Modified from Balke et al. (2020), reprinted by permission from Springer Nature. The figure is part of the licensed content title "AAV-Mediated Expression of Dominant-Negative ULK1 Increases Neuronal Survival and Enhances Motor Performance in the MPTP Mouse Model of Parkinson's Disease", published by Dirk Balke, Lars Tatenhorst, Vivian Dambeck et al. in Molecular Neurobiology. https://link.springer.com/journal/12035 © Springer Nature (2020)

4 Discussion

4.1 The role of autophagy and axonal degeneration in PD

PD is a common neurodegenerative disease with a prevalence of about 1 % in people aged over 60 (Tysnes and Storstein 2017). In the consequence of still missing valid biomarkers for an early diagnosis of the disease, in most of the cases the diagnosis cannot be ascertained until clinical disease symptoms emerge (Batistela et al. 2017). At this timepoint, already a severe neuronal loss and degeneration especially of the nigro-striatal system has taken place. This underlines the need of either efficient neurorestorative therapies or neuroprotective therapies in combination with reliable biomarkers. However, no causal therapy is available by now. This is in spite of or just due to the several pathomechanisms that have been elucidated during the last years and that are likely to be responsible for the most sporadic cases of PD in a multifactorial etiology (Salat et al. 2016).

Autophagy, as a highly conserved intracellular degradation and recycling process, is essential for maintaining cellular homeostasis (Mizushima and Komatsu 2011). Perturbation of this delicate process has been implicated not only in PD, but in a variety of neurodegenerative and also other disorders (Menzies et al. 2015). Among the most important pathomechanisms behind PD, are disrupted proteolysis and mitochondrial dysfunction, two systems with an existing crosstalk. Impaired autophagy includes disrupted mitophagy and leads to an accumulation of defective mitochondria, thereby increasing the burden of ROS and ultimately leading to cell death (Corti 2019). Vice versa, mitochondrial damage is able to impair the biogenesis of lysosomes, causing failure in the ALP (Plotegher and Duchen 2017). Consequently, the protection and retrieval of physiological autophagy and ALP function are crucial objectives in potential PD therapies.

An increase in autophagic vesicles in *post mortem* brain tissue of PD patients has been observed already more than 15 years ago, thereby suggesting that autophagy plays a role in the pathogenesis of PD (Zhu et al. 2003). However, the debate on how increased levels of autophagosome formation have to be interpreted when monitoring autophagy is still going on. They might indicate surplus production in terms of increased autophagic flux or accumulate in response to a reduced autophagic flux (Banerjee et al. 2010). Results of *post mortem* brain tissue analyses in PD patients showing perturbations of autophagy

protein levels may represent a causal aspect in the early stage of PD pathogenesis. Yet they could also represent the end state of a dysregulatory neurodegenerative process (Dagda et al. 2013).

Much attention has been paid to inclusion bodies, disrupted proteolysis and possible ways to protect cell somata of dopaminergic neurons, also with the help of autophagy stimulation (Miki et al. 2016; Cerri and Blandini 2018).

Until now, it has been largely overlooked that targeting the axonal compartment might be of even higher therapeutic value, due to the fact that the degeneration in human PD, as well as in the MPTP mouse model, does not start in the dopaminergic cell body but in the striatal projections. Therefore, increasing attention was paid to axonal degeneration (Kurowska et al. 2016). Autophagy has been shown to be involved in the degradation process in different cell culture and animal studies on AAD (Koch et al. 2010; Lingor et al. 2012; Ribas et al. 2017; Vahsen et al. 2020). Focusing on the axonal compartment in CNS diseases, previous work of our group pointed out that axonal degeneration is mediated by rapid and massive Ca^{2+} influx and exaggerated upregulation of autophagy (Knöferle et al. 2010). In this setting, inhibition of autophagy with 3-MA showed neuroprotective properties leading to attenuated ultrastructural changes and axonal loss (Koch et al. 2010).

The initiation complex of the autophagy cascade is comprised of ULK1, ATG13, FIP200 and ATG101, with ULK1 as the central player (Menzies et al. 2015). In an *in vitro* study on alpha-synuclein aggregation upregulation of ULK1 was reported, which might reflect attempts of a compensatory upregulation of autophagy to clear the excess protein (Miki et al. 2016). Furthermore, increasing levels of especially oligomeric alpha-synuclein have been linked to autophagy dysregulation (Bengoa-Vergniory et al. 2017). However, in brain tissue from human patients diseased with PD or dementia with Lewy bodies (DLB) no such upregulation of ULK1 could be detected (Miki et al. 2016). A subsequent study looking at autophagy protein levels in lympho- and monocytes obtained from PD patient's blood did show significantly increased levels of ULK1 compared with age-matched controls (Miki et al. 2018). Furthermore, ULK1 protein levels measured in those cells positively correlated with the levels of oligomeric alpha-synuclein and paralleled clinical severity of the disease. This may represent first *in vivo* evidence of an interaction between oligomeric alpha-synuclein and autophagy (Miki et al. 2018). As no change in the

expression of LC3 could be detected, the autophagic pathway is likely blocked at some stage before substrate degradation (Miki et al. 2018).

Besides its key role in autophagy initiation, ULK1 was shown to impact on axonal transport via regulation of motor-cargo association (Toda et al. 2008). Furthermore, there is evidence that ULK1 is required for orderly endocytosis of nerve growth factor (NGF) and suppression of profuse axonal branching during outgrowth (Zhou et al. 2007).

A dominant-negative form of ULK1 (ULK1.DN) was previously reported as a new approach to target the key protein of autophagy initiation. ULK1.DN leads to an isolated expression of the protein's C-terminal domain without the required kinase and phosphorylation sites for autophagic activity (Chan et al. 2009). ULK1.DN was successfully employed in previous studies of our group. In cell culture experiments with neurons derived from rat cortex that were transduced with an ULK1.DN expressing AAV1/2 vector, as well as in a model of spinal cord injury (SCI) and optic nerve crush experiments *in vivo,* autophagy was successfully competitively inhibited (Koch et al. 2010; Ribas et al. 2017; Vahsen et al. 2020). The inhibition resulted in decreased axonal degeneration and fostered neurite outgrowth after axotomy. The *in vivo* studies showed attenuated axonal degeneration after SCI and attenuated axonal degeneration after optic nerve crush when inhibiting autophagy via ULK1.DN expression, by employment of the ULK1 inhibitor SBI-0206965 (Vahsen et al. 2020). Based on this groundwork, this study intended to evaluate the neuroprotective potential of ULK1.DN-mediated inhibition of autophagy in the MPTP mouse model.

4.2 Limitations of the MPTP model

Today, the MPTP toxin model is one of the most commonly used ones to test for neuroprotective and neurorestorative treatments (Kin et al. 2019). The MPTP model has advantages over other toxin-induced PD models because it selectively targets dopaminergic structures and causes a virtually identical motor phenotype in men as Parkinson's disease does (Jackson-Lewis and Przedborski 2007). The toxin is employable in several species, but is applied in rodents and non-human primates with special emphasis. While the primates develop human-like motor symptoms and impairment, these tend to be much weaker and reversed over time in rodents. However, due to economical and ethical restraints, only few laboratories work with PD primate models. Based on the relative MPTP insensitivity of rats, mice are the most frequently used

animals for pre-clinical testing of neuroprotective and neurorestorative treatments (Schmidt and Ferger 2001). Unfortunately, in the past, many promising neuroprotective agents discovered in the mouse model failed when transferred into clinical trials. To bridge the gap between mice and men and as an encouraging alternative to the employment of primates, a recently established MPTP model in Göttingen minipigs (Nielsen et al. 2016) might help. Although Lewy bodies represent the histopathological hallmark of PD, they are neither found in MPTP treated mice nor in the minipigs or in the non-human primates.

We decided to give preference to the MPTP mouse model rather than the 6-Hydroxydopamine (6-OHDA) rat model for various reasons: As mentioned above, MPTP is more selective for DAergic neurons, while 6-OHDA also targets catecholaminergic neurons throughout the brain. Moreover, 6-OHDA requires intraparenchymal injection as it is incapable of blood-brain barrier transfer, but we already needed to inject the AAV.ULK1.DN directly into the SNpc. Finally, recent studies argue for a relevance of mitochondrial impairment in PD (Larsen et al. 2018) which is modelled better by employment of MPTP than 6-OHDA because MPTP predominately targets complex I of the respiratory chain.

The administration of MPTP was scheduled once a day for five consecutive days with a dose of 30mg/kg bw to generate a ‘subchronic PD model’ (Jackson-Lewis and Przedborski 2007). Considering the immunohistochemical analysis of TH^+ and Nissl cell count with a reduction of 50 % in total numbers per SN two weeks post MPTP treatment, it can be concluded that the model worked properly. This is strengthened by the depletion of > 90 % of dopamine in the murine striatum two weeks post MPTP treatment and in line with the literature published employing this particular MPTP regime (Tönges et al. 2012; Huang et al. 2017).

4.3 Autophagy inhibition via ULK1.DN overexpression exhibits beneficial properties in the MPTP mouse model of PD

4.3.1 ULK1.DN overexpression protects dopaminergic nigral cell bodies from MPTP-induced degeneration and preserves dopaminergic striatal terminals

The intracerebral injections of the AAV vectors had no influence on intranigral TH^+ cell numbers when PBS injected animals with and without stereotactic surgery were compared to assess possible harmful effects of the surgical procedure. Besides, the obtained numbers of the stereological counting of TH^+ and $Nissl^+$ cells were in line with previously published results (Tönges et al. 2012; Saal et al. 2015). Accordingly, no impact on the nigral DAergic cell count in the injected hemisphere by mechanic injury due to injection or the AAV itself was present.

Two weeks post MPTP treatment, a significant (> 50 %) reduction in TH^+ cells occurred in the MPTP CTRL mice as compared to the CTRL PBS mice. The fact that the quantification of $Nissl^+$ cells showed a similar decrease ruled out a mere downregulation of TH expression and proved that the observed reduction was due to toxin induced specific dopaminergic cell death. In animals expressing ULK1.DN, the reduction in TH^+ or $Nissl^+$ cell numbers due to MPTP exposure was not significant. However, the ULK1.DN MPTP group displayed a significantly higher amount of preserved DAergic cell bodies than the CTRL MPTP group, indicating a successful neuroprotection of the DAergic cell bodies from MPTP-induced cell death two weeks post MPTP treatment. The amount of preserved DAergic neurons at a rate of 95 % was even higher than in previous successful studies with the subchronic MPTP paradigm, reaching a rescue of 81 % after employing the rho kinase inhibitor fasudil (Tönges et al. 2012).

Considering the fact that PD pathology apparently starts in the axons and not in the cell body (Burke and O'Malley 2013), also the striatal TH^+ fiber density was evaluated two weeks post MPTP treatment. As expected, the degeneration of the terminals was more pronounced than the one of the cell bodies: In the CTRL MPTP group only 45 % of the TH^+ signal intensity was preserved compared to the CTRL PBS group two weeks post treatment. The reduction in relative striatal density of ULK1.DN MPTP in comparison to ULK1.DN PBS was also significant but less pronounced than for the CTRL MPTP/CTRL PBS group. Again, the ULK1.DN MPTP group shows a significantly higher preservation in comparison to the CTRL MPTP group, indicating a morphologically protective effect

of the ULK1.DN overexpression and subsequent autophagy impairment. The lower protection efficiency compared to the protective effect on the nigral DAergic cell bodies may be due to the fact that the degeneration described as a ‘dying back’ in literature (Dauer and Przedborski 2003) starts in the terminals and is just more advanced in the striatum than in the SNpc two weeks post treatment. This sequence has not only been assumed for PD in humans but has already been confirmed in the MPTP mouse model (Li et al. 2009). Another reason may be the fact that the AAV vector was injected into the SNpc and had to be transported along the axons into the striatum. Consequently, a higher transduction of the nigral perikarya ensured better protection of the cell soma in comparison to the distal terminals.

Six weeks post MPTP treatment, a recovery of striatal density values to the amount of the PBS treated CTRL group was observed in the CTRL MPTP group. Thus, there was not only no MPTP effect visible anymore, but a complete morphological restoration of TH^+ fibers had taken place. This phenomenon was already described before (Jakowec et al. 2004) and may be explained by genuine enzyme replacement or simple reoccurrence of TH^+ immunoreactivity after temporary suppression. For ULK1.DN MPTP, the same observation of complete morphological restauration was made. Thus, with the exceptionality that the relative striatal density in fact surpassed the one of the ULK1.DN PBS group, thereby indicating the possibility of a positive long-term effect on neuro-regeneration and stabilization of dopaminergic terminals. This observation emphasizes the findings of the improved behavioral performance in the cylinder rearing test six weeks post MPTP treatment. The improved rearing behavior may be explained by a higher number of functional dopaminergic fibers and/or synapses in the murine striatum leading to quantifiable enhanced number of free rears as a valid indicator of improved balance and motor coordination. Alternatively, a positive modulatory effect of ULK1.DN expression on extrastriatal dopaminergic projections might be a suitable explanation for the improved motor function, as alterations of these were recently encountered in PD patients (Masilamoni and Smith 2018; Pilotto et al. 2019)

The absolute number of TH^+ and $Nissl^+$ cells remained higher for MPTP exposed ULK1.DN animals compared to CTRL MPTP animals (and also higher for the respective ULK1.DN PBS group compared to CTRL PBS) six weeks post MPTP treatment. However, opposed to the analysis two weeks post MPTP treatment, the cell count of ULK1.DN MPTP was not significantly elevated in comparison to CTRL MPTP anymore.

This reduction of effect might be due to several factors, one most likely being intrinsic, compensatory neuro-regeneration (Mitsumoto et al. 1998). Rodents are capable of this self-repair mechanism to a much bigger extent than humans (Obernier and Alvarez-Buylla 2019). Another contributing factor might be a weakened expression of the ULK1.DN gene product during time and/or reactive modulation of downstream intracellular signaling pathways, thereby reducing the initial effect size.

4.3.2 ULK1.DN overexpression does not rescue intrastriatal dopamine levels from MPTP-induced depletion

In search of a correlation between preserved striatal fiber density and preserved levels of DA and its metabolites as a possible indicator of functional maintenance, a HPLC analysis of striatal lysates was conducted. The extent of DA depletion was much higher than the reduction of striatal fiber density: Two weeks post MPTP treatment, nearly total DA depletion was found in both ULK1.DN MPTP and CTRL MPTP animals. Therefore, ULK1.DN overexpression was not able to lessen MPTP effects on intrastriatal neurochemical homeostasis. The observation of a stronger reduction of dopamine and metabolite levels in the striatum compared to the reduction of relative striatal density however, is in line with findings from earlier studies (Tönges et al. 2012; Tatenhorst et al. 2014; Saal et al. 2015). At six weeks post MPTP treatment, the DA levels were partly restored, but there was no significant difference between the CTRL MPTP and the ULK1.DN MPTP group. A prominent MPTP effect was still present, meaning the CTRL PBS and ULK1.DN PBS group had significantly higher values of DA than the respective MPTP groups. Considering absolute values, ULK1.DN PBS and ULK1.DN MPTP showed slightly higher DA levels than the corresponding CTRL PBS and MPTP group. However, the difference in DA levels between ULK1.DN MPTP and CTRL MPTP is too minimal to be held responsible for the displayed improved motor behavior of ULK1.DN MPTP animals in the cylinder test six weeks post MPTP treatment. This strongly suggests that it is not the level of the neurotransmitter which is crucial for the enhanced motor performance in this case. Otherwise there must have also been a significant impairment of motor behavior already two weeks post MPTP treatment in MPTP treated animals because the DA levels of the PBS treated experimental groups at that time point exceeded the ones of the ULK1.DN MPTP group six weeks post MPTP treatment without raising any significant differences in motor behavior at two weeks post MPTP. Another

explanation may be a higher number of dopaminergic axons which is supported by the elevated striatal density in ULK1.DN MPTP groups at six weeks post MPTP treatment and/or synapses and consequently enhanced functionality due to an increased sprouting of terminals under the influence of ULK1.DN expression upon MPTP treatment.

Along with the depletion of DA, there was also a diminished amount of DOPAC and HVA found in the MPTP treated experimental groups two weeks post treatment. These reductions were not as pronounced as the one of dopamine but still highly significant and in line with previous studies (Tönges et al. 2012).

4.3.3 ULK1.DN overexpression improves long-term motor behavior after MPTP treatment

Of the three employed behavioral tests, only the cylinder rearing test yielded significant changes in the motor behavior of the animals. The Catwalk XT gait analysis did not show any differences between the treatment groups and time points. While the Noldus software proved itself in assessment of gait disturbances due to spinal cord injury (Bhimani et al. 2017), synucleinopathy (Tatenhorst et al. 2016) or multiple sclerosis (Bernardes and Oliveira 2017), it failed to reveal discreet MPTP related motor alterations. The difficulty in analyzing the effects of this toxic agent, of course, is the systemic effect in comparison to 6-OHDA, which is a unilateral lesion model of PD and therefore was successfully assessed with the catwalk software before (Saal et al. 2015).

Interestingly, neither the rotarod nor the cylinder test displayed significant differences in terms of endurance, equilibrioception and motor coordination between the PBS and the MPTP treated animals two weeks post MPTP treatment. This is contradictory to already published results using the same MPTP model (Tönges et al. 2012). However, other studies using the same subchronic MPTP model even found improved motor performance e.g. on the rotarod in the MPTP treated group compared to CTRL animals (Zhang et al. 2017). In contrast to the Catwalk XT gait analysis, the rotarod and cylinder rearing tests were chosen for behavior assessment especially because they have been used and considered appropriate for evaluation of motor performance in the MPTP paradigm in our group before (Tönges et al. 2012).

The cylinder rearing test did not display a MPTP effect two weeks post MPTP treatment and also no difference between the treatment groups. However, the proportion of “both”

rears in the CTRL MPTP group was elevated and the proportion of free rears was reduced four weeks post MPTP treatment in comparison to the ULK1.DN MPTP group. These findings were significant for the increase in free rears in the ULK1.DN MPTP group in comparison to CTRL MPTP and got even more pronounced at six weeks post MPTP treatment, indicating a possible, beneficial long-term effect of ULK1.DN overexpression. To characterize possible long-term effects of ULK1.DN overexpression, further studies are certainly needed. However, modulation of extrastriatal dopaminergic projections might be one contributing mechanism to the ULK1.DN expression-mediated motor effects (Rommelfanger and Wichmann 2010; Pilotto et. al. 2019).

As the ULK1.DN-dependent improved rearing behavior occurred only in the lesioned, MPTP treated animals, one might speculate that nigrostriatal damage and the concomitant dysregulation of autophagy act as a trigger for reinforced autophagy inhibition and downstream signaling. Concurrently, the PBS injected animals showed no divergent rearing behavior at two, four, or six weeks post MPTP.

Although the rotarod analysis did not bring up significant results, a trend similar to results of the cylinder test analysis was visible: In the actual experiment, no significant difference in the average timespans on the rod was observed, while in literature both reduced time on the rotarod (Tönges et al. 2012) and significantly increased time on the rod (Zhang et al. 2017) at two weeks post MPTP (with the same sub chronic MPTP model) have been reported. However, four weeks post MPTP treatment, absolute values were higher for ULK1.DN MPTP compared to CTRL MPTP. Six weeks post MPTP treatment, this difference was even bigger showing a statistical trend ($p = 0.06$) to enhanced endurance of ULK1.DN MPTP animals in comparison to the CTRL MPTP animals. This finding is in line with the significantly improved rearing behavior in the cylinder test and further supports the theory of potential beneficial long-term effects of ULK1.DN overexpression.

4.3.4 ULK1.DN overexpression regulates autophagy and activates mTOR signaling

Western blot analysis of mouse midbrain tissue was conducted six weeks post MPTP treatment. The analysis of the ULK1.DN MPTP group revealed increased levels of p62, indicating a significant reduction of autophagic activity due to ULK1.DN overexpression. Interestingly, the LC3-II/I ratio, a parameter expected to be reduced in the case of reduced

autophagosome formation, was not significantly altered. However, similar results were obtained in *in vitro* experiments applying ULK1.siRNA to HEK293 cells (Chan et al. 2007) or directly expressing ULK1.DN in HEK293 cells *in vitro* (Chan et al. 2009). AMPK and mTOR are two important upstream regulators of ULK1 (Alers et al. 2012). However, ULK1 also is able to exert inhibitory influence on the mTOR/pS6 kinase pathway (Lee et al. 2007). While mTOR suppresses autophagy by inhibitory phosphorylation of ULK1 in a nutrient-rich environment, AMPK positively regulates autophagy in a nutrient-deprived status via inhibitory phosphorylation of mTOR and activating phosphorylation of ULK1 (Alers et al. 2012). Despite the disability of ULK1.DN to directly interact with AMPK and mTOR because of the missing key structures (Chan et al. 2009), significantly altered mTOR levels were detected after ULK1.DN expression (Balke et al. 2020). While the AMPK protein levels remained unchanged upon ULK1.DN expression and MPTP treatment, mTOR levels were significantly elevated in the ULK1.DN MPTP group compared to CTRL PBS and to a lesser, but still significant extent in the ULK1.DN PBS group compared to CTRL PBS. This also supports the possibility of toxin damage as a trigger for reinforced autophagy inhibition and downstream signaling. ERK1 and ERK2 protein levels were analyzed because ERK was shown to contribute to mitochondrial injury in 6-OHDA and MPP^+ models of PD, most likely via stimulation of mitophagy (Chu et al. 2007). Therefore, inhibition of ERK prevented MPP^+-induced autophagic vacuole formation and degradation, but not ultrastructural damage to the mitochondria (Chu et al. 2007). There is evidence that ERK enhances autophagy/mitophagy when ROS are induced (Dagda et al. 2013) and that it contributes to cell death in the MPTP model (Zhang et al. 2015). However, ERK levels were not found to be significantly changed by ULK1.DN expression (Balke et al. 2020). The inhibition of S6 was reported to induce autophagy through Mitogen-activated protein kinase 7 (MAP3K7)-mediated AMPK activation in NSC34 hybrid mouse motoneuron cells (Sun J et al. 2018). In this context, also inhibitory qualities of ULK1 in regard to S6 phosphorylation were reported, which led to enhanced MPP^+ toxicity in the cell culture setup (Li et al. 2015). However, analysis of pS6 expression levels did not reveal disparities between the ULK1.DN MPTP and CTRL group.

Over all, the Western blot analysis was conducted on samples from tissue of the entire midbrain, therefore containing not only the DAergic neuronal cell population of interest but also other neurons and glial cells, which are not equally affected by the MPTP

exposure and AAV.ULK1.DN transduction. In consequence, discreet changes in neuronal protein expression might be hardly detectable with this approach (Balke et al. 2020). However, despite this drawback, we were able to observe a significant activation of mTOR, which is well in line with other recent studies. For example, anodal transcranial direct current stimulation in the MPTP mouse model was described to inhibit autophagy and its upstream markers while significantly increasing mTOR signaling, thereby reducing MPTP-induced neurotoxicity (Lee et al. 2018). Since mTOR is a master regulator, not only affecting autophagy but regulating several other molecular pathways like cell growth, proliferation and transcriptional regulation, it may be considered an interesting molecular alternative to ULK1 in order to target axonal degeneration in PD (Zhu et al. 2019).

4.4 Targeting autophagy in PD therapy

Autophagy is a highly preserved biological process. It is inevitable for cellular homeostasis and survival, continuously taking place to degrade old organelles, misfolded proteins and to produce energy under conditions of nutrient starvation (Mizushima 2007). After Yoshinuri Ohsumi discovered the essential autophagy genes in yeast in the early 1990's and then continued to unravel the underlying mechanisms, we achieved a great understanding of the physiological process of autophagy (Tooze and Dikic 2016). With temporal delay the involvement of autophagy dysregulation in the genesis of neurodegenerative disorders, cancer or chronic illnesses like diabetes mellitus is now also studied (Komatsu and Ichimura 2010) and Yoshinuri Ohsumi received the Nobel Prize for his achievements (Tooze and Dikic 2016).

Although there are promising preclinical studies on autophagy modulation employing cell culture and animal models like the MPTP model for PD (Lee et al. 2018; Ouyang et al. 2018; Sun S et al. 2018; Liu et al. 2019), results should be interpreted with caution. Despite tremendous research effort and impressive neuroprotective effects in animal studies, hardly any therapeutic agent or strategy was successfully transferred into clinical studies and none succeeded in patient care so far (Tagliaferro and Burke 2016).

As already mentioned, the role of ULK1 and autophagy in PD is still under fierce debate. While Su et al. (2015), Lee et al. (2018) and Zhao et al. (2020) support our findings of neuroprotective inhibition of autophagy in the MPTP mouse model, there are also

conflicting, methodically equivalent studies (Jang et al. 2018; Ouyang et al. 2018; Pupyshev et al. 2019). For example Ouyang et al. (2018) could show that their small molecule activator of ULK1, *33i* was able to enhance autophagy and thereby protect SH-SY5Y cells from neurotoxicity caused by MMP^+. Furthermore, it also rescued MPTP-induced motor dysfunction and neuronal demise in the *in vivo* model (Ouyang et al. 2018).

Without limiting the analysis of autophagy modulation to the MPTP model, it can be noted that autophagy serves different and sometimes opposing roles depending on the clinical context and pathology. Many tumors rely on autophagy to promote cell survival, especially for their nutrient-deprived core in later stages, and the SBI-0206965 inhibitor of ULK1 for instance was found to have detrimental effects on cell survival in small cell lung cancer (Egan et al. 2015; Tang et al. 2017). However, a different role of autophagy in tumor initiation is presumed, and additional induction of autophagy might be helpful in early stages to improve clearance of mutant proteins and to reduce oxidative stress (White 2015). Dysregulation of autophagy has also been linked to several chronic illnesses e.g. diabetes (Komatsu and Ichimura 2010). Diminished autophagic activity was linked to impaired ß-cell function, increased insulin resistance and the development of diabetic complications like diabetic nephropathy (Barlow and Thomas 2015). Therefore, available data argue for the merits of autophagy induction in diabetic illness (Barlow and Thomas 2015). At least some of the antidiabetic effects of the new antidiabetic drugs are mediated by induction of autophagy, thereby alleviating oxidative stress and improving insulin signaling (Ashrafizadeh et al. 2019). Unfortunately, the picture is not that coherent in the field of neurodegenerative disorders and PD.

On the one hand, impaired autophagy is at least partly contributing to cellular malfunction, a formation of inclusion bodies and has just recently been linked to an accumulation of alpha-synuclein in patients with idiopathic PD in an *in vivo* study (Miki et al. 2018). Therefore, a reinforcement of autophagy to protect the dopaminergic neurons and alter the disease progression appears possible. On the other hand, it has been shown that axonal degeneration as key early event in the sequence of PD pathology comes along with exaggerated autophagy activation that contributes to degeneration (Koch et al. 2010). Furthermore, nuclear ULK1 promotes necrotic cell death due to ROS exposure, which constitutes a driving force in PD pathophysiology (Joshi et al. 2016). Probably both phenomena ultimately contribute to neuronal death in a chronologically detached manner. Generally, both exaggerated and insufficient autophagy harm physiological neuronal

function and are to be prevented. Therefore, an accurate titration of the delicate autophagy process is required to keep autophagic activity within the physiological boundaries (Banerjee et al. 2010).

While targeting autophagy in the MPTP mouse model with the help of a stereotactic AAV vector injection into the SN is a smart way of administration to rule out systemic side effects, this approach is not the first choice for patient care. There are classic risks of surgery as bleeding and infection, but also the possibility of brain injury due to injection. Although the approach of intracerebral injections has already been employed in a few clinical studies and therefore is not an insuperable obstacle (Choudhury et al. 2017), an oral or intravenous application would be much more favorable. In the last five years, several pharmacological compounds e.g. the ULK1 inhibitors SBI-0206965 or ULK1-100 have been developed and successfully used in cell cultures (Egan et al. 2015; Martin et al. 2018). Due to its position as the sole kinase involved in the initial steps of the autophagy cascade, ULK1 represents an attractive drug target (Egan et al. 2015). Therefore, its activity can be easily modulated by direct phosphorylation (Kim et al. 2011). Meanwhile, there is also first *in vivo* evidence of its functionality available for the SBI-0206965 inhibitor (Vahsen et al. 2020). However, studies on tolerance and the absence of critical side effects in other organs when administered in vertebrates are not yet available. For the benefit of PD patients, it will be necessary to determine which of the numerous inhibitors has the best safety profile.

Finally, in consideration of the successful modulation of the autophagic process by expression of ULK1.DN, resulting in attenuation of MPTP toxicity and subsequent reduced neurodegeneration *in vivo*, ULK1 appears as an auspicious future target for the treatment of neurodegeneration in PD.

5 Summary

Parkinson's disease (PD) is a widespread neurodegenerative condition. Owing to the absence of suitable biomarkers, a diagnosis can only be made upon onset of clinical symptoms like tremor, rigidity or bradykinesia. They occur mainly due to degeneration of the nigrostriatal system, but other brain areas and autonomic nerves are also affected by PD. The demise of dopaminergic neurons and the presence of Lewy bodies in affected neuronal somas and axons represent the most recognized histopathologic hallmark of PD. With exception of the monogenetic forms of PD, its etiology is multifactorial and based on gene-environment interaction. Autophagy, as a highly conserved homeostatic and vital process, is dysregulated in Parkinson diseased brains and contributes to axonal and neuronal death. Therefore, the present study aimed to assess neuroprotective and neurorestorative properties of competitive autophagy inhibition via Adeno-associated virus-mediated ULK1.DN gene expression in the 1-Methyl-4-phenyl-1,2,3,6-tetrahydropyridine (MPTP) mouse model. It could be demonstrated that ULK1.DN expression was able to rescue dopaminergic cell bodies from MPTP-induced neurotoxicity two weeks post MPTP treatment. Furthermore, also dopaminergic striatal fibers were significantly protected as compared to controls. Western blot analysis confirmed a downregulation of autophagy by ULK1.DN overexpression and showed a significant activation of Mammalian target of rapamycin (mTOR) signaling. While striatal dopamine levels could not be rescued by ULK1.DN gene expression, a beneficial effect in motor behavior in the cylinder rearing test was observed six weeks post MPTP treatment, pointing towards beneficial long-term effects of ULK1.DN expression. Part of a possible explanation for these findings may be the modulation of extrastriatal dopaminergic projections and an enhanced sprouting and synapse formation. Taking all these aspects into consideration, competitive autophagy inhibition via ULK1.DN expression shows promising neuroprotective properties as well as beneficial long-term effects on motor skills. Consequently, competitive autophagy inhibition may be considered a promising target in future therapeutic approaches of PD.

6 References

Alers S, Löffler AS, Wesselborg S, Stork B (2012): Role of AMPK-mTOR-Ulk1/2 in the regulation of autophagy: cross talk, shortcuts, and feedbacks. Mol Cell Biol 32, 2–11

Andreyev AY, Kushnareva YE, Starkov AA (2005): Mitochondrial metabolism of reactive oxygen species. Biochemistry 70, 200–214

Ashrafizadeh M, Yaribeygi H, Atkin SL, Sahebkar A (2019): Effects of newly introduced antidiabetic drugs on autophagy. Diabetes Metab Syndr Clin Res Rev 13, 2445–2449

Auricchio A, Kobinger G, Anand V, Hildinger M, O'Connor E, Maquire AM, Wilson JM, Bennett J (2001): Exchange of surface proteins impacts on viral vector cellular specificity and transduction characteristics: the retina as a model. Hum Mol Genet 10, 3075–3081

Bach JP, Ziegler U, Deuschl G, Dodel R, Doblhammer-Reiter G (2011): Projected numbers of people with movement disorders in the years 2030 and 2050. Mov Disord 26, 2286–2290

Balke D, Tatenhorst L, Dambeck V, Ribas VT, Vahsen BF, Michel U, Bähr M, Lingor P (2020): AAV-mediated expression of dominant-negative ULK1 increases neuronal survival and enhances motor performance in the MPTP mouse model of Parkinson's disease. Mol Neurobiol 57, 685–697

Bandres-Ciga S, Diez-Fairen M, Kim JJ, Singleton AB (2020): Genetics of Parkinson's disease: An introspection of its journey towards precision medicine. Neurobiol Dis 137, 104782

Banerjee R, Starkov AA, Beal MF, Thomas B (2009): Mitochondrial dysfunction in the limelight of Parkinson's disease pathogenesis. Biochim Biophys Acta - Mol Basis Dis 1792, 651–663

Banerjee R, Beal MF, Thomas B (2010): Autophagy in neurodegenerative disorders: pathogenic roles and therapeutic implications. Trends Neurosci 33, 541–549

Bankiewicz KS, Plunkett RJ, Jacobowitz DM, Porrino L, di Porzio U, London WT, Kopin IJ, Oldfield EH (1990): The effect of fetal mesencephalon implants on primate MPTP-induced parkinsonism. Histochemical and behavioral studies. J Neurosurg 72, 231–244

Barlow AD, Thomas DC (2015): Autophagy in diabetes: β-cell dysfunction, insulin resistance, and complications. DNA Cell Biol 34, 252–260

Bartlett JS, Wilcher R, Samulski RJ (2000): Infectious entry pathway of adeno-associated virus and adeno-associated virus vectors. J Virol 74, 2777–2785

Batistela MS, Josviak ND, Sulzbach CD, de Souza RLR (2017): An overview of circulating cell-free microRNAs as putative biomarkers in Alzheimer's and Parkinson's Diseases. Int J Neurosci 127, 547–558

Beach TG, Adler CH, Sue LI, Peirce JB, Bachalakuri J, Dalsing-Hernandez JE, Lue LF, Caviness JN, Connor DJ, Sabbagh MN et al. (2008): Reduced striatal tyrosine hydroxylase in incidental Lewy body disease. Acta Neuropathol 115, 445–451

Beck G, Singh A, Papa SM (2018): Dysregulation of striatal projection neurons in Parkinson's disease. J Neural Transm 125, 449–460

Bednarczyk M, Zmarzły N, Grabarek B, Mazurek U, Muc-Wierzgoń M (2018): Genes involved in the regulation of different types of autophagy and their participation in cancer pathogenesis. Oncotarget 9, 34413–34428

Bender A, Krishnan KJ, Morris CM, Taylor GA, Reeve AK, Perry RH, Jaros E, Hersheson JS, Betts J, Klopstock T (2006): High levels of mitochondrial DNA deletions in substantia nigra neurons in aging and Parkinson disease. Nat Genet 38, 515–517

Bengoa-Vergniory N, Roberts RF, Wade-Martins R, Alegre-Abarrategui J (2017): Alpha-synuclein oligomers: a new hope. Acta Neuropathol 134, 819–838

Bernardes D, Oliveira ALR (2017): Comprehensive catwalk gait analysis in a chronic model of multiple sclerosis subjected to treadmill exercise training. BMC Neurol 17, 160

Berns KI, Linden RM (1995): The cryptic life style of adenoassociated virus. BioEssays 17, 237–245

Beyer K, Domingo-Sàbat M, Ariza A (2009): Molecular pathology of Lewy body diseases. Int J Mol Sci 10, 724–745

Bhimani AD, Kheirkhah P, Arnone GD, Nahhas CR, Kumar P, Wonais M, Hidrogo H, Aguilar E, Spalinski D, Gopalka M et al. (2017): Functional gait analysis in a spinal contusion rat model. Neurosci Biobehav Rev 83, 540–546

Boerger M, Funke S, Leha A, Roser AE, Wuestemann AK, Maass F, Bähr M, Grus F, Lingor P (2019): Proteomic analysis of tear fluid reveals disease-specific patterns in patients with Parkinson's disease – A pilot study. Park Relat Disord 63, 3–9

Booth LA, Tavallai S, Hamed HA, Cruickshanks N, Dent P (2014): The role of cell signalling in the crosstalk between autophagy and apoptosis. Cell Signal 26, 549–555

Braak H, del Tredici K, Rüb U, de Vos RAI, Jansen Steur ENH, Braak E (2003): Staging of brain pathology related to sporadic Parkinson's disease. Neurobiol Aging 24, 197–211

Branco DM, Arduino DM, Esteves AR, Silva DF, Cardoso SM, Oliveira CR (2010): Cross-talk between mitochondria and proteasome in Parkinson's disease pathogenesis. Front Aging Neurosci 2, 17

Breckenridge CB, Berry C, Chang ET, Sielken RL, Mandel JS (2016): Association between Parkinson's Disease and Cigarette Smoking, Rural Living, Well-Water Consumption, Farming and Pesticide Use: Systematic Review and Meta-Analysis. PLoS One 11, e0151841

Burke RE, O'Malley K (2013): Axon degeneration in Parkinson's disease. Exp Neurol 246, 72–83

Burke RE, Dauer WT, Vonsattel JPG (2008): A critical evaluation of the Braak staging scheme for Parkinson's disease. Ann Neurol 64, 485–491

Cerri S, Blandini F (2018): Role of Autophagy in Parkinson's Disease. Curr Med Chem 26, 3702–3718

Chan EYW, Kir S, Tooze SA (2007): siRNA screening of the kinome identifies ULK1 as a multidomain modulator of autophagy. J Biol Chem 282, 25464–25474

Chan EYW, Longatti A, McKnight NC, Tooze SA (2009): Kinase-Inactivated ULK Proteins Inhibit Autophagy via Their Conserved C-Terminal Domains Using an Atg13-Independent Mechanism. Mol Cell Biol 29, 157–171

Chen Y, Klionsky DJ (2011): The regulation of autophagy - unanswered questions. J Cell Sci 124, 161–170

Cheng HC, Ulane CM, Burke RE (2010): Clinical progression in Parkinson disease and the neurobiology of axons. Ann Neurol 67, 715–725

Choi DC, Chae YJ, Kabaria S, Chaudhuri AD, Jain MR, Li H, Mouradian MM, Junn E (2014): MicroRNA-7 protects against 1-methyl-4-phenylpyridinium-induced cell death by targeting RelA. J Neurosci 34, 12725–12737

Choi VW, McCarty DM, Samulski RJ (2006): Host cell DNA repair pathways in adeno-associated viral genome processing. J Virol 80, 10346–10356

Choudhury SR, Hudry E, Maguire CA, Sena-Esteves M, Breakefield XO, Grandi P (2017): Viral vectors for therapy of neurologic diseases. Neuropharmacology 120, 63–80

Christine CW, Starr PA, Larson PS, Eberling JL, Jagust WJ, Hawkins RA, Van Brocklin HF, Wright JF, Bankiewicz KS, Aminoff MJ (2009): Safety and tolerability of putaminal AADC gene therapy for Parkinson disease. Neurology 73, 1662–1669

Chu CT, Zhu J, Dagda RK (2007): Beclin 1-independent pathway of damage-induced mitophagy and autophagic stress: implications for neurodegeneration and cell death. Autophagy 3, 663–666

Connolly BS, Lang AE (2014): Pharmacological Treatment of Parkinson Disease. JAMA 311, 1670–1683

Cooper CA, Chahine LM (2016): Biomarkers in Prodromal Parkinson Disease: a Qualitative Review. J Int Neuropsychol Soc 22, 956–967

Corona Velazquez A, Corona AK, Klein KA, Jackson WT (2018): Poliovirus induces autophagic signaling independent of the ULK1 complex. Autophagy 14, 1201–1213

Corti O (2019): Neuronal Mitophagy: Lessons from a pathway linked to Parkinson's disease. Neurotox Res 36, 292–305

Dagda RK, Das Banerjee T, Janda E (2013): How Parkinsonian toxins dysregulate the autophagy machinery. Int J Mol Sci 14, 22163–22189

Dauer W, Przedborski S (2003): Parkinson ' s disease : Mechanisms and models. 39, 889–909

Daya S, Berns KI (2008): Gene therapy using adeno-associated virus vectors. Clin Microbiol Rev 21, 583–593

De Duve CRMJ (1963): The lysosome. Sci Am 208, 64–72

De Lau LM, Breteler MM (2006): Epidemiology of Parkinson's disease. Lancet Neurol 5, 525–535

Del Zompo M, Piccardi MP, Ruiu S, Quartu M, Gessa GL, Vaccari A (1993): Selective MPP+ uptake into synaptic dopamine vesicles: possible involvement in MPTP neurotoxicity. Br J Pharmacol 109, 411–414

Dexter DT, Jenner P (2013): Parkinson disease: from pathology to molecular disease mechanisms. Free Radic Biol Med 62, 132–144

Dorsey ER, Sherer T, Okun MS, Bloemd BR (2018): The emerging evidence of the Parkinson pandemic. J Parkinsons Dis 8, 3–8

Doxakis E (2010): Post-transcriptional regulation of alpha-synuclein expression by mir-7 and mir-153. J Biol Chem 285, 12726–12734

Ebrahimi-Fakhari D, Cantuti-Castelvetri I, Fan Z, Rockenstein E, Masliah E, Hyman BT, McLean PJ, Unni VK (2011): Distinct roles in vivo for the ubiquitin-proteasome system and the autophagy-lysosomal pathway in the degradation of alpha-Synuclein. J Neurosci 31, 14508–14520

Egan DF, Chun MGH, Vamos M, Zou H, Rong J, Miller CJ, Lou HJ, Raveendra-Panickar D, Yang CC, Sheffler DJ (2015): Small molecule inhibition of the autophagy kinase ULK1 and identification of ULK1 substrates. Mol Cell 59, 285–297

Eisbach SE, Outeiro TF (2013): alpha-Synuclein and intracellular trafficking: impact on the spreading of Parkinson's disease pathology. J Mol Med 91, 693–703

Elbaz A, Tranchant C (2007): Epidemiologic studies of environmental exposures in Parkinson's disease. J Neurol Sci 262, 37–44

Engelender S, Isacson O (2017): The threshold theory for Parkinson's disease. Trends Neurosci 40, 4–14

Fimia GM, Stoykova A, Romagnoli A, Giunta L, Di Bartolomeo S, Nardacci R, Corazzari M, Fuoco C, Ucar A, Schwartz P et al. (2007): Ambra1 regulates autophagy and development of the nervous system. Nature 447, 1121–1125

Fitch MT, Silver J (2008): CNS injury, glial scars, and inflammation: Inhibitory extracellular matrices and regeneration failure. Exp Neurol 209, 294–301

Ganley IG, Lam DH, Wang J, Ding X, Chen S, Jiang X (2009): ULK1.ATG13.FIP200 complex mediates mTOR signaling and is essential for autophagy. J Biol Chem 284, 12297–12305

Geng J, Klionsky DJ (2008): The Atg8 and Atg12 ubiquitin-like conjugation systems in macroautophagy. 'Protein modifications: beyond the usual suspects' review series. EMBO Rep 9, 859–864

Goedert M, Spillantini MG, del Tredici K, Braak H (2013): 100 years of Lewy pathology. Nat Rev Neurol 9, 13–24

Gray SJ, Matagne V, Bachaboina L, Yadav S, Ojeda SR, Samulski RJ (2011): Preclinical differences of intravascular AAV9 delivery to neurons and glia: a comparative study of adult mice and nonhuman primates. Mol Ther 19, 1058–1069

Gray SJ, Nagabhushan Kalburgi S, McCown TJ, Jude Samulski R (2013): Global CNS gene delivery and evasion of anti-AAV-neutralizing antibodies by intrathecal AAV administration in non-human primates. Gene Ther 20, 450–459

Grieger JC, Choi VW, Samulski RJ (2006): Production and characterization of adeno-associated viral vectors. Nat Protoc 1, 1412–1428

Harnett MM, Pineda MA, Latré de Laté P, Eason RJ, Besteiro S, Harnett W, Langsley G (2017): From Christian de Duve to Yoshinori Ohsumi: More to autophagy than just dining at home. Biomed J 40, 9–22

Heikkila RE, Hess A, Duvoisin RC (1984): Dopaminergic neurotoxicity of 1-methyl-4-phenyl-1,2,5,6-tetrahydropyridine in mice. Science 224, 1451–1453

Hocquemiller M, Giersch L, Audrain M, Parker S, Cartier N (2016): Adeno-associated virus-based gene therapy for CNS diseases. Hum Gene Ther 27, 478–496

Holdorff B (2002): Friedrich Heinrich Lewy (1885-1950) and his work. J Hist Neurosci 11, 19–28

Hovland DN, Boyd RB, Butt MT, Engelhardt JA, Moxness MS, Ma MH, Emery MG, Ernst NB, Reed RP, Zeller JR (2007): Reprint: Six-month continuous intraputamenal infusion toxicity study of recombinant methionyl human glial cell line-derived neurotrophic factor (r-metHuGDNF) in rhesus monkeys. Toxicol Pathol 35, 1013–1029

Huang D, Xu J, Wang J, Tong J, Bai X, Li H, Wang Z, Huang Y, Wu Y, Yu M et al. (2017): Dynamic changes in the nigrostriatal pathway in the MPTP mouse model of Parkinson's disease. Parkinsons Dis 2017, 9349487

Huang R, Liu W (2015): Identifying an essential role of nuclear LC3 for autophagy. Autophagy 11, 852–853

Huynh T (2011): The Parkinson's disease market. Nat Rev Drug Discov 10, 571–572

Ibáñez P, Bonnet AM, Débarges B, Lohmann E, Tison F, Agid Y, Dürr A, Brice A, Pollak P (2004): Causal relation between α-synuclein gene duplication and familial Parkinson's disease. Lancet 364, 1169–1171

Ichimura Y, Kirisako T, Takao T, Satomi Y, Shimonishi Y, Ishihara N, Mizushima N, Tanida I, Kominami E, Ohsumi M et al. (2000): A ubiquitin-like system mediates protein lipidation. Nature 408, 488–492

Imming P, Sinning C, Meyer A (2006): Drugs, their targets and the nature and number of drug targets. Nat Rev Drug Discov 5, 821–834

Jackson-Lewis V, Przedborski S (2007): Protocol for the MPTP mouse model of Parkinson's disease. Nat Protoc 2, 141–151

Jakowec MW, Nixon K, Hogg E, McNeill T, Petzinger GM (2004): Tyrosine hydroxylase and dopamine transporter expression following 1-Methyl-4-Phenyl-1,2,3,6-Tetrahydropyridine-induced neurodegeneration of the mouse nigrostriatal pathway. J Neurosci Res 76, 539–550

Jang YC, Hwang DJ, Koo JH, Um HS, Lee NH, Yeom DC, Lee Y, Cho JY (2018): Association of exercise-induced autophagy upregulation and apoptosis suppression with neuroprotection against pharmacologically induced Parkinson's disease. J Exerc Nutr Biochem 22, 1–8

Javitch JA, D'Amato RJ, Strittmatter SM, Snyder SH (1985): Parkinsonism-inducing neurotoxin, N-methyl-4-phenyl-1,2,3,6 -tetrahydropyridine: uptake of the metabolite N-methyl-4-phenylpyridine by dopamine neurons explains selective toxicity. Proc Natl Acad Sci U S A 82, 2173–2177

Jenner P (2003): The contribution of the MPTP-treated primate model to the development of new treatment strategies for Parkinson's disease. Park Relat Disord 9, 131–137

Joshi A, Iyengar R, Joo JH, Li-Harms XJ, Wright C, Marino R, Winborn BJ, Phillips A, Temirov J, Sciarretta S et al. (2016): Nuclear ULK1 promotes cell death in response to oxidative stress through PARP1. Cell Death Differ 23, 216–230

Junn E, Lee KW, Jeong BS, Chan TW, Im JY, Mouradian MM (2009): Repression of alpha-synuclein expression and toxicity by microRNA-7. Proc Natl Acad Sci U S A 106, 13052–13057

Kabaria S, Choi DC, Chaudhuri AD, Jain MR, Li H, Junn E (2015): MicroRNA-7 activates Nrf2 pathway by targeting Keap1 expression. Free Radic Biol Med 89, 548–556

Kamp F, Exner N, Lutz AK, Wender N, Hegermann J, Brunner B, Nuscher B, Bartels T, Giese A, Beyer K et al. (2010): Inhibition of mitochondrial fusion by α-synuclein is rescued by PINK1, Parkin and DJ-1. EMBO J 29, 3571–3589

Kang LH, Zhang S, Jiang S, Hu N (2019): Activation of autophagy in the retina after optic nerve crush injury in rats. Int J Ophthalmol 12, 1395–1401

Kaplitt MG, Feigin A, Tang C, Fitzsimons HL, Mattis P, Lawlor PA, Bland RJ, Young D, Strybing K, Eidelberg D et al. (2007): Safety and tolerability of gene therapy with an adeno-associated virus (AAV) borne GAD gene for Parkinson's disease: an open label, phase I trial. Lancet 369, 2097–2105

Karanasios E, Walker SA, Okkenhaug H, Manifava M, Hummel E, Zimmermann H, Ahmed Q, Domart MC, Collinson L, Ktistakis NT (2016): Autophagy initiation by ULK complex assembly on ER tubulovesicular regions marked by ATG9 vesicles. Nat Commun 7, 12420

Kaur J, Debnath J (2015): Autophagy at the crossroads of catabolism and anabolism. Nat Rev Mol Cell Biol 16, 461–472

Kaushik S, Cuervo AM (2012): Chaperone-mediated autophagy: a unique way to enter the lysosome world. Trends Cell Biol 22, 407–417

Kerschensteiner M, Schwab ME, Lichtman JW, Misgeld T (2005): In vivo imaging of axonal degeneration and regeneration in the injured spinal cord. Nat Med 11, 572–577

Kim J, Dalton VM, Eggerton KP, Scott SV, Klionsky DJ (1999): Apg7p/Cvt2p is required for the cytoplasm-to-vacuole targeting, macroautophagy, and peroxisome degradation pathways. Mol Biol Cell 10, 1337–1351

Kim J, Kundu M, Viollet B, Guan KL (2011): AMPK and mTOR regulate autophagy through direct phosphorylation of Ulk1. Nat Cell Biol 13, 132–141

Kin K, Yasuhara T, Kameda M, Date I (2019): Animal models for Parkinson's disease research: Trends in the 2000s. Int J Mol Sci 20, E5402

Kirisako T, Baba M, Ishihara N, Miyazawa K, Ohsumi M, Yoshimori T, Noda T, Ohsumi Y (1999): Formation process of autophagosome is traced with Apg8/Aut7p in yeast. J Cell Biol 147, 435–446

Kirisako T, Ichimura Y, Okada H, Kabeya Y, Mizushima N, Yoshimori T, Ohsumi M, Takao T, Noda T, Ohsumi Y (2000): The reversible modification regulates the membrane-binding state of Apg8/Aut7 essential for autophagy and the cytoplasm to vacuole targeting pathway. J Cell Biol 151, 263–276

Klionsky DJ (2008): Autophagy revisited: a conversation with Christian de Duve. Autophagy 4, 740–743

Klionsky DJ, Abdelmohsen K, Abe A, Abedin MJ, Abeliovich H, Acevedo Arozena A, Adachi H, Adams CM, Adams PD, Adeli K et al. (2016): Guidelines for the use and interpretation of assays for monitoring autophagy (3rd edition). Autophagy 12, 1–222

Knöferle J, Koch JC, Ostendorf T, Michel U, Planchamp V, Vutova P, Tönges L, Stadelmann C, Brück W, Bähr M et al. (2010): Mechanisms of acute axonal degeneration in the optic nerve in vivo. Proc Natl Acad Sci U S A 107, 6064–6069

Koch JC, Knöferle J, Tönges L, Ostendorf T, Bähr M, Lingor P (2010): Acute axonal degeneration in vivo is attenuated by inhibition of autophagy in a calcium-dependent manner. Autophagy 6, 658–659

Kolata G (1983): Monkey model of Parkinson's disease. Science 220, 705

Komatsu M, Ichimura Y (2010): Selective autophagy regulates various cellular functions. Genes Cells 15, 923–933

Kordower JH, Emborg ME, Bloch J, Ma SY, Chu Y, Leventhal L, McBride J, Chen EY, Palfi S, Roitberg BZ et al. (2000): Neurodegeneration prevented by lentiviral vector delivery of GDNF in primate models of Parkinson's disease. Science 290, 767–773

Kotin RM, Siniscalco M, Samulski RJ, Zhu XD, Hunter L, Laughlin CA, McLaughlin S, Muzyczka N, Rocchi M, Berns KI (1990): Site-specific integration by adeno-associated virus. Proc Natl Acad Sci U S A 87, 2211–2215

Kraytsberg Y, Kudryavtseva E, McKee AC, Geula C, Kowall NW, Khrapko K (2006): Mitochondrial DNA deletions are abundant and cause functional impairment in aged human substantia nigra neurons. Nat Genet 38, 518–520

Kuma A, Mizushima N, Ishihara N, Ohsumi Y (2002): Formation of the approximately 350-kDa Apg12-Apg5.Apg16 multimeric complex, mediated by Apg16 oligomerization, is essential for autophagy in yeast. J Biol Chem 277, 18619–18625

Kurowska Z, Kordower JH, Stoessl AJ, Burke RE, Brundin P, Yue Z, Brady ST, Milbrandt J, Trapp BD, Sherer TB et al. (2016): Is axonal degeneration a key early event in Parkinson's disease? J Parkinsons Dis 6, 703–707

Kwon I, Schaffer DV (2008): Designer gene delivery vectors: molecular engineering and evolution of adeno-associated viral vectors for enhanced gene transfer. Pharm Res 25, 489–499

Langston JW, Ballard P, Tetrud JW, Irwin I (1983): Chronic Parkinsonism in humans due to a product of meperidine-analog synthesis. Science 219, 979–980

Larsen SB, Hanss Z, Krüger R (2018): The genetic architecture of mitochondrial dysfunction in Parkinson's disease. Cell Tissue Res 373, 21–37

Lee EJ, Tournier C (2011): The requirement of uncoordinated 51-like kinase 1 (ULK1) and ULK2 in the regulation of autophagy. Autophagy 7, 689–695

Lee JW, Park S, Takahashi Y, Wang HG (2010): The association of AMPK with ULK1 regulates autophagy. PLoS One 5, e15394

Lee SB, Kim S, Lee J, Park J, Lee G, Kim Y, Kim JM, Chung J (2007): ATG1, an autophagy regulator, inhibits cell growth by negatively regulating S6 kinase. EMBO Rep 8, 360–365

Lee SB, Kim HT, Yang HO, Jang W (2018): Anodal transcranial direct current stimulation prevents methyl-4-phenyl-1,2,3,6-tetrahydropyridine (MPTP)-induced neurotoxicity by modulating autophagy in an in vivo mouse model of Parkinson's disease. Sci Rep 8, 15165

Le Grand JN, Gonzalez-Cano L, Pavlou MA, Schwamborn JC (2015): Neural stem cells in Parkinson's disease: a role for neurogenesis defects in onset and progression. Cell Mol Life Sci 72, 773–797

Li LH, Qin HZ, Wang JL, Wang J, Wang XL, Gao GD (2009): Axonal degeneration of nigra-striatum dopaminergic neurons induced by 1-Methyl-4-phenyl-1,2,3, 6-tetrahydropyridine in mice. J Int Med Res 37, 455–463

Li XK, Guo AC, Zuo PP (2003): Survival and differentiation of transplanted neural stem cells in mice brain with MPTP-induced Parkinson disease. Acta Pharmacol Sin 24, 1192–1198

Li Y, Zhang J, Yang C (2015): UNC-51-like kinase 1 blocks S6k1 phosphorylation contributes to neurodegeneration in Parkinson's disease model in vitro. Biochem Biophys Res Commun 459, 196–200

Lill CM (2016): Genetics of Parkinson's disease. Mol Cell Probes 30, 386–396

Lin LF, Doherty DH, Lile JD, Bektesh S, Collins F (1993): GDNF: a glial cell line-derived neurotrophic factor for midbrain dopaminergic neurons. Science 260, 1130–1132

Lin MT, Beal MF (2006): Mitochondrial dysfunction and oxidative stress in neurodegenerative diseases. Nature 443, 787–795

Lin SY, Li TY, Liu Q, Zhang C, Li X, Chen Y, Zhang SM, Lian G, Liu Q, Ruan K et al. (2012): GSK3-TIP60-ULK1 signaling pathway links growth factor deprivation to autophagy. Science 336, 477–481

Lingor P, Tönges L, Pieper N, Bermel C, Barski E, Planchamp V, Bähr M (2007): ROCK inhibition and CNTF interact on intrinsic signalling pathways and differentially regulate survival and regeneration in retinal ganglion cells. Brain 131, 250–63

Lingor P, Koch JC, Tönges L, Bähr M (2012): Axonal degeneration as a therapeutic target in the CNS. Cell Tissue Res 349, 289–311

Liou HH, Tsai MC, Chen CJ, Jeng JS, Chang YC, Chen SY, Chen RC (1997): Environmental risk factors and Parkinson's disease: a case-control study in Taiwan. Neurology 48, 1583–1588

Liu C, Huang X, Qiu S, Chen W, Li W, Zhang H, Wang T, Wang X, Wu X (2019): Chinese herbal complex „Bu Shen Jie Du Fang" (BSJDF) modulated autophagy in an MPP +-induced cell model of Parkinson's disease. Evid Based Complement Alternat Med 13, 2019:8920813

Liu J, Gao H, Wang X (2015): The role of the Rho/ROCK signaling pathway in inhibiting axonal regeneration in the central nervous system. Neural Regen Res 10, 1892–1896

Loh SHY, Francescut L, Lingor P, Bähr M, Nicotera P (2008): Identification of new kinase clusters required for neurite outgrowth and retraction by a loss-of-function RNA interference screen. Cell Death Differ 15, 283–298

Lowe J, McDermott H, Landon M, Mayer RJ, Wilkinson KD (1990): Ubiquitin carboxyl-terminal hydrolase (PGP 9.5) is selectively present in ubiquitinated inclusion bodies characteristic of human neurodegenerative diseases. J Pathol 161, 153–160

Maass F, Michalke B, Leha A, Boerger M, Zerr I, Koch JC, Tönges L, Bähr M, Lingor P (2018): Elemental fingerprint as a cerebrospinal fluid biomarker for the diagnosis of Parkinson's disease. J Neurochem 145, 342–351

Maass F, Michalke B, Willkommen D, Leha A, Schulte C, Tönges L, Mollenhauer B, Trenkwalder C, Rückamp D, Börger M et al. (2020): Elemental fingerprint: Reassessment of a cerebrospinal fluid biomarker for Parkinson's disease. Neurobiol Dis 134, 104677

Mallet N, Delgado L, Chazalon M, Miguelez C, Baufreton J (2019): Cellular and synaptic dysfunctions in Parkinson's disease: Stepping out of the striatum. Cells 8, E1005

Martin KR, Celano SL, Solitro AR, Gunaydin H, Scott M, O'Hagan RC, Shumway SD, Fuller P, MacKeigan JP (2018): A potent and selective ULK1 inhibitor suppresses autophagy and sensitizes cancer cells to nutrient stress. iScience 8, 74–84

Masat E, Pavani G, Mingozzi F (2013): Humoral immunity to AAV vectors in gene therapy: Challenges and potential solutions. Discov Med 15, 379–389

Masilamoni GJ, Smith Y (2018): Chronic MPTP administration regimen in monkeys: a model of dopaminergic and non-dopaminergic cell loss in Parkinson's disease. J Neural Transm 125, 337–363

Menzies FM, Fleming A, Rubinsztein DC (2015): Compromised autophagy and neurodegenerative diseases. Nat Rev Neurosci 16, 345–357

Meyer K, Ferraiuolo L, Schmelzer L, Braun L, McGovern V, Likhite S, Michels O, Govoni A, Fitzgerald J, Morales P et al. (2015): Improving single injection CSF delivery of AAV9-mediated gene therapy for SMA: a dose-response study in mice and nonhuman primates. Mol Ther 23, 477–487

Miki Y, Tanji K, Mori F, Utsumi J, Sasaki H, Kakita A, Takahashi H, Wakabayashi K (2016): Alteration of upstream autophagy-related proteins (ULK1, ULK2, Beclin1, VPS34 and AMBRA1) in Lewy body disease. Brain Pathol 26, 359–370

Miki Y, Shimoyama S, Kon T, Ueno T, Hayakari R, Tanji K, Matsumiya T, Tsushima E, Mori F, Wakabayashi K et al. (2018): Alteration of autophagy-related proteins in peripheral blood mononuclear cells of patients with Parkinson's disease. Neurobiol Aging 63, 33–43

Mills JC, Stone NL, Erhardt J, Pittman RN (1998): Apoptotic membrane blebbing is regulated by myosin light chain phosphorylation. J Cell Biol 140, 627–636

Mitsumoto Y, Watanabe A, Mori A, Koga N (1998): Spontaneous regeneration of nigrostriatal dopaminergic neurons in MPTP-treated C57BL/6 mice. Biochem Biophys Res Commun 248, 660–663

Mittermeyer G, Christine CW, Rosenbluth KH, Baker SL, Starr P, Larson P, Kaplan PL, Forsayeth J, Aminoff MJ, Bankiewicz KS (2012): Long-term evaluation of a phase 1 study of AADC gene therapy for Parkinson's disease. Hum Gene Ther 23, 377–381

Mizuno Y, Sone N, Saitoh T (1987): Effects of 1-methyl-4-phenyl-1,2,3,6-tetrahydropyridine and 1-methyl-4-phenylpyridinium ion on activities of the enzymes in the electron transport system in mouse brain. J Neurochem 48, 1787–1793

Mizushima N (2007): Autophagy: process and function. Genes Dev 21, 2861–2873

Mizushima N, Levine B, Cuervo AM, Klionsky DJ (2008): Autophagy fights disease through cellular self-digestion. Nature 451, 1069–1075

Mizushima N, Komatsu M (2011): Autophagy: renovation of cells and tissues. Cell 147, 728–741

Molino D, Nascimbeni AC, Giordano F, Codogno P, Morel E (2017a): ER-driven membrane contact sites: Evolutionary conserved machineries for stress response and autophagy regulation? Commun Integr Biol 10, e1401699

Molino D, Zemirli N, Codogno P, Morel E (2017b): The journey of the autophagosome through mammalian cell organelles and membranes. J Mol Biol 429, 497–514

Moreau K, Ravikumar B, Renna M, Puri C, Rubinsztein DC (2011): Autophagosome precursor maturation requires homotypic fusion. Cell 146, 303–317

Nah J, Yuan J, Jung YK (2015): Autophagy in neurodegenerative diseases: from mechanism to therapeutic approach. Mol Cells 38, 381–389

Nakamura K, Nemani VM, Azarbal F, Skibinski G, Levy JM, Egami K, Munishkina L, Zhang J, Gardner B, Wakabayashi J et al. (2011): Direct membrane association drives mitochondrial fission by the Parkinson disease-associated protein alpha-synuclein. J Biol Chem 286, 20710–20726

Nascimbeni AC, Codogno P, Morel E (2017): Phosphatidylinositol-3-phosphate in the regulation of autophagy membrane dynamics. FEBS J 284, 1267–1278

Naso MF, Tomkowicz B, Perry WL, Strohl WR, Strohl WR (2017): Adeno-associated virus (AAV) as a vector for gene therapy. BioDrugs 31, 317–334

Nerius M, Fink A, Doblhammer G (2017): Parkinson's disease in Germany: prevalence and incidence based on health claims data. Acta Neurol Scand 136, 386–392

Nicklas WJ, Youngster SK, Kindt MV, Heikkila RE (1987): MPTP, MPP+ and mitochondrial function. Life Sci 40, 721–729

Nielsen MS, Glud AN, Møller A, Mogensen P, Bender D, Sørensen JC, Doudet D, Bjarkam CR (2016): Continuous MPTP intoxication in the Göttingen minipig results in chronic parkinsonian deficits. Acta Neurobiol Exp (Wars) 76, 199–211

Noda NN, Mizushima N (2016): Atg101: Not just an accessory subunit in the autophagy-initiation complex. Cell Struct Funct 41, 13–20

Obernier K, Alvarez-Buylla A (2019): Neural stem cells: Origin, heterogeneity and regulation in the adult mammalian brain. Dev 146, dev156059

Obeso JA, Rodríguez-Oroz MC, Benitez-Temino B, Blesa FJ, Guridi J, Marin C, Rodriguez M (2008): Functional organization of the basal ganglia: Therapeutic implications for Parkinson's disease. Mov Disord 23, 548–559

Ouyang L, Zhang L, Zhang S, Yao D, Zhao Y, Wang G, Fu L, Lei P, Liu B (2018): Small-molecule activator of UNC-51-like kinase 1 (ULK1) that induces cytoprotective autophagy for Parkinson's disease treatment. J Med Chem 61, 2776–2792

Palfi S, Gurruchaga JM, Ralph GS, Lepetit H, Lavisse S, Buttery PC, Watts C, Miskin J, Kelleher M, Deeley S et al. (2014): Long-term safety and tolerability of ProSavin, a lentiviral vector-based gene therapy for Parkinson's disease: a dose escalation, open-label, phase 1/2 trial. Lancet 383, 1138–1146

Pan PY, Yue Z (2014): Genetic causes of Parkinson's disease and their links to autophagy regulation. Park Relat Disord 20, 154–157

Pan T, Kondo S, Le W, Jankovic J (2008): The role of autophagy-lysosome pathway in neurodegeneration associated with Parkinson's disease. Brain 131, 1969–1978

Pardal R, López-Barneo J (2012): Neural stem cells and transplantation studies in Parkinson's disease; in: Advances in experimental medicine and biology 741, 206–216

Park JM, Seo M, Jung CH, Grunwald D, Stone M, Otto NM, Toso E, Ahn Y, Kyba M, Griffin TJ et al. (2018): ULK1 phosphorylates Ser30 of BECN1 in association with ATG14 to stimulate autophagy induction. Autophagy 14, 584-597

Parkinson J (2002): An essay on the shaking palsy. J Neuropsychiatry Clin Neurosci 14, 223–236

Parzych KR, Klionsky DJ (2014): An overview of autophagy: morphology, mechanism, and regulation. Antioxid Redox Signal 20, 460–473

Pasquier B (2016): Autophagy inhibitors. Cell Mol Life Sci 73, 985–1001

Pattingre S, Tassa A, Qu X, Garuti R, Liang XH, Mizushima N, Packer M, Schneider MD, Levine B (2005): Bcl-2 antiapoptotic proteins inhibit Beclin 1-dependent autophagy. Cell 122, 927–939

Paxinos G, Franklin KBJ (2007): The mouse brain in stereotaxic coordinates. Third edition; Academic Press, Cambridge 2007

Pen AE, Jensen UB (2017): Current status of treating neurodegenerative disease with induced pluripotent stem cells. Acta Neurol Scand 135, 57–72

Petherick KJ, Conway OJ, Mpamhanga C, Osborne SA, Kamal A, Saxty B, Ganley IG (2015): Pharmacological inhibition of ULK1 kinase blocks mammalian target of rapamycin (mTOR)-dependent autophagy. J Biol Chem 290, 28726

Pfisterer SG, Bakula D, Frickey T, Cezanne A, Brigger D, Tschan MP, Robenek H, Proikas-Cezanne T (2014): Lipid droplet and early autophagosomal membrane targeting of Atg2A and Atg14L in human tumor cells. J Lipid Res 55, 1267–1278

Pilotto A, Schiano di Cola F, Premi E, Grasso R, Turrone R, Gipponi S, Scalvini A, Cottini E, Paghera B, Garibotto V et al. (2019): Extrastriatal dopaminergic and serotonergic pathways in Parkinson's disease and in dementia with Lewy bodies: a ^{123}I-FP-CIT SPECT study. Eur J Nucl Med Mol Imaging 46, 1642–1651

Plotegher N, Duchen MR (2017): Crosstalk between lysosomes and mitochondria in Parkinson's disease. Front cell Dev Biol 5, 110

Postuma RB, Aarsland D, Barone P, Burn DJ, Hawkes CH, Oertel W, Ziemssen T (2012): Identifying prodromal Parkinson's disease: Pre-Motor disorders in Parkinson's disease. Mov Disord 27, 617–626

Postuma RB, Berg D, Stern M, Poewe W, Warren Olanow C, Oertel W, Obeso J, Marek K, Litvan I, Lang AE et al. (2015b): MDS clinical diagnostic criteria for Parkinson's disease. Mov Disord 30, 1591–1599

Postuma RB, Iranzo A, Hogl B, Arnulf I, Ferini-Strambi L, Manni R, Miyamoto T, Oertel W, Dauvilliers Y, Ju YE et al. (2015a): Risk factors for neurodegeneration in idiopathic rapid eye movement sleep behavior disorder: A multicenter study. Ann Neurol 77, 830–839

Postuma RB, Berg D (2016): Advances in markers of prodromal Parkinson disease. Nat Rev Neurol 12, 622–634

Pupyshev AB, Tikhonova MA, Akopyan AA, Tenditnik MV, Dubrovina NI, Korolenko TA (2019): Therapeutic activation of autophagy by combined treatment with rapamycin and trehalose in a mouse MPTP-induced model of Parkinson's disease. Pharmacol Biochem Behav 177, 1–11

Rabanal-Ruiz Y, Otten EG, Korolchuk VI (2017): mTORC1 as the main gateway to autophagy. Essays Biochem 61, 565–584

Ribas VT, Schnepf B, Challagundla M, Koch JC, Bähr M, Lingor P (2015): Early and sustained activation of autophagy in degenerating axons after spinal cord injury. Brain Pathol 25, 157–170

Ribas VT, Koch JC, Michel U, Bähr M, Lingor P (2017): Attenuation of axonal degeneration by calcium channel inhibitors improves retinal ganglion cell survival and regeneration after optic nerve crush. Mol Neurobiol 54, 72–86

Rommelfanger KS, Wichmann T (2010): Extrastriatal dopaminergic circuits of the basal ganglia. Front Neuroanat 4, 139

Rosenbusch KE, Kortholt A (2016): Activation mechanism of LRRK2 and its cellular functions in Parkinson's disease. Parkinsons Dis 2016, 7351985

Roser AE, Caldi Gomes L, Halder R, Jain G, Maass F, Tönges L, Tatenhorst L, Bähr M, Fischer A, Lingor P (2018): miR-182-5p and miR-183-5p act as GDNF mimics in dopaminergic midbrain neurons. Mol Ther Nucleic Acids 11, 9–22

Rott R, Szargel R, Haskin J, Bandopadhyay R, Lees AJ, Shani V, Engelender S (2011): -Synuclein fate is determined by USP9X-regulated monoubiquitination. Proc Natl Acad Sci 108, 18666–18671

Saal KA, Koch JC, Tatenhorst L, Szego ÉM, Ribas VT, Michel U, Bähr M, Tönges L, Lingor P (2015): AAV.shRNA-mediated downregulation of ROCK2 attenuates degeneration of dopaminergic neurons in toxin-induced models of Parkinson's disease in vitro and in vivo. Neurobiol Dis 73, 150–162

Salat D, Noyce AJ, Schrag A, Tolosa E (2016): Challenges of modifying disease progression in prediagnostic Parkinson's disease. Lancet Neurol 15, 637–648

Schallert T, Fleming SM, Leasure JL, Tillerson JL, Bland ST (2000): CNS plasticity and assessment of forelimb sensorimotor outcome in unilateral rat models of stroke, cortical ablation, parkinsonism and spinal cord injury. Neuropharmacology 39, 777–787

Schapira AH, Cooper JM, Dexter D, Jenner P, Clark JB, Marsden CD (1989): Mitochondrial complex I deficiency in Parkinson's disease. Lancet 1, 1269

Schapira AH, Tolosa E (2010): Molecular and clinical prodrome of Parkinson disease: implications for treatment. Nat Rev Neurol 6, 309–317

Schlossmacher MG, Frosch MP, Gai WP, Medina M, Sharma N, Forno L, Ochiishi T, Shimura H, Sharon R, Hattori N et al. (2002): Parkin localizes to the Lewy bodies of Parkinson disease and dementia with Lewy bodies. Am J Pathol 160, 1655–1667

Schmidt N, Ferger B (2001): Neurochemical findings in the MPTP model of Parkinson's disease. J Neural Transm 108, 1263–1282

Schober A (2004): Classic toxin-induced animal models of Parkinson's disease: 6-OHDA and MPTP. Cell Tissue Res 318, 215–224

Sidhu A, Wersinger C, Moussa CE, Vernier P (2004): The role of alpha-synuclein in both neuroprotection and neurodegeneration. Ann N Y Acad Sci 1035, 250–270

Simon DK, Pulst SM, Sutton JP, Browne SE, Beal MF, Johns DR (1999): Familial multisystem degeneration with parkinsonism associated with the 11778 mitochondrial DNA mutation. Neurology 53, 1787–1793

Singleton AB (2011): VPS35: A new player in Parkinson's disease. Mov Disord 26, 1803

Smith Y, Bevan MD, Shink E, Bolam JP (1998): Microcircuitry of the direct and indirect pathways of the basal ganglia. Neuroscience 86, 353–387

Spillantini MG, Schmidt ML, Lee VM, Trojanowski JQ, Jakes R, Goedert M (1997): Alpha-synuclein in Lewy bodies. Nature 388, 839–840

Srivastava A, Lusby EW, Berns KI (1983): Nucleotide sequence and organization of the adeno-associated virus 2 genome. J Virol 45, 555–564

Su LY, Li H, Lv L, Feng YM, Li GD, Luo R, Zhou HJ, Lei XG, Ma L, Li JL et al. (2015): Melatonin attenuates MPTP-induced neurotoxicity via preventing CDK5-mediated autophagy and SNCA/α-synuclein aggregation. Autophagy 11, 1745–1759

Sullivan AM, Toulouse A (2011): Neurotrophic factors for the treatment of Parkinson's disease. Cytokine Growth Factor Rev 22, 157–165

Summerford C, Samulski RJ (1998): Membrane-associated heparan sulfate proteoglycan is a receptor for adeno-associated virus type 2 virions. J Virol 72, 1438–1445

Sun J, Mu Y, Jiang Y, Song R, Yi J, Zhou J, Sun J, Jiao X, Prinz RA, Li Y et al. (2018): Inhibition of p70 S6 kinase activity by A77 1726 induces autophagy and enhances the degradation of superoxide dismutase 1 (SOD1) protein aggregates. Cell Death Dis 9, 407

Sun S, Han X, Li X, Song Q, Lu M, Jia M, Ding J, Hu G (2018): MicroRNA-212-5p prevents dopaminergic neuron death by inhibiting SIRT2 in MPTP-induced mouse model of Parkinson's disease. Front Mol Neurosci 11, 381

Tagliaferro P, Burke RE (2016): Retrograde axonal degeneration in Parkinson disease. J Parkinsons Dis 6, 1–15

Takahashi Y, Coppola D, Matsushita N, Cualing HD, Sun M, Sato Y, Liang C, Jung JU, Cheng JQ, Mulé JJ et al. (2007): Bif-1 interacts with Beclin 1 through UVRAG and regulates autophagy and tumorigenesis. Nat Cell Biol 9, 1142–1151

Tang F, Hu P, Yang Z, Xue C, Gong J, Sun S, Shi L, Zhang S, Li Z, Yang C et al. (2017): SBI0206965, a novel inhibitor of Ulk1, suppresses non-small cell lung cancer cell growth by modulating both autophagy and apoptosis pathways. Oncol Rep 37, 3449–3458

Tanida I (2011): Autophagy basics. Microbiol Immunol 55, 1–11

Tanji K, Mori F, Kakita A, Takahashi H, Wakabayashi K (2011): Alteration of autophagosomal proteins (LC3, GABARAP and GATE-16) in Lewy body disease. Neurobiol Dis 43, 690–697

Tatarewicz SM, Wei X, Gupta S, Masterman D, Swanson SJ, Moxness MS (2007): Development of a maturing T-cell-mediated immune response in patients with idiopathic Parkinson's disease receiving r-metHuGDNF via continuous intraputaminal infusion. J Clin Immunol 27, 620–627

Tatenhorst L, Tönges L, Saal KA, Koch JC, Szegő ÉM, Bähr M, Lingor P (2014): Rho kinase inhibition by fasudil in the striatal 6-Hydroxydopamine lesion mouse model of Parkinson disease. J Neuropathol Exp Neurol 73, 770–779

Tatenhorst L, Eckermann K, Dambeck V, Fonseca-Ornelas L, Walle H, Lopes da Fonseca T, Koch JC, Becker S, Tönges L, Bähr M et al. (2016): Fasudil attenuates aggregation of α-synuclein in models of Parkinson's disease. Acta Neuropathol Commun 4, 39

Tekriwal A, Kern DS, Tsai J, Ince NF, Wu J, Thompson JA, Abosch A (2016): REM sleep behaviour disorder: prodromal and mechanistic insights for Parkinson's disease. J Neurol Neurosurg Psychiatry 88, 445–451

Thyagarajan D, Bressman S, Bruno C, Przedborski S, Shanske S, Lynch T, Fahn S, DiMauro S (2000): A novel mitochondrial 12SrRNA point mutation in parkinsonism, deafness, and neuropathy. Ann Neurol 48, 730–736

Toda H, Mochizuki H, Flores R, Josowitz R, Krasieva TB, LaMorte VJ, Suzuki E, Gindhart JG, Furukubo-Tokunaga K, Tomoda T (2008): UNC-51/ATG1 kinase regulates axonal transport by mediating motor-cargo assembly. Genes Dev 22, 3292–3307

Tönges L, Koch JC, Bähr M, Lingor P (2011): ROCKing regeneration: Rho kinase inhibition as molecular target for neurorestoration. Front Mol Neurosci 4, 39

Tönges L, Frank T, Tatenhorst L, Saal KA, Koch JC, Szegő ÉM, Bähr M, Weishaupt JH, Lingor P (2012): Inhibition of rho kinase enhances survival of dopaminergic neurons and attenuates axonal loss in a mouse model of Parkinson's disease. Brain 135, 3355–3370

Tooze SA, Dikic I (2016): Autophagy Captures the Nobel Prize. Cell 167, 1433–1435

Tysnes OB, Storstein A (2017): Epidemiology of Parkinson's disease. J Neural Transm 124, 901–905

Umemura A, Oyama G, Shimo Y, Nakajima M, Nakajima A, Jo T, Sekimoto S, Ito M, Mitsuhashi T, Hattori N et al. (2016): Current topics in deep brain stimulation for Parkinson disease. Neurol Med Chir (Tokyo) 56, 613–625

Vahsen BF, Ribas VT, Sundermeyer J, Boecker A, Dambeck V, Lenz C, Shomroni O, Caldi Gomes L, Tatenhorst L, Barski E et al. (2020): Inhibition of the autophagic protein ULK1 attenuates axonal degeneration in vitro and in vivo, enhances translation, and modulates splicing. Cell Death Differ 27, 2810–2827

Velikkakath AKG, Nishimura T, Oita E, Ishihara N, Mizushima N (2012): Mammalian Atg2 proteins are essential for autophagosome formation and important for regulation of size and distribution of lipid droplets. Mol Biol Cell 23, 896–909

Vila M, Vukosavic S, Jackson-Lewis V, Neystat M, Jakowec M, Przedborski S (2000): Alpha-synuclein up-regulation in substantia nigra dopaminergic neurons following administration of the parkinsonian toxin MPTP. J Neurochem 74, 721–729

Wang D, Tai PWL, Gao G (2019): Adeno-associated virus vector as a platform for gene therapy delivery. Nat Rev Drug Discov 18, 358–378

Webb JL, Ravikumar B, Atkins J, Skepper JN, Rubinsztein DC (2003): Alpha-synuclein is degraded by both autophagy and the proteasome. J Biol Chem 278, 25009–25013

Weidberg H, Shvets E, Shpilka T, Shimron F, Shinder V, Elazar Z (2010): LC3 and GATE-16/GABARAP subfamilies are both essential yet act differently in autophagosome biogenesis. EMBO J 29, 1792–1802

Weidberg H, Shpilka T, Shvets E, Abada A, Shimron F, Elazar Z (2011): LC3 and GATE-16 N termini mediate membrane fusion processes required for autophagosome biogenesis. Dev Cell 20, 444–454

Weindler FW, Heilbronn R (1991): A subset of herpes simplex virus replication genes provides helper functions for productive adeno-associated virus replication. J Virol 65, 2476–2483

White E (2015): The role for autophagy in cancer. J Clin Invest 125, 42–46

Wilkaniec A, Lenkiewicz AM, Czapski GA, Jęśko HM, Hilgier W, Brodzik R, Gąssowska-Dobrowolska M, Culmsee C, Adamczyk A (2019): Extracellular alpha-synuclein oligomers induce parkin S-nitrosylation: Relevance to sporadic Parkinson's disease etiopathology. Mol Neurobiol 56, 125–140

Wong E, Cuervo AM (2010): Autophagy gone awry in neurodegenerative diseases. Nat Neurosci 13, 805–811

Wu DC, Tieu K, Cohen O, Choi DK, Vila M, Jackson-Lewis V, Teismann P, Przedborski S (2002): Glial cell response: A pathogenic factor in Parkinson's disease. J Neurovirol 8, 551–558

Xu C, Zhang W, Liu S, Wu W, Qin M, Huang J (2018): Activation of the SphK1/ERK/p‑ERK pathway promotes autophagy in colon cancer cells. Oncol Lett 6, 9719–9724

Yang Z, Klionsky DJ (2010a): Mammalian autophagy: core molecular machinery and signaling regulation. Curr Opin Cell Biol 22, 124–131

Yang Z, Klionsky DJ (2010b): Eaten alive: a history of macroautophagy. Nat Cell Biol 12, 814–822

Yorimitsu T, Klionsky DJ (2005): Autophagy: molecular machinery for self-eating. Cell Death Differ 12, 1542–1552

Zachari M, Ganley IG (2017): The mammalian ULK1 complex and autophagy initiation. Essays Biochem 61, 585–596

Zavodszky E, Seaman MN, Moreau K, Jimenez-Sanchez M, Breusegem SY, Harbour ME, Rubinsztein DC (2014): Mutation in VPS35 associated with Parkinson's disease impairs WASH complex association and inhibits autophagy. Nat Commun 5, 3828

Zhang H, Yang B, Mu X, Ahmed SS, Su Q, He R, Wang H, Mueller C, Sena-Esteves M, Brown R et al. (2011): Several rAAV vectors efficiently cross the blood–brain barrier and transduce neurons and astrocytes in the neonatal mouse central nervous system. Mol Ther 19, 1440–1448

Zhang H, Duan C, Yang H (2015): Defective autophagy in Parkinson's disease: Lessons from genetics. Mol Neurobiol 51, 89–104

Zhang M, Wang Y, Ge L (2018): Endomembrane remodeling in autophagic membrane formation. Autophagy 14, 918–920

Zhang QS, Heng Y, Mou Z, Huang JY, Yuan YH, Chen NH (2017): Reassessment of subacute MPTP-treated mice as animal model of Parkinson's disease. Acta Pharmacol Sin 38, 1317–1328

Zhao J, Yang M, Li Q, Pei X, Zhu X (2020): MiR-132-5p regulates apoptosis and autophagy in MPTP model of Parkinson's disease by targeting ULK1. Neuroreport 31, 959–965

Zhou X, Babu JR, da Silva S, Shu Q, Graef IA, Oliver T, Tomoda T, Tani T, Wooten MW, Wang F (2007): Unc-51-like kinase 1/2-mediated endocytic processes regulate filopodia extension and branching of sensory axons. Proc Natl Acad Sci U S A 104, 5842–5847

Zhu JH, Guo F, Shelburne J, Watkins S, Chu CT (2003): Localization of phosphorylated ERK/MAP kinases to mitochondria and autophagosomes in Lewy body diseases. Brain Pathol 13, 473–481

Zhu Z, Yang C, Iyaswamy A, Krishnamoorthi S, Sreenivasmurthy SG, Liu J, Wang Z, Tong BCK, Song J, Lu J et al. (2019): Balancing mTOR signaling and autophagy in the treatment of Parkinson's disease. Int J Mol Sci 20, E728

Acknowledgements

I would like to express special thanks to Prof. Dr. Paul Lingor for giving me the opportunity to conduct my MD thesis in his laboratory and to work on this interesting project. I am very thankful for his support, ideas and permanent availability. I am also very grateful for the supervision of Dr. Lars Tatenhorst, his guidance and also his help with the experiments.

Additionally, I want to thank Prof. Dr. Stadelmann-Nessler for being part of my thesis committee, her helpful suggestions and our discussions during the progress report meetings. I also thank Prof. Dr. Mathias Bähr and the Department of Neurology for giving me the chance to be part of the "VorSPrUNG Promotionskolleg" and to benefit not only from the concomitant bursary, but also from the regular seminars held for the doctoral students.

I really appreciated being part of the Lingor working group and all the helpful advice everybody provided during my time in the lab. Furthermore, I am especially thankful for the excellent technical support I received from Sabine and Vivian. Finally, I want to express my gratitude to my predecessor Björn who gave me an excellent introduction into the lab and recommended relevant literature from the field of neurodegeneration and autophagy to me.